Seismic isolation structure for pool-type LMFBR – Isolation building with vertically isolated floor for NSSS

A.Sakurai, H.Shiojiri, S.Aoyagi & T.Matsuda
Central Research Institute of Electric Power Industry, Abiko, Japan
S.Fujimoto & Y.Sasaki
R & D Center, Toshiba Corporation, Kawasaki, Japan
H.Hirayama
Advanced Reactor Engineering Department, Toshiba Corporation, Yokohama, Japan

1 Introduction

In the design of nuclear power plants, a critical issue is the determination of loadings and response due to earthquakes. A key principle in structural developments of nuclear power plants is the need to maintain elastic behavior during earthquake. Therefore, usual aseismic design requires stiffened structural design for equipments as well as buildings in order to avoid excessive response to seismic waves and to maintain elasticity.

On the other hand, for a fast breeder reactor which is operated under as low pressure as atmospheric pressure and at elevated temperature thin-walled structure is designed to avoid high thermal stresses during operation. In the majority of cases, wall thickness of the main vessel and the core support structure is determined by earthquake condition.

Seismic isolation is an alternative approach of design for earthquake which aims to reduce seismic input to buildings and equipments. Using isolation structure, there is potential of simplification of structure, cost reduction, and improvement of reliability of plant.

2 Seismically Isolated FBR Plant

In high seismic zone, vertical as well as horizontal isolation structure for a FBR plant may be required, because a reactor structure is dependent on not only horizontal but also vertical seismic characteristics. In the case of horizontally and vertically isolated plant, the plant configuration depends on absorption methods for relative displacement between isolated area and non-isolated area. Especially, for sodium pipings, long length pipings are required in order to absob relative displacement by using the piping flexibility. However, it is difficult to design the long length sodium piping.

In this studies, combination of horizontally isolated building and vertically isolated floor for NSSS (Nuclear Steam Supply System) as shown in Fig. 1 was selected as a reference seismically isolated structure for FBR plant. In this plant, all sodium components are installed on the NSSS vertical isolation floor. The relative displacement caused by earthquake is absorbed by non-sodium components. The NSSS isolation floor is 40 m x 40 m and about 20000 ton in weight including installed components. Vertical isolators for the floor are

composed of coil springs and dampers. Further, rubber bearings are set up on the floor side wall as side support bearing. In the horizontal isolation building, horizontal isolators are composed of rubber bearings and dampers.

3 Seismic Response Analysis

3.1 Analytical Model and Condition

Seismic response analyses were performed in order to investigate effects of building structural features, damper characteristics for isolators and soil conditions on responses of the reactor buildings and equipments. For building structural features, two structure categories were considered. One was a conventional structure, designed by usual seismic design methods. The other is a seismic isolation structure, as shown in Fig. 1.

Analytical models in the horizontal direction and the vertical direction for these building were considered. Horizontal model for the seismic isolation building is shown in Fig. 2. The NSSS isolation floor position corresponds to main vessel support position (mass point 4) in Fig. 2. Horizontal natural frequency of the isolation building is 0.5 Hz for the rubber bearing support only. In the vertical analytical model for the isolation building, the NSSS isolation floor is simplified by a linear single-degree-of-freedom system, which moves only in a vertical direction. Vertical natural frequency of the NSSS floor is 1.5 Hz for the coil spring support only. For dampers, 3 kinds of dampers (linear viscuous damper, friction damper and elasto-plastic damper [ex. Lead shear damper]) were considered for horizontal isolator (see Fig. 2). Further, a linear viscous damper was considered for the vertical isolator in the NSSS floor. Three kinds of soil shear stiffness were considered (V_S = 700, 1500 and 2000 m/s).

3.2 Response Calculation

Input seismic wave for seismic isolation design was developed, based on the observed earthquake data. Wave form and response spectrum for the input are shown in Fig. 3. In the response analyses, this seismic wave was used as both horizontal and vertical inputs. But, maximum accelerations for horizontal and vertical inputs are 3 and 2.1 m/s^2, respectively.

First, in eigen value analysis, 1st, 2nd and 3rd natural frequencies of the conventional building (V_S = 1500 m/s) are 3.57, 4.97 and 10.44 Hz, respectively. Natural frequencies and participation factors for the isolation building without dampers are shown in Table 1 and 2.

Second, in horizontal seismic response analysis, response acceleration time history of the main vessel support position, in the case of the isolation building with the elasto-plastic dampers (50 gal trigger), is shown in Fig. 4. Floor response acceleration spectrum on the main vessel support positions for the conventional building and the isolation building with 3 dampers are shown in Fig. 5. Effects of viscous damper damping ratio and trigger level of the friction and elasto-plastic dampers on maximum relative displacement of the isolator are shown in Fig. 6. Further, effects of the above-mentioned damper parameter on maximum response acceleration for the main vessel support position in the isolation building are shown in Fig. 7.

Third, in vertical seismic response analysis, maximum vertical response acceleration and relative displacement for the NSSS isolation floor are 1.692 m/s^2 and 0.0175 m, respectively. It is assumed that vertical damper damping ratio is 0.30.

3.3 Results

(1) Effective seismic isolation for the reactor components can be expected by adopting the proposed isolation building.
(2) In the isolation building, low frequency range responses, in which liquid sloshing in the main vessel increases, are not amplified by using the hysteric dampers.
(3) The viscous damper is most effective for response acceleration control, but is not effective for relative displacement control. The friction damper is most effective for relative displacement control, but is not effective for acceleration control. The elasto-plastic damper is relatively excellent for practical frequency range in the three kinds of dampers. Proper trigger level for this damper is about 50 gal.

4 Scale Model Test on NSSS Isolation Floor

4.1 Scale Model Structure

A 1/18 scale model, in which the NSSS floor, the main vessel, the S/G and the pump are simplified, was used (see Fig. 8) in order to investigate vibration characteristics for the NSSS isolation floor and side support bearing effects on rocking responses for the isolation floor. The similarity rule on the dynamic properties between scale model and actual structures was applied for fundamental natural frequency, structual vertical stiffness and masses. The scale model, whose total mass is 3.45×10^3 kg, is supported by 8 coil springs and 4 oil dampers. Further, 4 or 8 high damping rubber bearings are set up between the floor side wall and the pedestal as side support bearings in order to restrain horizontal floor motion and control rocking motion. Designed vertical natural frequencies for the floor model and the main vessel model are 4.5 Hz and 18 Hz, which correspond to 1.5 Hz and 6 Hz for actual structure frequencies.

4.2 Model Tests

In model tests, static loading test for a vertical isolator, vibration test for model components and vibration test for the scale model in Fig. 8 , were performed in order to investigate load-displacement relation of the isolator, vibration characteristics of the model components and the whole isolation floor model. Load-displacement relation for the vertical siolators, containing 8 coil springs and 4 rubber bearings, is shown in Fig. 9. Resonant frequencies for the model components and the scale model are shown in Table 3.

In seismic vibration tests, response wave on the main vessel support position of the isolation building with the elasto-plastic damper for the seismic wave in Section 3, Akita wave (1983), and El Centro wave (1949) were used as seismic inputs. Maximum response accelerations for isolated scale model and non-isolated scale model for the seismic inputs, whose time scale was reduced to 1/3 for the actual scale, are shown in Table 4.

4.3 Results

(1) The NSSS isolation floor vibration characteristics were made clear. Especially, the side support bearing (rubber bearing) is effective for horizontal floor motion restraint and rocking motion control.
(2) Seismic isolation effects for responses of the reactor components can be sufficiently expected, using the vertical seismic isolation floor.

5 Conclusion

From the analytical and experimental studies, the following has been concluded:

(1) Seismic isolation structure, which is suitable for large pool-type LMFBR, were proposed.

(2) Seismic response characteristics of the seismic isolation structure were investigated. It was made clear that the proposed seismic isolation (Combination of the isolated building and the isolated NSSS floor) was effective.

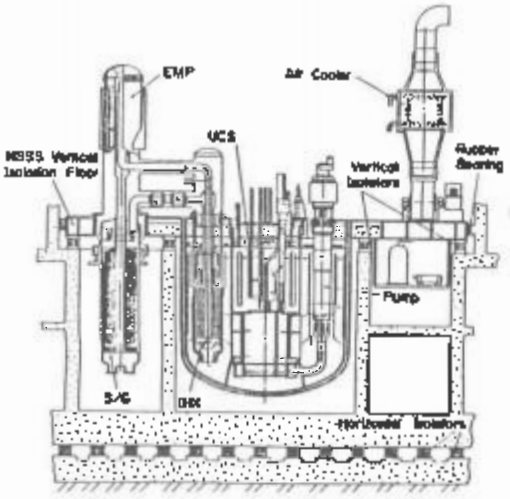

Fig.1 Reference seismic isolation structure for FBR plant

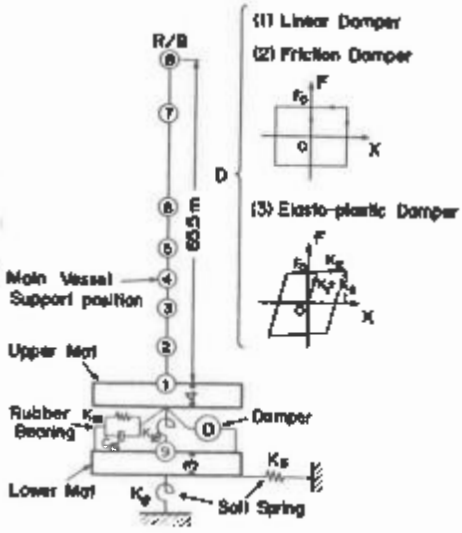

Fig.2 Analytical model for seismic isolation building (Horizontal direction)

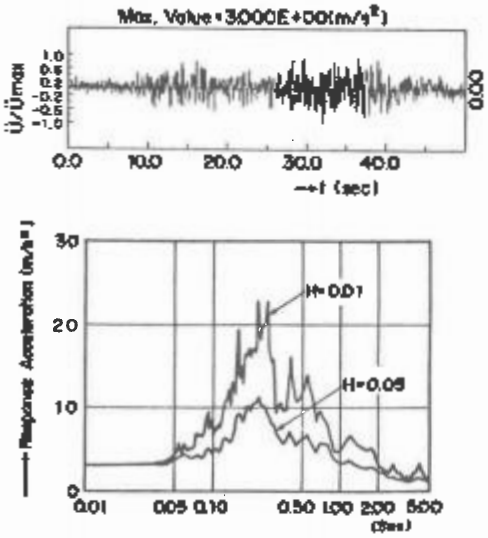

Fig.3 Time history of acceleration and response spectrum for seismic wave input (Wave B)

Table 1 Horizontal eigen value of seismic isolation building

mode	Vs (m/s)	N.Frequency (Hz)	Period (sec)	Participation Factor
1	700	0.485	2.020	1.060
	1500	0.498	2.007	1.048
	2000	0.498	2.006	1.046
2	700	2.64	0.379	0.047
	1500	2.68	0.373	0.046
	2000	2.69	0.372	0.046
3	700	5.79	0.173	0.040
	1500	9.32	0.107	0.026
	2000	9.82	0.102	0.018
4	700	9.92	0.101	0.259
	1500	9.96	0.100	0.035
	2000	10.23	0.098	0.022
5	700	10.22	0.098	0.977
	1500	17.01	0.059	0.056
	2000	18.99	0.053	0.024

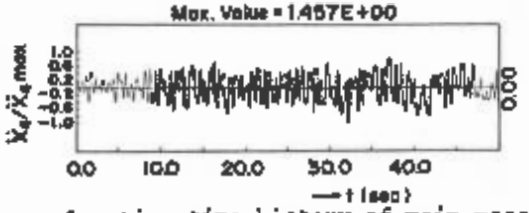

Fig.4 Response acceleration time history of main vessel support position in the case of elasto-plastic damper (50 gal trigger)

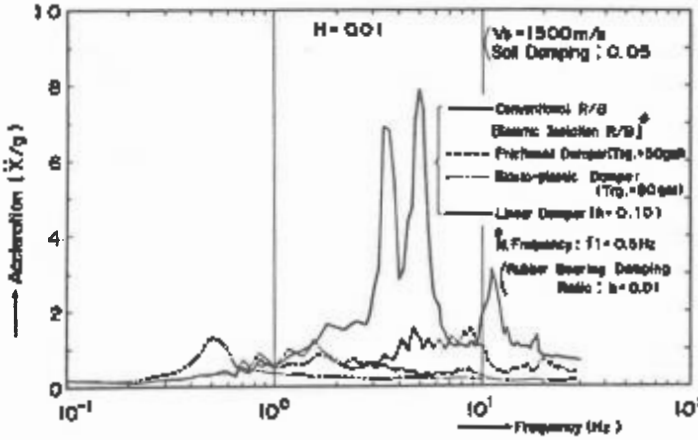

Fig.5 Response acceleration spectrum on main vessel support position (Comparison of conventional building with isolation building)

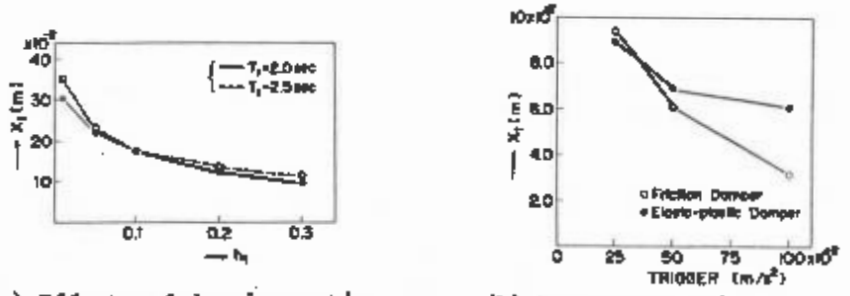

(a) Effects of damping ratio (Viscous damper)

(b) Effects of trigger level (Hysterisis damper)

Fig.6 Maximum response relative displacements for three kinds of damper

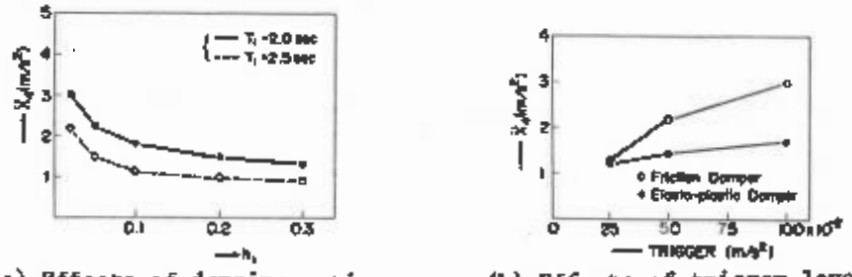

(a) Effects of damping ratio (Viscous damper)

(b) Effects of trigger level (Hysterisis damper)

Fig.7 Maximum response accelerations of main vessel support position for three kinds of damper

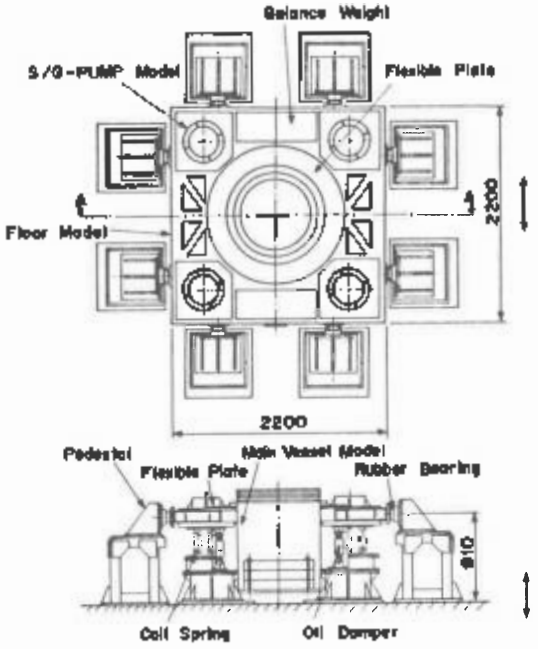

Fig.8 Scale model of NSSS isolation floor

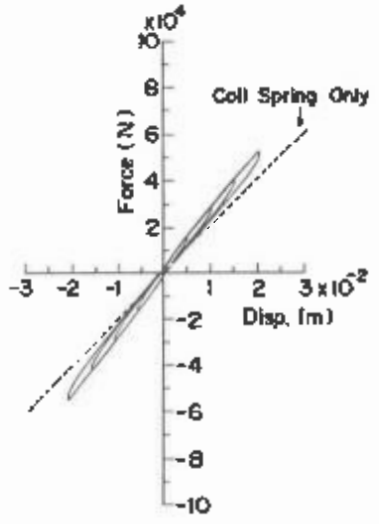

Fig.9 Load-displacement relation for vertical isolators

Table 2 Vertical eigen value of seismic isolation building

mode	Vs (m/s)	N.Frequency (Hz)	Period (sec)	Participation Factor
1	700	1.491	0.671	1.095
	1500	1.497	0.668	1.027
2	700	5.158	0.194	1.251
	1500	9.535	0.105	2.872
3	700	12.50	0.081	0.352
	1500	12.76	0.078	1.965
4	700	27.64	0.036	0.086
	1500	30.04	0.033	0.337
5	700	45.04	0.022	0.045
	1500	45.17	0.022	0.177

Table 3 Resonant frequency of NSSS isolation floor model

Test Case	Resonant Frequency (Hz)	Mode
Model Components Test	10.6	Hor. 1st (M/V Rocking)
	15.8	Ver. 1st (M/V)
Isolated Model Test (Coil Springs Only)	2.2	Hor. 1st (Floor)
	3.8	Ver. 1st (Floor)
	4.2	Rocking 1st (Floor)
	25.0	Ver. 2nd (M/V)
Isolated Model Test (Coil Springs, Rubber Bearings, Oil dampers)	5.0	Ver. 1st (Floor)
	10.0	Hor. 1st (M/V Rocking)
	22.6	Rocking 1st (Floor)
	25.8	Ver. 2nd (M/V)

Table 4 Maximum seismic response acceleration of NSSS isolation floor model (Comparison of isolated floor with non-isolated floor)

Seismic Wave (Floor Response)	Max. Input Acceleration (m/s^2)	Floor Support Type	Max. Response Acceleration (m/s^2)		
			Floor Hor.	M/V Lower End Hor.	M/V Lower End Ver.
Wave 8	Hor. 0.74	Non Isolation	0.93	2.33	4.67
	Ver. 1.80	Isolation	1.27	1.10	1.69
Akita Wave	Hor. 1.13	Non Isolation	1.24	1.93	3.87
	Ver. 1.49	Isolation	1.30	1.40	1.76
El Centro Wave	Hor. 0.58	Non Isolation	1.13	1.27	4.72
	Ver. 4.42	Isolation	1.15	0.69	3.30

A study on the seismic isolation of fast breeder reactor plant 3-D seismic isolation of reactor structure

Y.Sonoda, K.Sekine & M.Madokoro
Advanced Reactor Department, Hitachi Works, Hitachi Ltd, Japan
H.Kasai
Mechanical Engineering Research Laboratory, Hitachi Ltd, Japan
A.Sakurai, S.Shiomi, S.Aoyagi & Y.Matsuda
Central Research Institute of Electric Power Industries

1. SUMMARY

Seismic load is most important for the structural design of Liquid Metal Fast Breeder Reactors (LMFBRs) because of the relatively low operational pressure of the coolant. This indicates that the reduction of earthquake excitation will result in a reduction of the structural mass and an increase of the structural reliability.

Based on the abovementioned background, the feasibility of applying a three dimensional seismic isolation to the reactor structure of LMFBR have been studied. The paper is composed of the following two parts, 1) experimental study on the force-displacement relation of the seismic isolation device 2) earthquake response analysis of a three dimensionally isolated reactor structure. The feasibility and the effectiveness of a three dimensional seismic isolation of LMFBR is shown by the study. But at the same time, it is indicated that for a more detailed analysis on the seismic behavior, the restoring force characteristics under bi-axial loading had better be taken into account in the modelization.

2. INTRODUCTION

Preceding studies on the application of seismic isolation to nuclear plants are the study by Jolivet et al, Kunar et al and Sonoda et al for example (Jolivet 1977, Kunar 1979, Sonoda 1986). But they are the studies on the horizontal seismic isolation of the nuclear reactor building. As for the reactor structure of the LMFBR, seismic isolation in the vertical direction may be also effective due to the large diameter of the reactor. Three dimensional seismic isolation is studied by a few researchers such as Huffmann, Kelly and Staudacher (Huffmann 1985, Kelly 1983, Staudacher 1985). But their studies treat the seismic behavior in a small displacement range. It is and yet essential to understand the seismic behavior of a three dimensionally isolated structure in an extreme seismic condition to evaluate its feasibility for nuclear facilities. Therefore an emphasis has been laid in the present study on the understanding of the load-deflection behavior in an extreme deformation condition.

Three dimensional seismic isolation by means of helical springs and viscous dampers at the support of the reactor structure was selected for study because of its compactness. Other method of three dimensional seismic isolation is to combine a vertical isolation of the reactor structure with a horizontal isolation of reactor building. But this method is not studied in the paper.

Tabel 1 The Loading Condition

Series	Test No.	Horizontal Load (kN)	Vertical Load (kN)
A	1	6.2	0~28.1
	2	3.1	
	3	6.2	
	4	9.3	
	5	1.1	
B	6	0~12	28.1
	7		18.7
	8		9.3

Table 2 Dimensions of the Coil Spring

Nominal Load	160	ton
Cent./ Diameter of Coil	400	mm
Dia. of Wire	100	mm
Effective Length of Coil	1400	mm
Effective Winding Number	5	turn

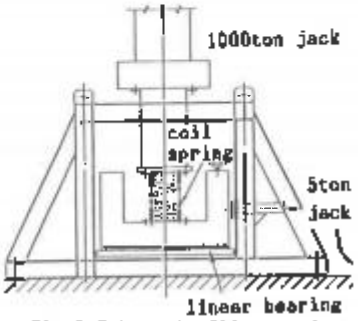

Fig 1 Schematic Illustration of Test Facility

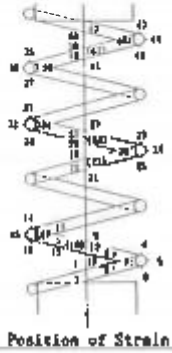
Fig 2 Position of Strain Gauges

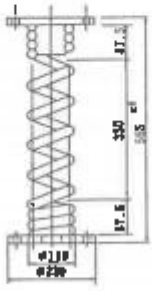
Fig 3 Schematic Illustration of Test Specimen

3. BI-AXIAL LOAD-DEFLECTION TEST OF COIL SPRINGS

3.1 Objective and composition of the test

Few test data are provided on the load-deflection relationship of helical springs in the horizontal (transversal) direction while sufficient test data are available in the vertical (axial) direction. Therefore, bi-axial load-deflection tests were performed in order to evaluate the effect of horizontal load to the vertical load-deflection relationship and vice versa. Table 1 shows the loading conditions. Fig. 1 shows the test facility. Tests are composed of the tests series A and series B. Series A comprises the vertical load-deflection tests for varied horizontal off-set displacements. Series B comprises the horizontal load-deflection tests under varied vertical initial load. Load, deflection and 162 strain components are measured in each test. Fig. 2 shows the position of strain gauges. Experimental stiffness and strain are compared to an analytical formulation and the FEM results.

3.2 Design of coil spring

The reactor structure weighing around 8,000 ton is supposed to be supported by 50 isolation devices which realize the natural frequency of 1.0 Hz in the horizontal direction and 2.0 Hz in the vertical direction. Based on the preliminary earthquake response analysis, the maximum response acceleration is estimated to be around 0.5G in the horizontal direction and 1.5G (including the gravity) in the vertical direction for an S_2 earthquake. Dimensions of the coil spring designed under the abovementioned conditions are described in Table 2. The effective hight is 1,700 mm, central diameter of the coil is 375 mm, diameter of the wire is 100 mm and the number of effective roll is five. The diameter of the wire of 100 mm is adopted because this is the maximum fabricatable diameter though a fatter wire is desirable for the increase of space efficiency. The test specimens are 1/4 scale models of the actual coil springs (Fig. 3).

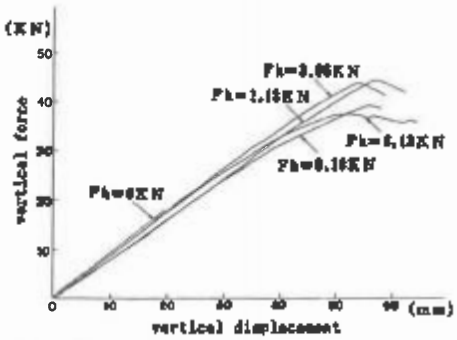

Fig 4 Results of The Test Series 1

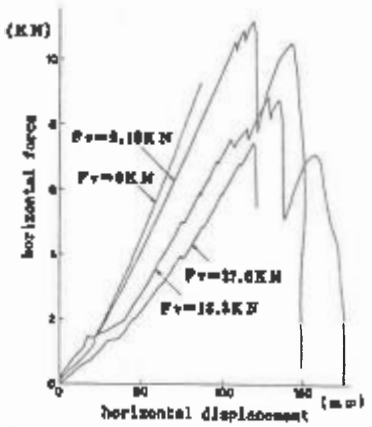

Fig 5 Results of The Test Series 2

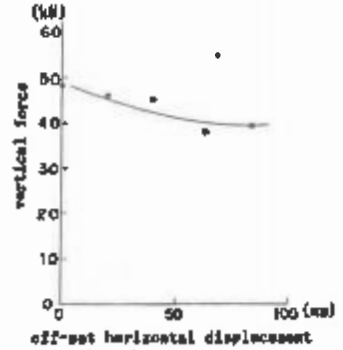

Fig 6 Maximum Vertical Tolerable Load For Different Horizontal Off-Sets

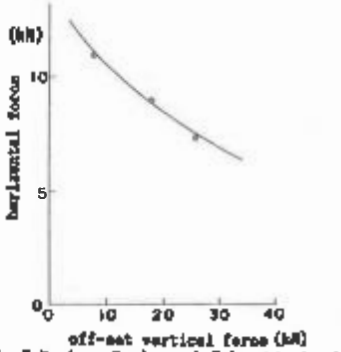

Fig 7 Maximum Horizontal Tolerable Load For Different Vertical Off-Sets

3.3 Results of load-deflection test

Fig. 4 represents the results of the tests series 1, Fig. 5 represents the test series 2. The dotted lines denote the FEM analysis taking into account the geometrical non-linearity in the large deformation range. The arrows denote the stiffness estimated by the analytical formulation.

Series 1 The deviation of the vertical stiffness for varied horizontal off-set displacements is ±10% and it does not show any obvious tendency as a function of the off-set. So, the effect of horizontal off-set can be neglected for design purposes. The relation between the vertical load and deflection is linear up to a certain extent. After that point, the vertical load does not increase while the vertical displacement increases. The behavior after the maximum load is explained as following. Because the horizontal actuator is load-constant type, it fractured the coil spring after the P-δ effect of the vertical load canceled the horizontal restoring force of the spring. Decrease of the horizontal restoring force corresponding to the increase of the vertical load also assures the explanation. Common fracture mode of the coil spring under the load combination of Series 1 is the loss of horizontal restoring force. Fig. 6 shows the maximum load for different horizontal off-sets. The maximum load decreases weakly corresponding to the increase of the horizontal off-set. The linear

load-deflection relationship and the fracture mode indicate that the geometrical non-linearity plays an important role compared to the material non-linearity in the load-deflection behavior.

Series 2 Fig. 5 indicates that the horizontal stiffness decreases with the increase of the vertical load. Horizontal load-deflection curve can be approximated by two straight lines. The increase of the stiffness in the large deformation is cause by the touching of spring wires each other. The fracture mode in the Series 2 was the fracture at the welding of the wire end. Fig. 7 shows the maximum horizontal loads for different vertical loads. Maximum horizontal load decreases with the increase of the vertical load.

Preliminary earthquake response analysis estimates that the maximum load for a spring will be around 10 ton horizontally and 30 ton vertically for an S_2 earthquake. Extrapolating the test results by using the law of simslarity, the maximum tolerable load of the actual isolation device will be 15 ton horizontally and 45 ton vertically at the same time. It is presumed therefore, that the coil spring has enough resistance (safety margin is 1.5) to be used as a seismic isolation device.

4. EARTHQUAKE RESPONSE OF THREE DIMENSIONALLY ISOLATED REACTOR

4.1 Determination of earthquake input

It is widely acknowledged that the input earthquake motion has a predominant effects on the earthquake response of seismically isolated nuclear facilities. Nevertheless, the design earthquakes for nuclear facilities which are used currently in Japan can not be relied as for its so called long period components (one to 10 seconds) because of insufficient observation data. On the contrary, they have enough reliability for their short period components. In the light of the abovementioned situation, an extensive earthquake observation is currently on the way. But it still does not supply with enough reliable data for the determination of the long period components of design earthquake waves. Therefore, an observational earthquake motion which had been obtained at a firm rock site at the occasion of a large earthquake was adopted for design earthquake in the study. The waveform is shown in Fig. 8, response spectrum is shown in Fig. 9. The amplitude of the observational earthquake motion was raised for the analytical use by more than ten times so as the maximum acceleration becomes 300 gal.

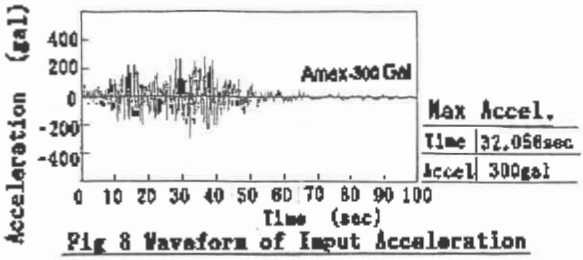

Fig 8 Waveform of Input Accelaration

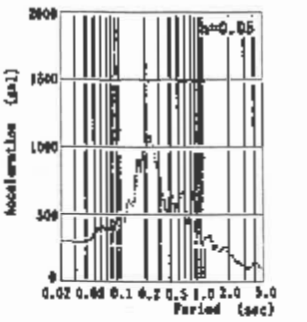

Fig 9 Response Spectrum of Input Accelaration

Table3 Natural Frequencies and Partipation Factores

model	period (sec)	frequency (Hz)	participation factor
1	4.54	0.22	1.386
2	2.49	0.40	0.564
3	1.88	0.66	−0.233
4	1.50	0.67	0.299
5	1.23	0.81	0.006
6	1.07	0.94	−0.128
7	1.02	0.98	−0.060
8	0.21	4.71	−0.857
9	0.20	5.07	−7.579
10	0.16	6.11	−0.552

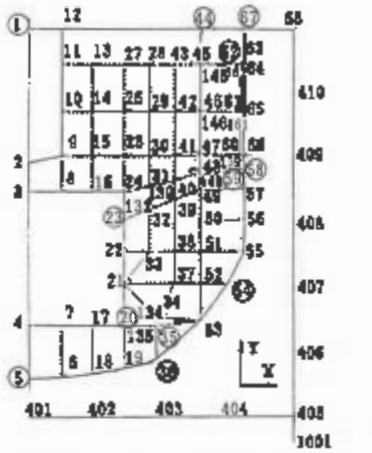

Fig 10 Axi-symmetric Analysis Model

Table 4

Node No.	Acceleration (Gal)	Displacement (cm)
1	293	1.82
44	285	1.62
67	285	1.82
2	287	1.86
26	286	1.63
65	225	1.36
84	210	1.29
20	274	1.82
25	274	1.62
25	225	1.20
50	210	1.29
87	272	1.84

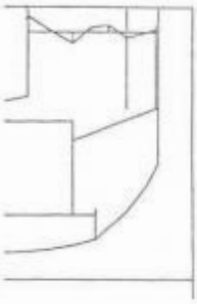

Fig.11 The First Sloshing Mode

4.2 Earthquake response of reactor structure

Fig. 10 shows the axi-symmetric model used for the response analysis. Liquid sodium is modelized by an added mass matrix taking the gravity effects into account. As shown in Fig. 11, the first sloshing mode appears at 0.22 Hz and the first vibration mode appears at 1.22 Hz (6th mode). At the 6th mode a coupling of sloshing and reactor structure vibration is distinguished. This is one of the important characteristics in the vibraiton mode of the three dimensionally isolated reactor structure. For the higher modes, the coupling is not obvious.

The maximum accelerations shown in Table 4 are not different much each other throughout the reactor which indicates that the reactor sways as a rigid body during earthquakes also. There is a weak ampilification of accleration through the reactor vessel. But it is rather due to the rocking motion of the reactor structure according to the vertical deformation of the isolation devices than due to the deformation of the reactor vessel itself. Vertical acceleration is also reduced by the seismic isolation. But the vertical accleration at the periphery of the roof-deck is higher than that at the center. Compared to the earthquake response of a non-isolated case, the horizontal maximum acceleration is reduced from 2 G to 0.3 G (0.15) and the vertical maximum acceleration is reduced from 1 G to 0.2 G (0.2). That enables the reduction of the thickness of vessel from 50 mm to 20 mm yet increasing the structural margin.

Fig. 12 Sloshing Time History

The sloshing time history is shown in Fig. 12. Maximum wave height reaches 0.8m but because sloshing pressure is much lower than that of the fluid structure interaction, it is not impedimental from the point of view of the structural design.

5. CONCLUSION

Feasibility of a three dimensional seismic isolation of the reactor was studied through the experiments on coil springs and the seismic response analysis of the reactor structure. The load-deflection test on the coil spring has shown that it could be possible to use coil springs as three dimensional seismic isolation device but the coupling effects of horizontal and vertical loads on the horizontal restoring characteristics had better be tested more intensively for a more detailed evaluation. The response analysis has indicated that the three dimensional seismic isolation is effective for the reduction of seismic load but an interaction between sloshing and isolated reactor have to be taken into account properly.

6. REFERENCE

Huffmann, G.K. 1985, Full base isolation for earthquake protection by helical springs and viscodampers, Nuclear Eng. & Design: 331 - 338.

Jolivet, F. & Richli, M. 1977. Aseismic foundation system for nuclear power stations, 4th SMiRT Conference, K9/2.

Kelly, J.M. 1983. The use of base isolation and energy absorbing restrainers for the seismic protection of a large power plant component, NP-2918 Research Project 810-8, EPRI

Kunar, R.R. & Malni, T. 1979. A review of seismic isolation for nuclear structures, NP-1220-SR, EPRI.

Pan, T.C. & Kelly, J.M. 1984. Seismic response of base-isolated structures with vertical-rocking coupling, Earthq. Eng. & Structural Dynamics: 681 - 702

Sonoda, Y. et al. 1986. A study in the seismic isolation of a fast breeder reactor plant, 7th Japan earthquake engineering symposium : 1651 - 1656

Staudacher, K. 1985. Protection for structures in extreme earthquakes: Full base isolation(3-D) by the Swiss seismofloat system, Nuclear Eng. & Design: 343-357

Feasibility study on the seismic isolation of pool-type LMFBR
1. Horizontal seismic isolation of Nuclear Island Building

Y.Sonoda & M.Madokoro
Advanced Reactor Department, Hitachi Works, Hitachi Ltd, Japan
K.Takabayashi
Nuclear Engineering Department, Kajima Corporation, Tokyo, Japan
K.Mizukoshi & T.Takenaka
Kobori Research Complex, Kajima Corporation, Tokyo, Japan
H.Koshida
Kajima Institute of Construction Technology, Kajima Corporation, Tokyo, Japan

1. INTRODUCTION

In case of pool-type liquid metal fast breeder reactors (LMFBRs), structural design is strongly influenced by the seismic loads because the operational coolant pressure is relatively low. This is one of the important differences of LMFBRs from light water reactors from the viewpoint of structural design. Therefore, the reduction of seismic force will be of great assistance for attaining a simple and lightweight LMFBR, especially when stringent seismic conditions are imposed as in Japan.

Based on the background, an intensive 3-year feasibility study was performed on the seismic isolation of LMFBRs. The objectives of the study were; firstly, to evaluate the effectiveness of seismic isolation for reducing structural masses and increasing structural margin, and secondly, to develop and validate seismic isolation techniques compatible with the strict requirement from nuclear facilities. The first part of the study is composed of the investigation into the input earthquake motion, a conceptual design study of the nuclear island building (NIB) and the reactor structure, and the investigation into the seismic behaviors of the structures. The second part of the study comprises of material tests, scale model tests of isolation devices and the confirmation of mechanical characteristics by prototype models. Shaking table tests of an NIB model was performed in order to confirm both the seismic behaviors of the structures and the mechanical characteristics of the isolation devices.

This paper presents the former part of the study, where as the latter part will be covered by two separate papers in this session.

2. DETERMINATION OF INPUT EARTHQUAKE MOTION

The seismic response of isolated structures is strongly influenced by the low frequency components (0.5 - 1.0 Hz) of the ground motion, while that of conventional nuclear facilities is sensible to higher frequency components. Considering the recent earthquake observations in Japan and the U.S. NRC spectrum, a synthetic ground motion has been generated which has larger low frequency components than Japanese conventional ones.

As a result, the response spectrum at 1.0 Hz is twice as high as the conventional spectrum in the synthetic earthquake motion. Fig. 1 shows the response spectrum of the earthquake motion defined at a free surface of the base stratum.

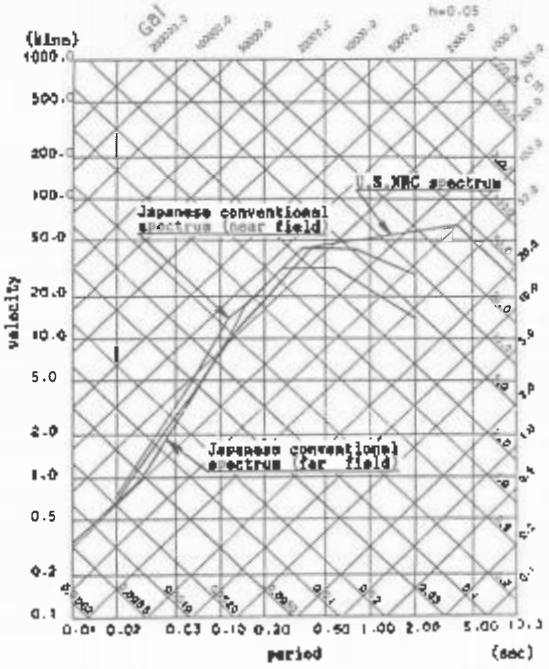

Fig 1 Floor Response of Input Acceleration

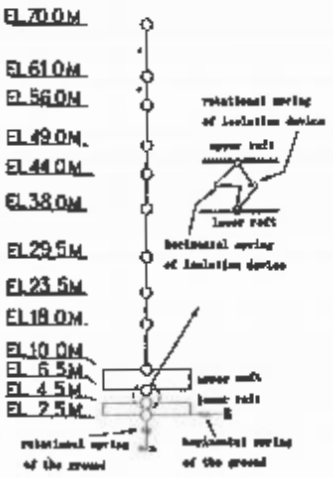

Fig 2 Analysis model (A-building)

Table 1 Characteristics of seismic isolation devices

Natural frequency \ No.		1	2	3	4	5
Horizontal	f 1 (Hz)	1.6		1.0		
	f 2 (Hz)	0.5				1.0
Vertical	f (Hz)	2.0				
Yield level		0.05 W	0.025 W	0.05 W	0.025 W	—

Table 2 Conceptual frameworks of NIBs

concept / elevation		A	B	C
EL>17.0 m		Reinforced concrete frame	Steel frame	Steel frame
EL≤ 17.0m	Outer part		Reinforced concrete frame	
	Inner part	reinforced concrete wall		

3. EARTHQUAKE RESPONSE OF NIB

Table 1 shows the characteristics of the seismic isolation devices. Five mechanical properties, four elasto-plastic and an elastic ones, are selected based on the preliminary selection of mechanical properties. Table 2 shows three types of the conceptual frameworks A, B and C, of the NIB, studied. All three buildings are reduced in weight compared to a conventional (non-isolated) building. The NIB concept A is a reinforced concrete frame structure building whose wall thicknesses are drastically reduced reflecting the reduction of seismic force by isolation. In the NIB B, the upper half of the building is replaced by a steel frame. In the NIB C, the whole building except for the neutron shielding walls is replaced by a steel frame and the two portions are connected by expansion joints. More drastic efforts for the mass reduction is employed in the NIB C than in concept A. The NIB B stands intermediate.

Fig. 2 shows the seismic analysis model. The soil is modelized as a so called sway-and-rocking model, the isolation devices are modelized by bi-linear springs and the building is modelized as shear-and-bending spring with concentrated masses. Fig. 3 shows the earthquake responses of the NIB A for each isolation characteristics. It also shows the response of the non-isolated building for comparison. The maximum response acceleration of the isolated buildings is 1/3 - 1/10 of that of the non-isolated building. The difference is remarkable at the top of the building. The maximum relative displacements of the isolated buildings are almost identical from the basemat to the top, which indicates that the building sways as a rigid body during earthquakes. Relative displacements between the isolated and the non-isolated buildings may cause a problem to the piping which runs between them. But the relative displacements can be absorbed without difficulties by expanding the support intervals as long as the relative displacement falls in the order of 10 cm as in this case.

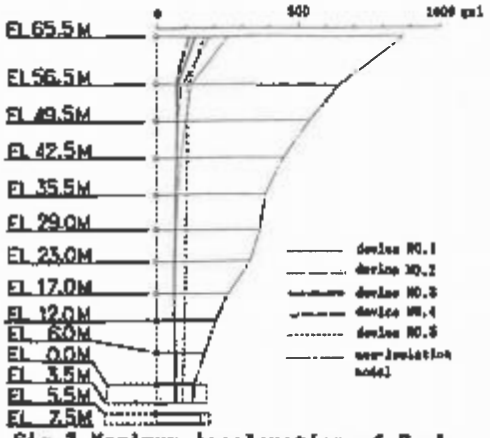

Fig 3 Maximum Acceleration of Each Isolation Devices

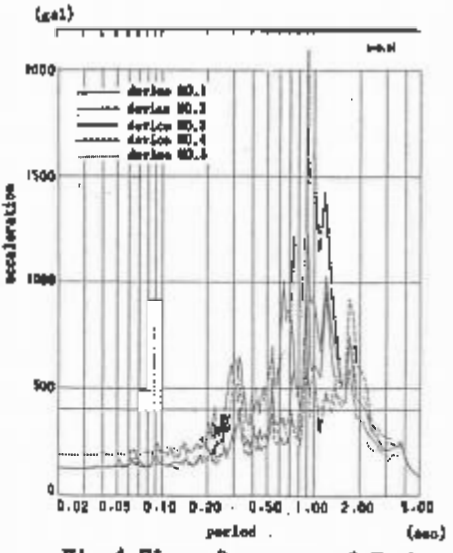

Fig 4 Floor Response of Each Isolation Devices

Fig. 4 shows the floor response spectrum (FRS) at the elevation of the reactor structure installation. When the elastic isolation device is used (Case 5), FRS of the isolated building becomes higher than that of the input ground motion at the first natural period of the isolated building itself (1.0 Hz). For the elasto-plastic isolation devices (Cases 1 to 4), on the other hand, the peaks at 0.5 -1.0 Hz are not evident. Table 3 shows the maximum FRS levels for the frequencies higher than 4 Hz which cover the natural frequencies of the reactor structure. The table shows that the characteristics of Devices 3 and 4 are most effective in reducing the response of the reactor structure. Therefore, the characteristics of Device 3 is adopted as a reference for the following comparisons.

Fig. 5 shows the natural modes of different structural frameworks based on the initial stiffness of the restoring characteristics of Device 3 . Participation factors of the first swaying modes are predominant for all framnworks. Deformations at the top of the building is larger for the buildings B and C than for the building A because of their low stiffness at the upper part of the buildings. Fig. 6 shows the maximum earthquake response of the buildings. Amplification at the upper part of the building is observed in the buildings B and C. But they are still much lower than that of the non-isolated

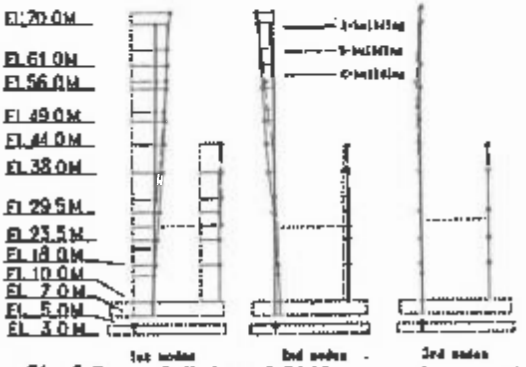

Fig 5 Natural Modes of Different Structural Frameworks

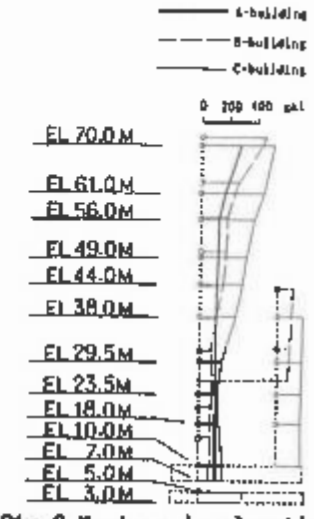

Fig 6 Maximum Acceleration of Different Structural Frameworks

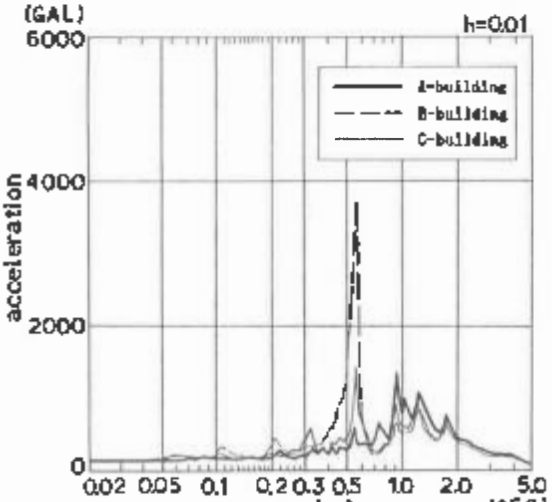

Fig 7 Floor Response of Differental Structual Frameworks

Table 3 Maximum FRS level at higher than 4Hz

service / Concept A	1	2	3	4	5
max. FRS (G)	0.41	0.26	0.21	0.22	0.35

building. The maximum relative displacement between the reinforced concrete cavity wall and the adjacent steel frame is around 3 cm, which is not impedimental for the piping design. The base shear coefficient and the overturning moment indicate that the building utilizes the seismic force reduction in increasing the stability and structural margin against the seismic force. FRS shown in Fig. 7 shows that it is reduced below around 0.4G for the frequencies higher than 4.0 Hz. Table 4 shows that the weight of the isolated NIBs is reduced to around 120,000 tons including the lower raft while that of non-isolated NIB is around 200,000 tons. Reduction reaches about 50%. A remarkable reduction is obtained together with increased structural margin by the seismic isolation. This is the largest merit of seismic isolations on the NIB.

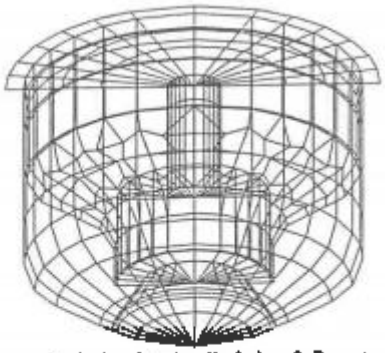

Fig 8 Analysis Model of Reactor Structure

Table 4 Weight of NIB

	Weight (ton)
Isolated NIB A	118,000
Isolated NIB B	108,000
Isolated NIB C	101,000
Non-Isolated NIB	198,000

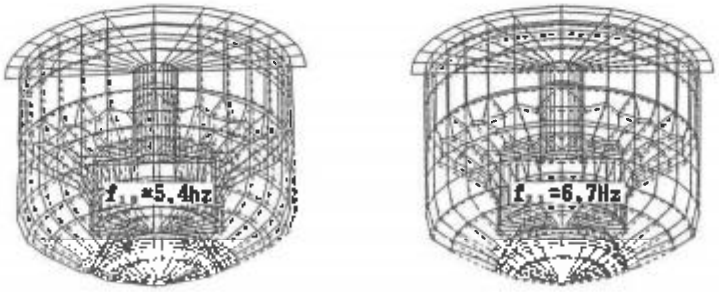

Fig.9 Typical vibration modes and frequencies

4. EARTHQUAKE RESPONSE OF REACTOR STRUCTURE

Fig. 8 shows the analysis model of the reactor structure, a three dimensional shell model, in which the liquid sodium is treated as a so called added mass matrix having significant non-diagonal terms. The effects of gravity, so the sloshing, is neglected in the analysis.

Fig. 9 shows the natural frequencies and modes of which the participation factors are significant. The most significant horizontal mode appears as the 18th mode (5.4 Hz) which is the in-phase horizontal deformation of the reactor vessel and the core. The most significant vertical mode is the 21st mode (6.7 Hz), which is the vertical in-phase deformation of the roof deck and the core. Time domain modal response analysis were performed based on the lowest 23 modes including the above mentioned two important modes. Fig. 10 shows the acceleration time history at the lower raft, the top of the cavity wall and the reactor core. The time history indicates that once an input acceleration is reduced by the isolators, it is no longer amplified significantly through the reactor building nor the reactor strucutre. This notably contrasts with the non-isolation case where the maximum acceleration at the core becomes more than ten times higher than the input at the ground.

Fig. 11 shows the resultant stresses at the reactor structure. The maximum stress of 11.5 kg/mm^2 appears at the junction of the bottom head and the core support structure. At the other parts, the stress is much lower. It indicates that the reactor structure with 20 mm thick wall has enough strength to stand in the seismically isolated conditions. This is also a significant reduction of the thickness as well as the increased structural margin compared to the conventional seismic design of a reactor structure.

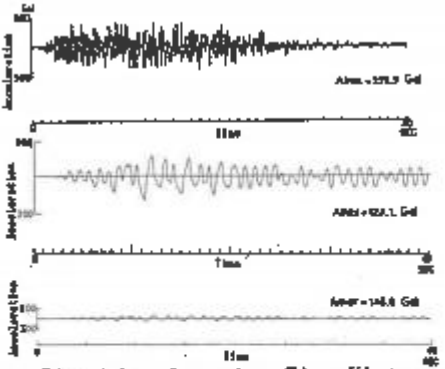

Fig 10 Acceleration Time History

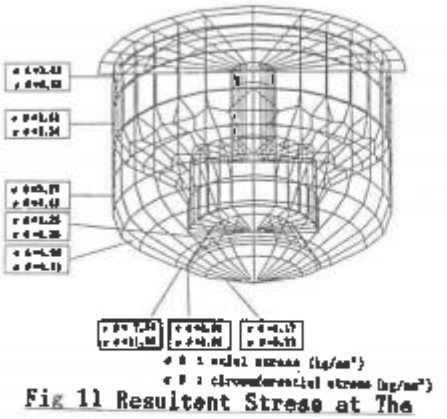

Fig 11 Resultant Stress at The Reactor Structure

5. CONCLUSION

Feasibilities and effectivenesses of a horizontal seismic isolation applied to the NIB of an LMFBR have been evaluated. The results are summarized as follows.

1) Seismic responses of seismically isolated NIBs and the reactor structure are characterized by a large sway motion displacement as a rigid body with low acceleration. The maximum response acceleration is reduced to 1/3 - 1/10 for the NIB and and reactor structure when isolated.
2) Structural integrity of a seismically isolated NIB is shown by the study not withstanding nearly 50% of the weight has been reduced compared to the non-isolated building.
3) As for the reactor structure, the seismic isolation can result in reduced wall thicknesses down to about 20 mm or, around 20% in weight.
4) The stability and structural margin of the building and the reactor yet increase in spite of the above-mentioned weight reduction of the structures.

By the experimental studies on the seismic isolation devices that will be presented in the succeeding papers, the seismic isolation is found feasible and effective for LMFBRs of Japan.

This study was carried out under the sponsorship of the Ministry of International Trade and Industry of Japan.

6. REFERENCE

Eidinger, J.M., 1979. Seismic isolation for nuclear power plants. Proc. of 7th SMIRT K16/2 pp 533-540.

Jolivet, F. & Richli, M. 1979. Aseismic foundation system for nuclear power stations. Proc. of 4th SMiRT conference, K/2

Kurihara, M, Iizuka, M. et al. 1986. Feasibility study of a seismic isolation system for fast breeder reactor plants. Proc. of the 7th Japanese earthquake engineering symposium. p 1657 - 1668.

Plichon, C et al. 1980. Protection of nuclear power plants against seism. Nuclear technology. pp 295-306.

Sonoda, Y et al. 1986. A study on the seismic isolation of a fast breeder reactor plant. Proc. of the 7th Japanese earthquake engineering symposium. pp 1651 - 1656.

Takabayashi, K. et al. 1986. Study on the seismic isolation of fast breeder reactor plants. Proceeding for Annual Meeting of architectural Institute of Japan. pp 983 - 988.

Seismic qualification of nuclear control board by using base isolation technique

T.Koizumi & N.Tsujiuchi
Central Research Laboratory, Mitsubishi Electric Corp., Amagasaki, Japan
T.Fujita
Institute of Industrial Science, University of Tokyo, Japan

1 INTRODUCTION

Seismic qualification is essential for any kind of electric equipment or control board especially for nuclear use. Therefore, for the safety of nuclear power, plant, structural analysis and experimental verification have been needed to qualify the earthquake loading according to the demand of nuclear safety regulation. . Eventually, structural rigidity has been regarded as the most prior characteristics for structural designing and this causes excessive weight and complexity of shape.

The purpose of the author's investigation here is to adopt base isolation technique(Fujita et al 1984) as a new approach for seismic qualification of nuclear control board. First part of this paper, basic concept of base isolation technique is expressed. In here, two dimensional linear motion mechanism with pre-tensioned coil springs and some dampers are included in the isolation device. Control board is regarded as a lamped mass system with inertia moment. Fundamental movement of this device and control board is calculated as a non-linear response problems.

After this fundamental analysis and numerical estimation, experimental investigation has been undertaken using an actual size control board. Sufficient agreement was recognized between experimental results and numerical estimation.

2 STRUCTURAL CONFIGURATION OF BASE ISOLATION DEVICE

The fundamental configuration of this base isolation device is composed of a orthogonally coupled linear motion mechanism(Figure 1 and Figure 2 (a),(b)). By using this mechanism, the upper table is movable in any direction of two dimensional plane. These two rails of X and Y direction shown in Figure 1 are composed of a couple of plate and 2 set of roller bearings for vertical loading. Therefore this structure has sufficient endurance for toppling moment. A set of coil springs and oil filled viscous dampers are installed between base frame and movable table. The coil spring works as a linear spring, however the damper behaves non-linearly depending on its' magnitude. This reason is that the damper is located at right angle to displacement direction. Another friction damper is installed as shown in Figure 1 and 2. This works to fix the table to the base frame as far as the seismic movement runs up to a certain extent.

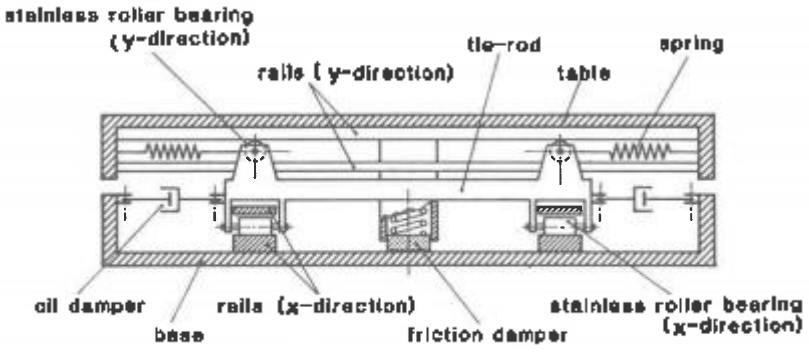

Figure 1. Fundamental configuration of base isolation device

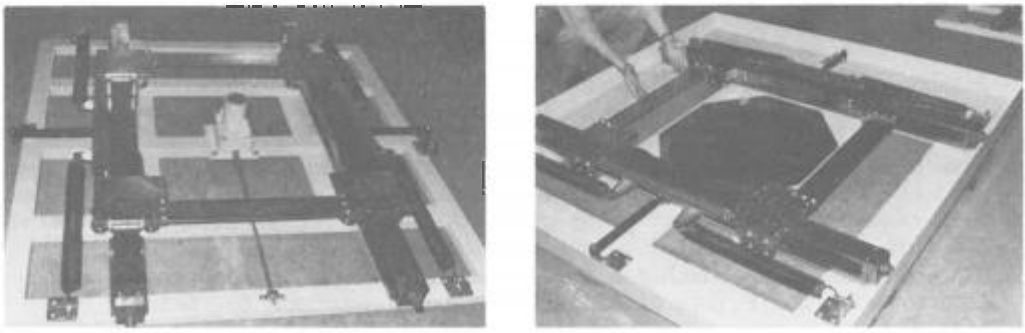

(a) (b)

Figure 2. Inside view of isolation mechanism

3 RESPONSE ANALYSIS

To investigate the effect of base isolation technique, a typical control board for nuclear power plant use was selected. Some specification of this board is that the external dimension is $1350^{W} \times 1000^{D} \times 2300^{H}$ (in mm) and total weight is approximately 1200 kg with dummy weights to represent the electric instrumentations. These two structures of base isolation device and control board were connected rigidly, so the analytical model was considered as shown below(Figure 3).

The equation of motion derived from this analytical model is as follows ;

(i) In the case of no friction damper slippage is involved - Phase I

(1) $x_1 = \text{const.}, \quad \dot{x}_1 = 0$

(2) $m_2\ddot{x}_2 + c_2(\dot{x}_2 - H\dot{\psi}) + k_2(x_2 - H\psi - x_1) = -m_2\ddot{z}$

(3) $I\ddot{\psi} + c_3\dot{\psi} + c_2H(H\dot{\psi} - \dot{x}_2) + k_3\psi + k_2H(H\psi + x_1 - x_2) = 0$

(ii) In the case of friction damper slippage is occured - Phase II

(4) $m_1\ddot{x}_1 + c_1\{x_1^2/(x_1^2 + h^2)\}\dot{x}_1 + \{(m_1 + m_2)g\mu_1 + F\mu_2\}\mathrm{sgn}(\dot{x}_1)$
$+ c_2(\dot{x}_1 - \dot{x}_2 + H\dot{\psi}) + k_1x_1 + k_2(x_1 - x_2 + H\psi) = -m_1\ddot{z}$

(5) $m_2\ddot{x}_2 + c_2(\dot{x}_2 - H\dot{\psi} - \dot{x}_1) + k_2(x_2 - H\psi - x_1) = -m_2\ddot{z}$

(6) $I\ddot{\psi} + c_3\dot{\psi} + c_2H(H\dot{\psi} + \dot{x}_1 - \dot{x}_2) + k_3\psi + k_2H(H\psi + x_1 - x_2) = 0$

(iii) Switching condition from Phase I to Phase II is anticipated when,

(7) $|m_2\ddot{z} - c_2(\dot{x}_2 - H\dot{\psi}) + k_1x_1 + k_2(x_2 - x_1 + H\psi)| > (m_1 + m_2)g\mu_1 + F\mu_2$ is satisfied.

On the other hand, when

(8) $x_1 = 0$ and

$|m_1(\ddot{x}_1 + \ddot{z}) - c_2(\dot{x}_2 - H\dot{\psi}) + k_1x_1 + k_2(x_1 - x_2 + H\psi)| \leq (m_1 + m_2)g\mu_1 + F\mu_2$,then Phase II to Phase I shift is anticipated.

Where x_1 and x_2 are relative displacements of movable table and gravity center of board respectively in reference to the installation floor, ψ is the rotational angle of the panel, I and m_2 are the moment of inertia around the gravity center and mass of board. H is the height of gravity center, k_2 and c_2 are the spring constant of the board for shearing and damping coefficient, k_3 and c_3 are the spring constant of the board for rotation and damping coefficient. And m_1 is the mass of isolation table, k_1 and c_1 are the spring constant and damping coefficient of isolation device, h is the length of viscous damper installed, and μ_1 and μ_2 are the friction coefficient of roller part and friction damper. F is depressing force of the friction damper, g is gravity constant, and $\ddot{z}$ is the horizontal acceleration of the floor on which the device is located. According to this configuration the resultant friction coefficient $\bar{\mu}$ is given as,

(9) $\bar{\mu} = \mu_1 + \mu_2F / \{(m_1 + m_2)g\}$

And also resonant period T of total system and the critical damping ratio ζ_1' are defined as,

(10) $T = 2\pi\sqrt{(m_1 + m_2) / k_1}$

(11) $\zeta_1' = c_1 / \{2\sqrt{(m_1 + m_2)k_1}\}$

A simulation software program was coded for this nonlinear equations. The Newmark's β method was used for direct integration in the condition of $\beta = 1/6$. Results from this simulation is compared with experimental data and that is discussed in the following chapter.

4 EXPERIMENTAL VERIFICATION AND FURTHER DISCUSSION

As the verification of this technique, experimental analysis was undertaken using large scale two dimensional (horizontal / vertical) shaker table (Takahashi et al 1981). The horizontal vibration was imposed to X direction of the specimen and the control board was installed on the shaker table in such a manner as the direction of the vibration being

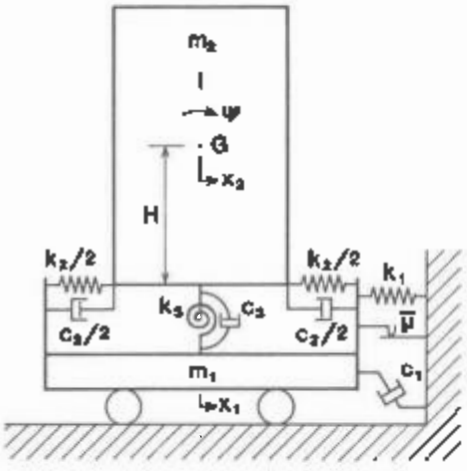

Figure 3. Analytical model of base isolation system

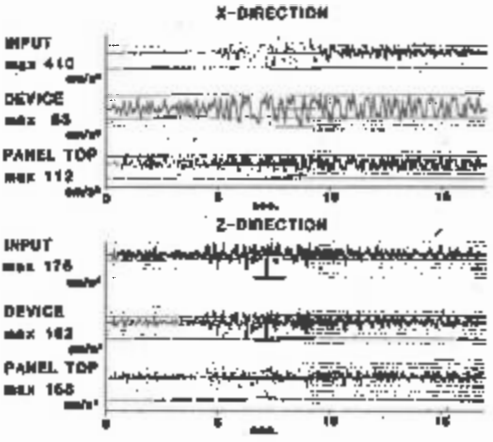

Figure 5. A typical result of experimental verification

Figure 4. Experimental setup of vibration test using two dimensional shaker table

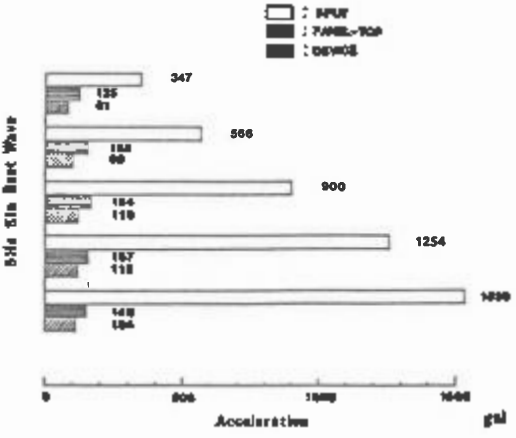

Figure 6. Experimental verification of base isolation effect for sine beet waveform input

conformity with the transversal direction of the board (Figure 4). One of the typical exsample of the experimental records is shown (Figure 5) in the condition of simultaneous vibrations of horizontal and vertical directions. An actual seismic waveform records of E41°S and UD at Ofunato site on Off-Miyagi Earthquake (1978,Japan) was used for exciting input. Referring from the results shown on Figure 5, it could be said that an adequate vibration isolation effect was realized in horizontal direction, while no amplification was noticed in vertical direction at all. The slite amplification of vibration from the device to the panel top of control board was recognized in Figure 5. However it was proven experimentally that this amplification stayed under a certain level even the input vibration level exceeded more than 1.5 G (Figure 6).

Comparison between computer simulation and experimantal results has been performed using same seismic waveform as shown in Figure 5. Sufficient agreement can be obtained (Figure 7) and this result allows us to conclude that the simulation model and argorithm could be usable for further estimation of the base isolation effect. And as far as this structural conbination is applied, the magnitude of horizontal vibration is suppressed under one-third of input level without any amplification of vertical vibration.

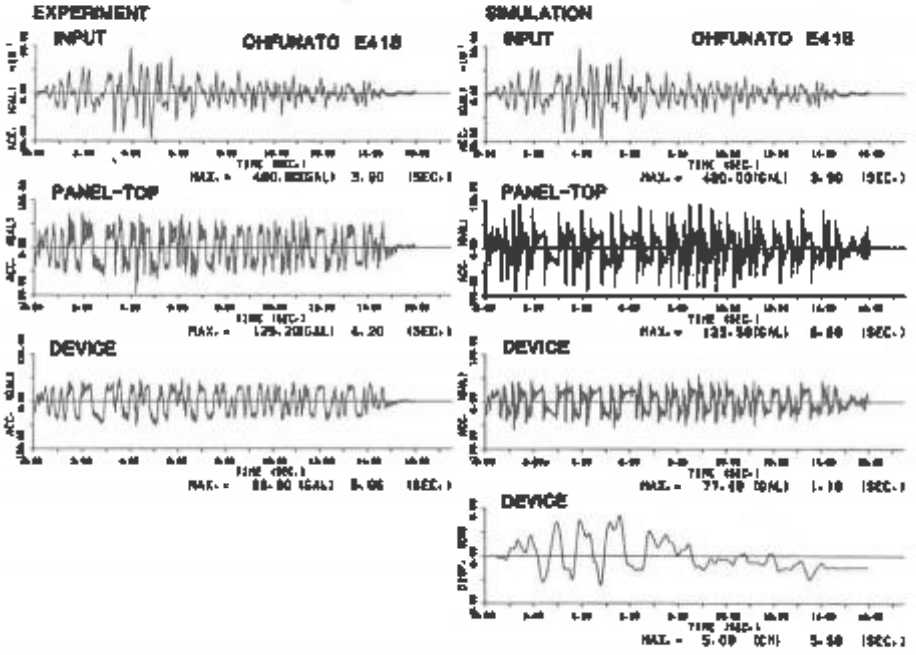

Figure 7. comparison between experimantal result and analytical simulation for actual earthquake waveform excitation

In order to obtain the design parameters which would be needed when a control board is installed with this isolation device in some nuclear power plant, response behaivior has been simulated under the condition of a certain floor response spectrum (Figure 8). Some results of the response analysis related to T (Figure 9) express the characteristics of this device, and as T = 3.5 s, $\overline{\gamma}$ = 0.02 and ζ' = 0.0. In here,the oil filled damper is omitted because of the reason that the stroke displacement of this damper is negligibly small and also it might be a limitation to use this kind of oil filled part for nuclear power plant. Accordingly the floor response waveform is estimated using these design parameters and an artificial earthquake waveform (Figure 10). As it can be recognized from the figure that more remarkable effect of base isolation is achieved and the response level of panel top decreases at least one-forth of input level.

5 CONCLUSIVE REMARKS

Consequently following conclusive remarks could be proposed.

(i) As far as this type of base isolation device would be used, the

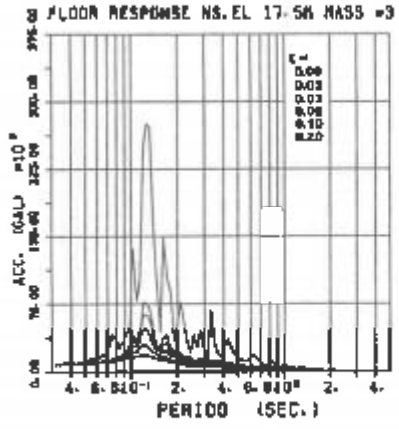

Figure 8. Floor response spectrum of a certain nuclear power plant

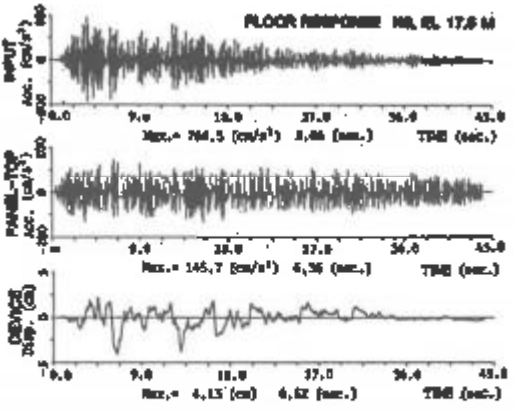

Figure 10. Simulated floor response

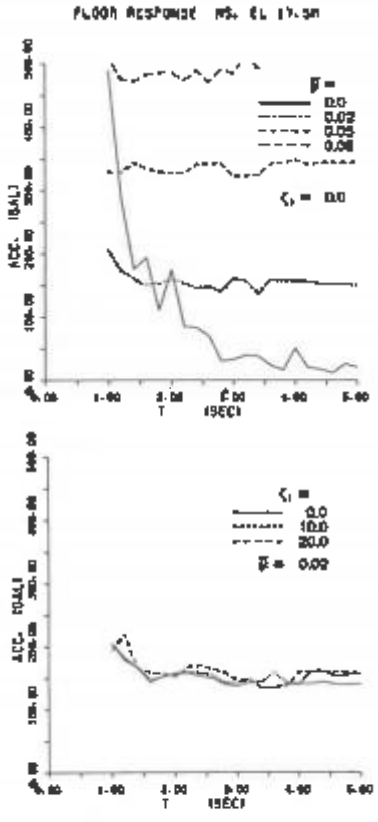

Figure 9. Design parameters estimation using floor response spectrum

mechanism of isolation has been appropriately formulated and simulated with the verification of experimental observations.

(ii) The effect of reduction by using this isolation technique would be estimated at least one-third in vibrational level for arbitraty earthquake waveforms in averaged level.

(iii) Seismic qualification of control board would have been controllable by using this new technique for any nuclear power plant use.

Finally authors would like to express their appreciation to Mr.Saruyama and Mr.Sawada of Mitsubishi Atomic Power Industries, Inc. who extended their cooperational association about nuclear power plant designing.

REFERENCES

Fujita,T. , K.Yogo, T.Omi & T.Koizumi 1984. An earthquake isolation device using linear motion mechanism. JSME 50.456 : 1339-1350

Takahashi,Y., N.Okutsu, T.Motoyoshi, M.Kono & T.Miyamoto 1981. Horizontal vertical two dimensional seismic qualification test. Mitsubishi-Denki-Giho 55.8 : 593-597

A new method of base isolation against earthquake damage using natural material

S.Tang, G.König & O.Kroggel
Institut für Massivbau, Technical University, Darmstadt, FR Germany

1. INTRODUCTION

Structures, especially structures of reactors and the equipment in those structures, in earthquake-endangered areas should be protected from failure caused by subsoil vibration. Structure subsoil-isolation can be used ingeniously to achieve this aim, especially for low and middle-rise buildings. In this paper, a new isolation method using soil-liquefaction is studied.

Generally speaking soil-liquefaction is almost always a catastrophe during earthquakes, because the liquefied soil is squeezed out of its original place under the foundation of the building and the foundation looses its stability and bearing capacity. This gives rise to very large settlement and tilting of the building. However, if the volume of the soil is kept constant, the foundation failure will be avoided. Due to the reduction of the stiffness of the soil after liquefaction, the transmission of the subsoil vibration into the superstructures will be greatly decreased. There are examples of cases, in which buildings survived earthquake attacks under natural ground conditions. One of them was in Japan /1/.

2. A NEW ISOLATION METHOD AND ITS CHARACTERS

Based on the above-mentioned idea, a new isolation method is being developed. The construction of the structure subsoil-isolation system using this method is shown in Fig. 1: the superstructure is built on several isolators, which separate it from the subsoil. The isolators are composed of a layer of artificially selected and mixed soil, the relative density (symbol Dr) of which is low. Around the soil is an impermeable and elastic wall keeping its volume constant. Through a network of pipes, the soil in the isolators is constantly water-saturated.

How this system functions and how it satisfies the specifications of structure-base isolation, can be explained on the basis of what we know about soil-liquefaction and base-isolation:

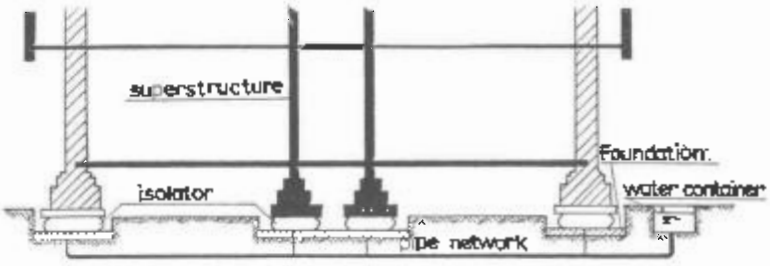

Fig. 1 Construction of the isolation system

a) The vibration energy input into the structure should be limited to an amount which does not lead to any structural damage. As we know from the results of soil experiments /2/, a loose, non-cohesive and saturated soil will liquefy after a number of shear loading cycles. The number of loading cycles to liquefaction depends on the soil density and the loading intensity (Fig. 2). To put it more exactly: the higher the loading intensity and the lower the soil density, the less is the number of loading cycles to liquefaction. That means that the vibration energy input in the soil till liquefaction will be confined. Accordingly, the energy transmitted into the superstructure before the soil liquefies will be limited too. The soil mixture and its relative density in the isolator will be selected so that the soil liquefies in a strong earthquake before the transmitted vibration energy can cause any structural damage.

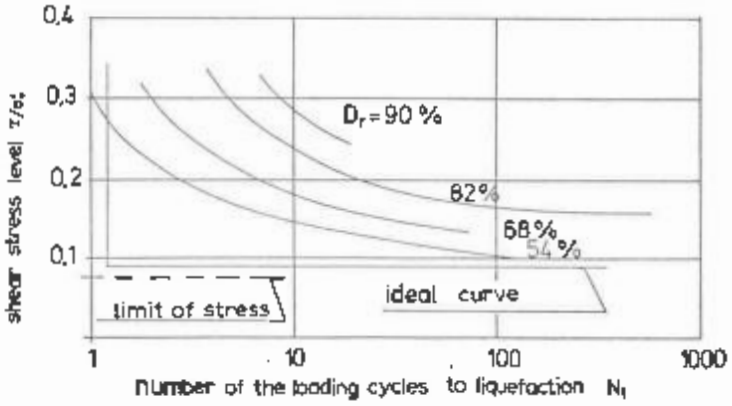

Fig. 2 Shear stress vs loading cycles to liquefaction

After the liquefied soil layer in isolators has lost its stiffness, the eigenfrequency of the isolated building will be shifted to a very low range, and thereby out of the most damaging frequency range of most earthquakes. Consequently, there will be no strong response of the building under further earthquake load, after the soil in the isolators has liquefied in the first cycles.

b) In any case, an isolation system should support the superstructure stably. This is ensured by the new isolation system. By virtue of an

impermeable and elastic wall, the volume and the height of the isolator will not change. Therefore the settlement and tilting of the building above the isolators will not happen. Besides, instead of the soil grain the pore water will support the structure.

c) A structure subsoil-isolation system should be rigid enough to supply the superstructure stable resistance to attacks of everyday's ambient cyclic loading which is not dangerous to buildings. It is known that there is a limit of shear stress in the soil, under which liquefaction does not take place inspite of an almost unlimited number of loading cycles (Fig. 2). Construction parameters of the isolation system can be regulated so that the limit of shear stress is larger than the amplitude of the above-mentioned loading in soil layer. If the soil liqufies after only one or two loading cycles under a dangerous shear-load from an earthquake, this behavior of soil will be ideal for the isolation purpose (Fig 2, ideal curve).

d) Isolators should have a large damping coefficient to provide the isolated structure with an energy-absorbing capacity. The soil after liquefaction is a good damping material owing to the friction between soil grains under large shear strain.

The new method is in the developing phase. At present the suitable composition of the soil and its characteristics are in the process of being tested and studied. "Suitable" means that the curve of the relationship between the shear stress level and the number of loading cycles to liquefaction should lie as near as possible to the ideal curve (Fig. 2).

3. ANALYSIS OF THE EFFECT OF THE SYSTEM

The effect and dynamic reaction of the building isolated with the new method has been analyzed. In this analysis the response of the structure in time was calculated both with and without isolator. For the description of soil-liquefaction process a model from Martin, Finn and Seed has been used /4/,/5/. A two-mass oscillator was used modelling the isolated structure. The superstructure was considered as linear-elastic with an eigenfrequency of 2Hz, and the isolator as a non-linear element. It was assumed that the isolator was filled with saturated natural fine sand having a relative density which can be achieved in reality.(This kind of sand is not the optimal material for the purpose.) With regard to the soil vibration signals, some recorded soil acceleration time histories of earthquakes in USA. and Europe and one earthquake wave artificialiy made for Europe have been used.

A part of the results of the analysis are shown in Table 1 and Fig. 3& 4. The response of the structural model with isolation is compared with that without isolation.

The results of the analysis show:

a) The isolator greatly reduces the energy input into the structural model. (Table 1 E_{dv} and E_{rs})
b) The maximum of response of the structure model is reduced considerably too.(Table 1 $\ddot{y}_{max}$)
c) The strong motion duration of the superstructure is shortened distinctly (Table 1 TTB).

Table 1: Response of the structural model

Stimulations	Systems	Response of the structural model					
		$\ddot{y}_{max}$	E_y	E_{dv}	E_{dg}	TTB	T_{VL}
Tolmezzo76 NS $\ddot{y}_{max}$=3.27 E_y=4.3,TTB=4.34	with Iso.	2.80	5.23	157	172	2.78	5.42
	without Iso.	11.8	282		9760	4.9	
TAFT52 N21E $\ddot{y}_{max}$=1.74 E_y=3.39,TTB=30.3	with Iso.	2.42	5.30	141	143	3.86	9.46
	without Iso.	5.05	75.4		2570	24.1	
ELCENTRO40 NS $\ddot{y}_{max}$=3.42 E_y=10.2,TTB=24.4	with Iso.	5.55	11.1	283	316	8.02	2.58
	without Iso.	10.1	196		6600	26.5	
artificial earthquake $\ddot{y}_{max}$=2.88 E_y=3.66,TTB=4.48	with Iso.	2.89	5.80	138	140	3.02	3.18
	without Iso.	4.57	29.6		1090	9.00	

Definition of the symbols:
$\ddot{y}_{max}$ -maximum acceleration (m/s²)
E_y -energy of acceleration in strong motion duration (m²/s³) /5/
E_{dv} -energy input into the structure before liquefaction (Nm)
E_{dg} -energy input into the structure in the whole duration (Nm)
TTB -strong motion duration (90% of E_{dg}) (s)
T_L -time of liquefaction (s)

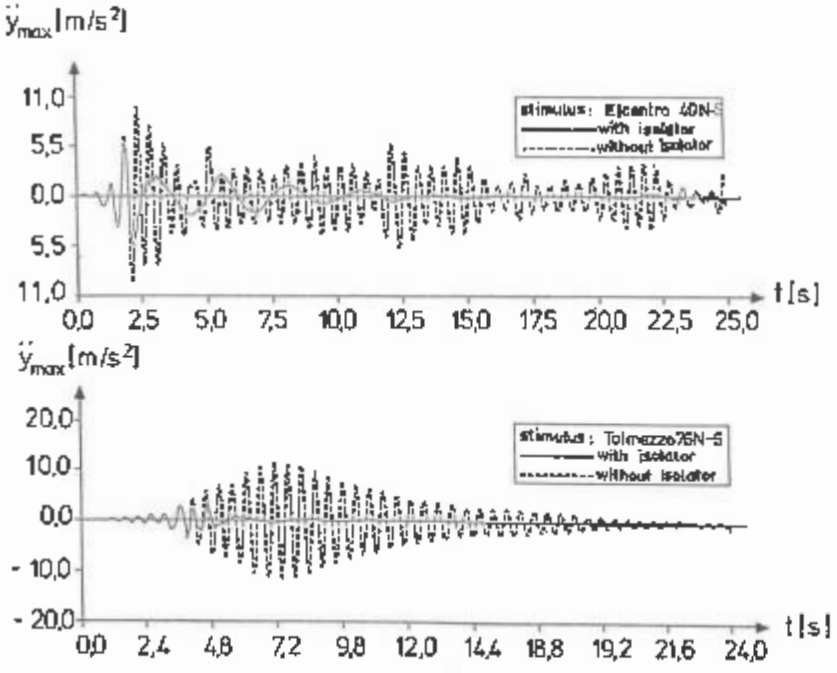

Fig. 3 & 4 Comparison of the responses between systems with and without isolator

After the experiments of the isolator-element have been finished, further analyses will be carried out so that the characteristics of the base-isolation system can be quantitatively described. In the analysis, a suitable model of soil composition according to the results of soil experiments will be used.

4.EXPERIMENTS

A test set-up for small-scale experiments has been made (Fig. 5). It consists of two parts: a structure model made of steel and an isolator model. In the isolator model, fine sand is filled in a rubber membrane. Through the valves and pipes leading into and the isolator model, the water volume within the membrane is controlled so that the sand is saturated and is kept in an undrained condition. During the test the structural model is vibrated horizontally by a small shaking table underneath, which produces a harmonic vibration.

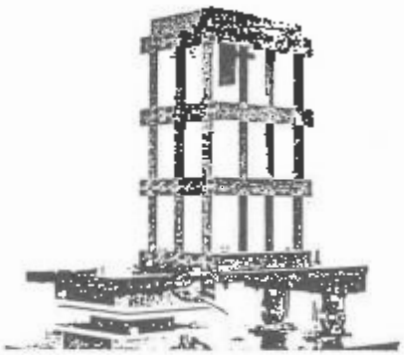

Fig. 5 Test set-up for the small-scale experiments

These experiments have already been done. The Fig. 6 shows two of the time histories of accelaration responses of the same structural model recorded during the experiments. Fig. 6a shows the time history with isolator, and Fig. 6b without isolator. There is a significant difference between the two diagrams.

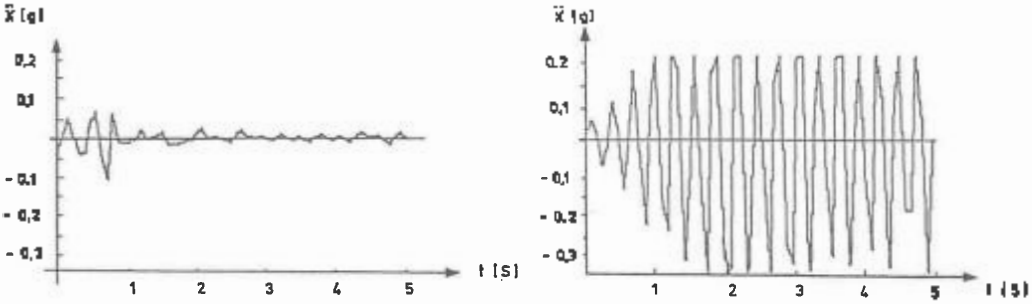

a) with isolator b) without isolator

Fig. 6 Top-acceleration of the structural model

The preparation for the middle-scale experiments on a shaking table in the laboratory is under way. The test equipment is made with the same principle of that of the small-scale one (Fig. 7). The experiments

will be carried out in two stages. In the first stage, the construction of the isolator will be tested. The parameters of the soil mixture obtained from soil experiments will be verified. The influence of the membrane on the isolator will be measured. In the second stage, the whole isolation system will be tested in order to obtain quantitive information about the characteristics of the system. The calculation model of the system based on the theoretical analysis will be modified through the results of the test.

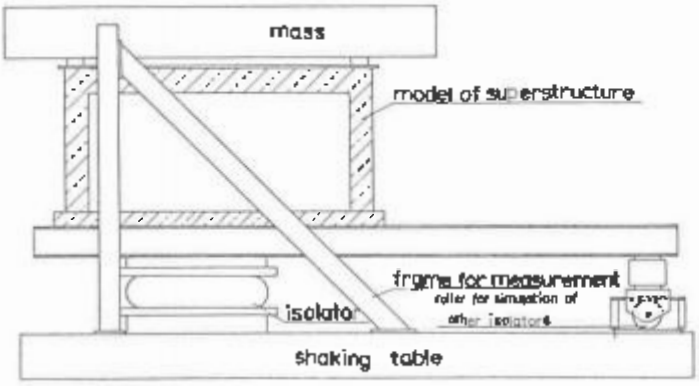

Fig. 7 Test set-up for the experiment on a shaking table

5. CONCLUSION

The new structure-subsoil isolation method is developed in view of practical usage. The analysis and tests previously done have proved the feasibility of this method. Furthermore, the material which is used comes directly from the nature, the construction of the isolation system is not complicated and maintenance is hardly needed. Therefore, it can be expected that this method will be an economical and practical approach towards structure isolation.

6. REFRENCES

/1/ Kelly, J. M. : Control of Seismic Response of Piping Systems and Other Structures by Base Isolation; Report No UCB/EERC-81/01, Earthquake Engineering Research Center, College of Engineering, University of California, Berkeley, California, January 1981

/2/ Shennon & Wilson, Inc.: Determination of Soil Liquefaction Characteristics by Large-Scale Laboratory Tests; U.S. Department of Commerce National Technical Information Service May 1975

/3/ Martin, G.R., Finn, W.D.L., Seed, H.B.: Fundamentals of Liquefaction Under Cylic Loading; Journal of the Geotechnical Engineering Division, May 1975

/4/ Finn, W.D.L., Byrne, P.M., Martin, G.R.: Seismic Response and Liquefaction of Sands; Journal of the Geotechnical Engineering Division, August 1976

/5/ Klein, H.-H.: Kenngrößen zur Beschreibung der Erdbebeneinwirkung Dissertation Darmstadt 1984

An experimental study of a base-isolation system using laminated rubber bearings and viscous dampers

M.Higashino, S.Aizawa & Y.Hayamizu
Takenaka Komuten Co. Ltd, Tokyo, Japan

ABSTRACT

The authors have performed tests on their earlier developed base-isolation system, which uses laminated rubber bearings and viscous dampers. In 1984, we constructed a full-scale model (supporting 505 ton of weight), and, using this system, carried out a free vibration test. Twelve seismometers were installed in this structure, enabling us to observe its earthquake response.

From the free vibration test, earthquake records, and a simulation analysis, we confirmed the effectiveness of the base-isolation system.

1 INTRODUCTION

Recently, the base-isolation system has been widely studied, and many kinds of systems have been developed. Presently, base-isolation systems using laminated rubber bearings are considered to be one of the most practical methods of reducing the acceleration response of buildings during earthquakes; and the system has been adopted for use in several countries. Especially in Japan, many kinds of systems have been developed in the past 2 or 3 years, but most of these systems use the histerisis of steel as an energy-absorbing device.

The authors started experimental study on the base-isolation system in 1982. Here the viscous damper, using the shear deformation of viscous fluid, is employed as an energy-absorbing device. The viscous damper does not have noticeable initial stiffness, as do steel dampers. This fact leads to the following characteristics: 1) the movement of the structure during an earthquake is smooth; 2) the viscous damper does not raise the natural frequency of the system; 3) the damping ratio can be set independently from the natural frequency of the system, (in other words, it is easy to design the system); and 4) base-isolation is effective for earthquakes whether large or small.

Having these characteristics, this system is suitable not only for buildings of regular use but also for high value-added buildings, such as precision environmental facilities, hospitals, etc., which can tolerate neither large nor small earthquakes.

The authors constructed a full-scale model, supporting 505 ton of weight with laminated rubber bearings and viscous dampers. We have carried out free vibration tests of this model and have been

also observing its behavior during earthquakes. The results of these studies are shown below.

2 VISCOUS DAMPER

The viscous damper has the mechanism shown in Fig.1. The damping force is provided by the shear deformation of the viscous fluid between the upper plate and the base plate. Fig. 2 shows the forced vibration test results of the damper itself (upper plate area A=908 cm^2). The figure shows the relationship between shear velocity (velocity divided by the thickness of the viscous fluid) and resistance force. From this test, the characteristics of this damper are expressed in the following formula:

$$F=0.42 \times e^{-0.043T} \times A \times (v/d)^{0.59} \qquad (1)$$

where F is the damping force (kg), T the temperature (°C), A the upper plate area (m^2), v the velocity of the upper plate to the base plate (cm/sec), and d the thickness of the fluid (cm).

3 THE MODEL AND FREE VIBRATION TEST

The model was built at the Takenaka Technical Laboratory site in Tokyo. The superstructure of the model was used for two other studies: "Variable Section Slip-Form Process Test," and "Coal-Storing Silo Test." It is 11.5 meters in height, 9 meters in diameter at the bottom, and its weight is 505 ton. This structure is supported by 9 laminated bearings. 6 viscous dampers are set beneath the superstructure.

The laminated rubber bearings are designed to make the natural frequency of the structure 0.5 Hz when they support 50 ton each. Each bearing is composed of 30 pieces of natural-rubber sheets (0.5 cm thick) and 29 pieces of steel plate (0.3 cm thick). The stiffness of one rubber bearing is 547 kg/cm in the horizontal direction and 6.07×10^5 kg/cm in the vertical direction (Fig. 4).

Fig. 5 shows the shape of the viscous damper. In this damper, the area of the upper plate is 755 cm^2, and the thickness of the viscous fluid is 0.6 cm. The damper is designed to show 10% damping ratio at 20 cm/sec velocity movement at 20°C temperature.

In the free vibration test, a notched steel rod (32ϕ) was attached to the superstructure. The free vibration was induced by pulling this rod with a center-holed jack until the rod was cut off. Fig. 6 shows the time histories of the free vibration. The broken line indicates the free vibration wave without viscous dampers, and the solid line indicates the free vibration with viscous dampers. From the test results, we can see that without the dampers the damping ratio is h_R=2.4%. We can see that the viscous damper is absorbing the vibration energy effectively. The observed damping ratio of free vibration with dampers is almost 12%.

Fig. 7 shows the relation between the natural period of the system and vibration amplitude. The natural period of the system is designed to be 2 seconds. But from the figure, we see that the period of the system becomes shorter in small-amplitude vibration when the viscous dampers are employed. The elasticity of the visco-elastic fluid was outstanding for small-amplitude vibration, but the variation of the

resonance frequency was small. As mentioned above, the damping ratio of the system is related to the velocity of the superstructure. The relation between these two is shown in Fig. 8. The results from the free vibration test (shown in dots) are distributed near the line calculated from formula (1). From this data, we can see that the system performed as designed.

4 BEHAVIOR DURING EARTHQUAKES

In the model, 12 seismometers (6 for horizontal and 6 for vertical) were installed to observe the acceleration response of the structure. In several earthquakes observed here, the one observed on October 4, 1985, was fairly large. Here we show the response of the model under this earthquake. Fig. 9 shows the acceleration record at the base of the model (below the system) and at the superstructure (above the system). From these records, it is known that the maximum acceleration levels were reduced by 0.63 and 0.37 for NS and EW directions, respectively. The difference between these two ratios was caused by the difference in input direction (Fig. 10). As the NS direction wave had spectrum peaks much closer to the structure's natural frequency than did the EW direction wave, the system did not reduce the NS direction acceleration as well as it reduced that of the EW direction.

In time histories and spectra, the response included higher frequency components; yet the natural frequency of the system is 0.5 Hz. This phenomenon is seen in the horizontal transfer function obtained from dividing the response spectrum by the input spectrum. In other words, the transfer function has many peaks that are higher than natural frequency. The rocking spectra at the base of the structure have peaks that are between 0 Hz and 10 Hz (Fig. 10). As the structure is tall in proportion, we can consider the higher frequency components to have been caused mainly by rocking vibration input.

A fairly large displacement occurred during this earthquake, and the displacement orbits are shown in Fig. 13. The recorded displacement orbit and the orbit obtained by integrating the acceleration record agree well.

5 THE SIMULATION ANALYSIS

The superstructure of the model is considered almost rigid. In the simulation analysis, the equation of motion is formulated in 1 mass 6 degrees of freedom system.

$$[M]\{\ddot{u}\}+\{F_D\}+[K]\{u\} = -[M]\{\ddot{g}\} \qquad (2)$$

where

$[M]$ is the Mass matrix
$\{u\} = \{X, Y, Z, \theta x, \theta y, \theta s\}^T$ <displacement vector>
$\{\ddot{g}\} = \{\ddot{X}g, \ddot{Y}g, \ddot{Z}g, \ddot{\theta}xg, \ddot{\theta}yg, \ddot{\theta}xg\}^T$ <input acceleration vector>

F_D is the sum of the damping force of the viscous dampers, given by formula (1), and the damping of the rubber bearings. In composing the stiffness matrix $[K]$, the visco-elasticity of the damper is taken into account when the displacement is small.

The input acceleration is composed by transforming

5 observed acceleration records (2 horizontal, and 3 vertical) at the base of the model to global coordinate. The illustration shown in Fig. 11 describes the analyzing procedure. The stiffness and damping matrices are updated at every step of analysis.

In Fig. 12, the analyzed response acceleration is shown in comparison with the recorded wave (the October 4, 1985 earthquake). The analyzed wave shows good agreement with the recorded wave. Also the calculated displacement orbit shown in Fig. 13 agrees well with the other two orbits (the recorded orbit and the orbit obtained by integrating the acceleration record). We can see that the clearness of the characteristics of the devices and the simplicity of the vibration model make this so.

The accumulated damping energy is calculated by the following formula:

$$E_D = \int \{\dot{u}\} \cdot \{F_D\} dt \tag{3}$$

where

$$\{F_D\} = \{F_x, F_y\}^T \quad \text{<damping force vector>} \tag{4-a}$$

$$\{\dot{u}\} = \{\dot{X}, \dot{Y}\} \quad \text{<velocity vector>} \tag{4-b}$$

Assuming the behavior of the structure as 1 mass 6 degrees of freedom, the damping forces are obtained as follows.

$$_RF_x = -M\ddot{Y} - M_I\ddot{\theta}_y - KY \tag{5-a}$$

$$_RF_y = -M\ddot{X} - M_I\ddot{\theta}_x - KX \tag{5-b}$$

where M is the mass of the superstructure; M_I the inertia effecting the horizontal vibration; $\ddot{X}$, $\ddot{Y}$, $\ddot{\theta}_x$, $\ddot{\theta}_y$ the recorded acceleration at the diaphragm of the superstructure; K the horizontal stiffness read from transfer function; X, Y the related displacement obtained by integrating the acceleration record.

In Fig. 14, the accumulated damping energy time histories are shown. The "non-linear analysis" shown in the figure indicates the analyzed result using formula (1). The analysis also agrees with the energy record.

The equivalent damping factor is given by the following formula:

$$C_E = \frac{\int F_D \cdot \dot{u} dt}{\int \dot{u}^2 dt} \tag{6}$$

where F_D is the damping force.

The calculated accumulated energy using C_E is also shown in Fig. 14. The time history closely agrees with the history obtained by using nonlinear C. In Fig. 15, the calculated velocity using C_E is shown in comparison with the velocity, which is obtained by integrating the acceleration record. As seen in the figure, the linear analysis is very accurate.

6 CONCLUSIONS

1) From the free vibration test, it is confirmed that the viscous damper has good damping ability. Also, the laminated rubber bearing has good deformation ability, and its movement is very smooth.

2) From earthquake observations, the system worked well. However, its effectiveness depended on the characteristics of the earthquakes. In designing the base-isolated structure, it is necessary to know the ground's vibration characteristics as well as possible.

3) The results of the simulation analysis agreed closely with observation records. Consequently, the response characteristics of the structure can be estimated very accurately at the designing stage.

4) The analysis using equivalent damping coefficient C_E gives good results. Consequently, linearizing the analyzing procedure is valuable to the design of structures.

Based on these studies, we are constructing a building (supporting 2,400 ton). It will be completed in March 1987.

7 ACKNOWLEDGEMENTS

The laminated rubber bearings used in this study are the products of the Bridgestone Corporation, and the viscous dampers are the products of Oiles, Inc. The authors would like to thank these two companies for the support they gave to our studies.

8 REFERENCES

Jolivet F., et al. 1977. A Seismic Foundation System for Nuclear Power Stations. Proceedings of the 4th SMIRT.

Kelly, J.M., et al. Experimental Study of Lead and Elastomeric Dampers for Base Isolation Systems. USC/EERC - 81/16.

Hayamizu, Y., et al. A Study of an Earthquake Base-Isolation System Using Laminated Rubber Bearings. AIJ Annual Meeting, 1984-86.

Fujita, T., et al. An Aseismic Base-Isolation System Using Laminated Rubber Bearings for Heavy Mechnical Equipment.(4th Report). SEISAN-KENKYU, University of Tokyo, Vol. 35, No. 4.

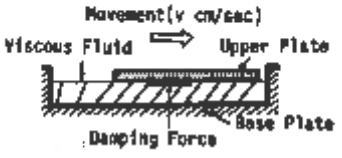

Fig.1 The Mechanism of Damping

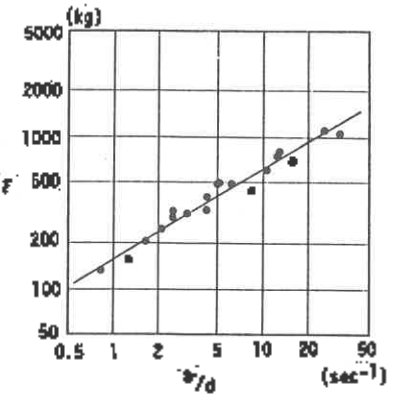

Fig.2 The Relation between Damping Force and Shear Velocity

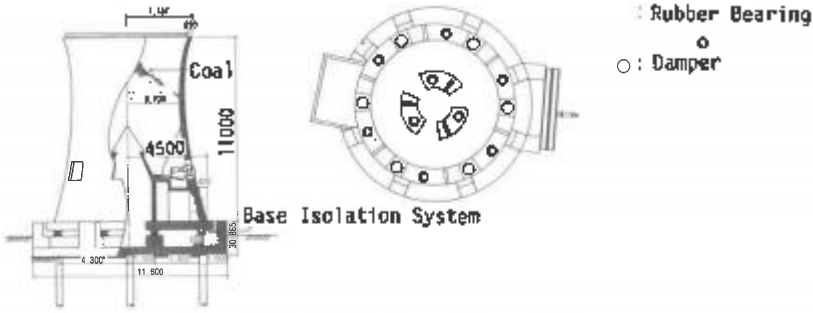

Fig.3 The Full Scale Model

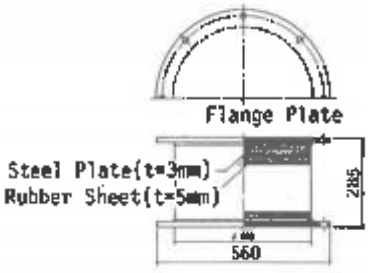

Fig.4 The Rubber Bearing

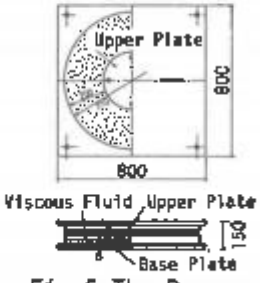

Fig.5 The Damper

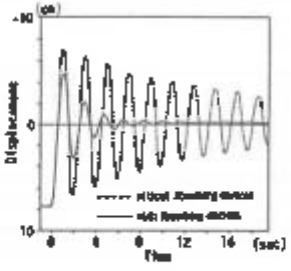

Fig.6 The Free Vibretion Time Histories

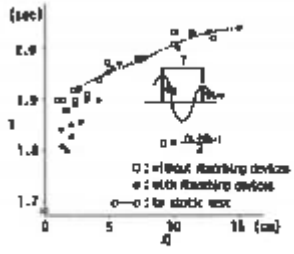

Fig.7 The Relation between Amplitude and Natural Period

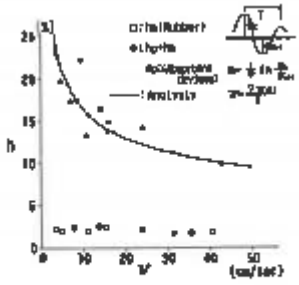

Fig.8 The Relation between Velocity and Damping Ratio

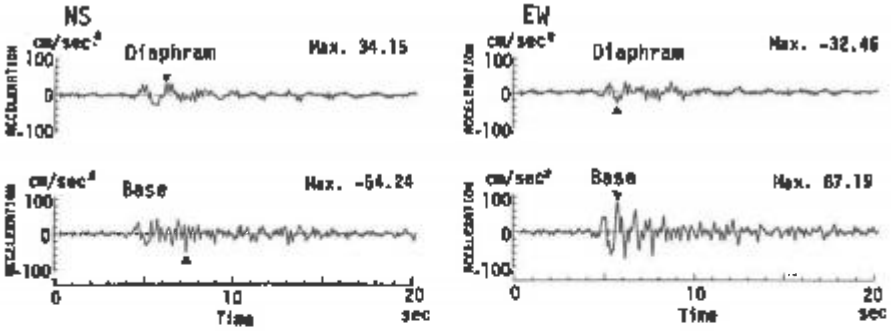

Fig.9 The Recorded Acceleration Time Histories of the Model
(Oct. 4 , 1985)

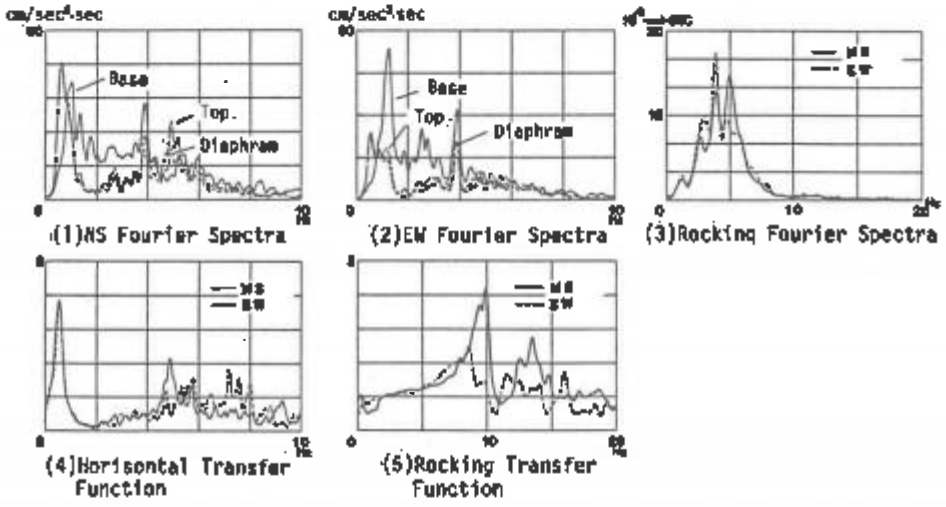

Fig.10 The Recorded Earthquake Acceleration Spectra (Oct.4.1985)

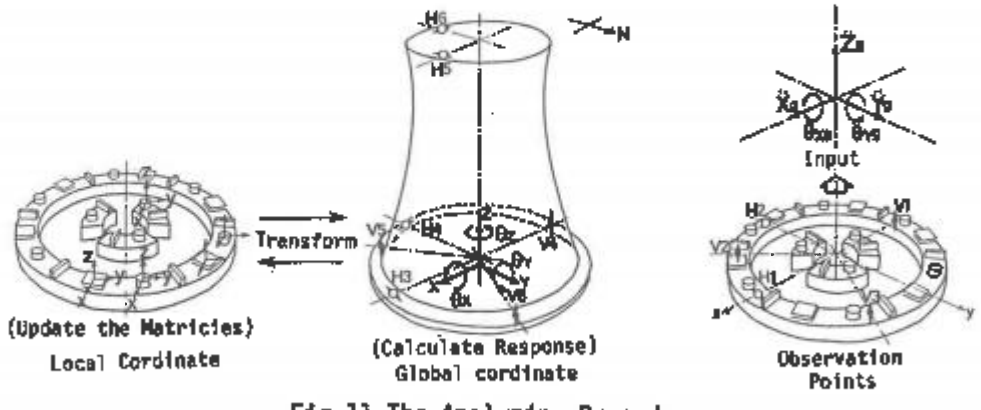

Fig.11 The Analyzing Procedure

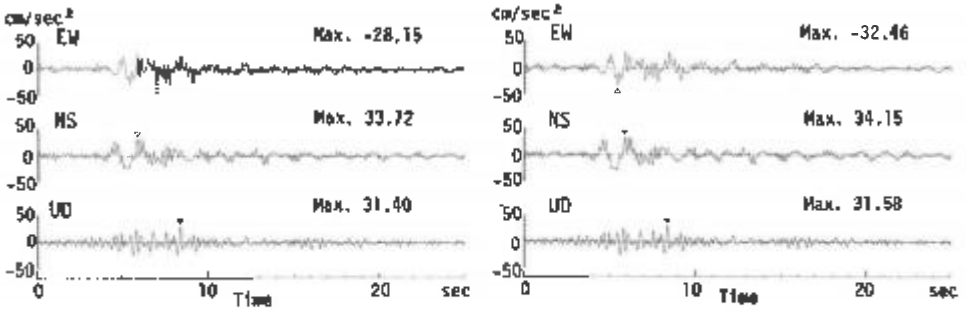

(1) Caluculated Response (2) Recorded Response

Fig.12 The Comparison of Acceleration Responses(Oct.4.1985)

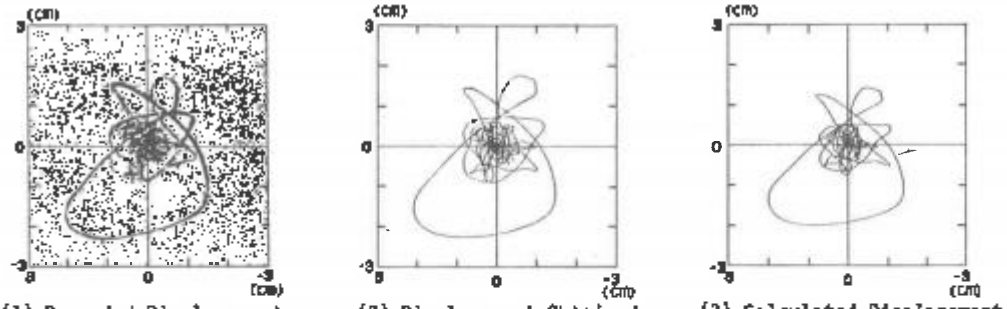

(1) Recorded Displacement (2) Displacement Obtained by Integrating Acceleration Record (3) Calculated Displacement

Fig.13 The Displacement Orbits

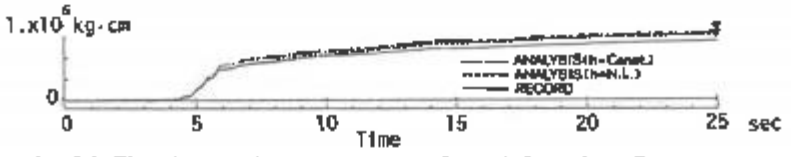

Fig.14 The Comparison of Accumulated Damping Energy

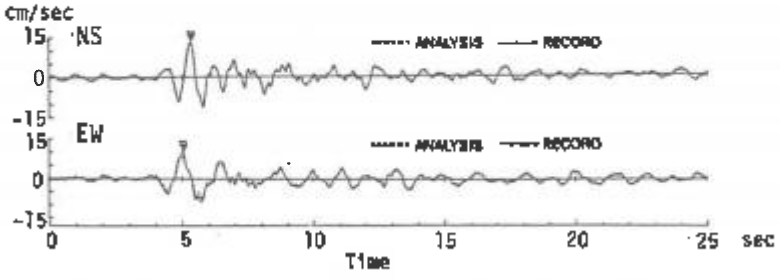

Fig.15 The Comparison of Response Velocity

Active optimal loop control to reduce the seismic response of a nonlinear isolation system

V.F.Poterasu & D.Condurache
Polytechnic Institute of Jassy, Romania

1 INTRODUCTION

Many systems are characterized by the fact that non-linear behaviour is restricted to certain points,particularly in the soil-interaction cases.The structure considered as a single degree of freedom is nonlinearly attached in a singular point,practically simulating the structure soil-interaction.In the first part of the paper we present the general problem for the situation when the dimensions of the state space and of the control are the same.Simple computations using Lie brackets of vector fields show that the optimal feedback law satisfies a system of quasi-linear first order partial differential equations.When the control does not appear in the criterion,this system degenerates into algebraic equations.For the polynomial nonlinearity and quadratic performance index we obtain by the original procedure the optimal law in the analytical form.The theoretical study is applied for to minimize the displacement of an idealized reactor building which is subject to horizontal earthquake-induced accelerations.The active control scheme developed uses a system of force actuators(most probable hydraulic)to counter the action of forcing input due to earthquake.The design problem concerns the optimal control input so that the system responds favourably.The paper is in a certain meaning an extension for the nonlinear optimal cases,soil-structure interaction,of the results of (Wolf,Madden 1981).As a practical examples we present the behaviour of a structure of shear beam linear type with a cubic nonlinearity confined to the connection between the foundation and the moving base.

2 OPTIMAL LOOP CONTROL LAW

We consider the system

$$(1) \qquad \dot{q}(t) = F(t,q(t),u(t)) \ , \ y(t) = h(q(t)).$$

where the state vector $q \in \mathbb{R}^n$,the control vector $u \in \mathbb{R}^m$, $n,m \in \mathbb{N}$.

The function $F:\mathbb{R}^{1+n+m}$ and the output function $h:\mathbb{R}^n \to \mathbb{R}^n$ are indefinitely derivables belonging C^∞. The optimal control problem considered has the Mayer's form without restrictions, with the initial state known, the final and free i.e. we optimize the output function $y(T) = h(q(T))$. We seek the optimal control under the feedback law form

$$(2) \qquad u = u(t,q), \quad u:\mathbb{R}^{1+n} \to \mathbb{R}^m$$

Pseudo-hamiltonian of the system (1)

$$(3) \qquad H = \langle p, F(t,q,u) \rangle = \sum_{k=1}^{n} p_k F^k(t,q,u)$$

where $p \in \mathbb{R}^n$ is the adjoint vector. The Hamilton's equations are given by

$$(4) \qquad \dot{q} = \frac{\partial H}{\partial p}, \qquad \dot{p} = -\frac{\partial H}{\partial q}$$

with the end conditions $q(0) = q_0, p(T) = -h_q(q(T))$.
According to Maximum principle, we have

$$(5) \qquad \frac{\partial H}{\partial u} = 0 \quad (0 \le t \le T), \quad H_{u_i} = \langle p, F_{u_i}(t,q,u) \rangle = 0 \quad i=\overline{1,m}$$

Since the optimal control has the form (2), in (4)

$$(6) \qquad \frac{\partial H}{\partial q^k} = \sum_{i=1}^{n} p_i \left[F^i_{q^k}(t,q,u) + \sum_{j=1}^{m} F^i_{u_j}(t,q,u) \frac{\partial u_j}{\partial q^k} \right]$$

Let $F = (F^1, F^2, \ldots, F^n)$ where $F^k:\mathbb{R}^{1+n+m} \to \mathbb{R}, k=\overline{1,n}$, and the fields vectors defined by the differential operators of the first order

$$(7) \qquad \begin{aligned} &A, F_{u_i}:\mathbb{R}^{n+1} \to \mathbb{R}^{n+1}, \quad A = \frac{\partial}{\partial t} + \sum_{k=1}^{n} F^k(t,q,u) \frac{\partial}{\partial q^k} \\ &F_{u_i} = \sum_{k=1}^{n} F^k_{u_i}(t,q,u) \frac{\partial}{\partial q^k}, \quad i=\overline{1,m} \end{aligned}$$

We consider the Lie brackets recurrsive iterative

$$(8) \qquad \mathrm{ad}_A^0 F_{u_i} = F_{u_i}, \quad \mathrm{ad}_A^1 F_{u_i} = [A, F_{u_i}], \quad \mathrm{ad}_A^{j+1} F_{u_i} = [A, \mathrm{ad}_A^j F_{u_i}] \quad j \ge 0$$

where $[A, F_{u_i}]$ are of the type

$$Z^k = \sum_{i=1}^{n} X^i \frac{\partial Y^k}{\partial q^i} - Y^i \frac{\partial X^k}{\partial q^i}$$

From the conditions, it results

$$(9) \qquad \frac{d^{\vartheta}}{dt^{\vartheta}} H_{u_i} = 0 \ , i=\overline{1,m} \ ; \ \vartheta = 0,1,2,\dots$$

Using (3),(8),(9) we obtain the necessary optimum conditions for the feedback law $u(t,q)$

$$(10) \qquad \langle p, \mathrm{ad}_A^{\vartheta} F_{u_i} \rangle = 0.$$

If we eliminate the adjoint vector p from (10) it obtains a system of quasi-linear partial differential equations. For a Bolza problem where the dimensions of the state space and of the control are the same it obtainsa system of equations of the first degree. Thus, the system with feedback loop law

$$(11) \quad \dot{q}(t)=F(t,q,u), \quad J=\phi(q(T))+\int_0^T F^0(t,q,u)\,dt$$

$$n=m$$

The system (11) is changed in a Mayer form with the new coordinate q^0:

$$\dot{q}^0(t)=F^0(t,q,u), \dot{q}(t)=F(t,q,u), y(t)=\phi(q)+q^0$$

$$q^0(0)=0$$

In this case the field vectors A is given by

$$\tilde{A} = \frac{\partial}{\partial t} + F^0(t,q,u)\frac{\partial}{\partial q^0} + \sum_{k=1}^{n} F^k(t,q,u)\frac{\partial}{\partial q^k} =$$

$$= \frac{\partial}{\partial t} + \tilde{F}, \qquad \tilde{F} = \sum_{l=0}^{n} F^l \frac{\partial}{\partial q^l}$$

For $\vartheta = 0,1$ the necessary conditions of optimum (10) are

$$\sum_{l=0}^{n} p_l F^l_{u_i}(t,q,u)=0, \quad \sum_{l=0}^{n} p_l \left[\tilde{A},\tilde{F}_{u_i}\right]^l = 0$$

where $[\cdot]^l$ is the l-th compenents of Lie brackets.

If the optimal problem has the Lagrange type

$$\dot{q}(t) = F(t,q,u), \quad J = \int_0^T F^0(t,q)\,dt$$

the feedback optimal loop law is given by the algebraic equations system:

$$(12) \qquad \sum_{k=1}^{n} F^0_{q^k} F^k_{u_i} = 0, \quad i=1,\dots,n$$

3 DYNAMIC MODEL OF SOIL-STRUCTURE INTERACTION PROBLEM

A major problem in the design of nuclear facilities is the satisfaction of the seismic response criteria.In this aim the active control concepts go further than passive control in significantly reducing the dynamic response.Reactor design dependence on the uncertainties of the amplitudes and of the frequency content of an actual earthquake is diminished.The forces can be applied by hydraulic or electromagnetic actuators.In this paper we consider an one-dimensional linear system attached at a point P to an external non-linear compliant constraint,as indicated in Figure 1.

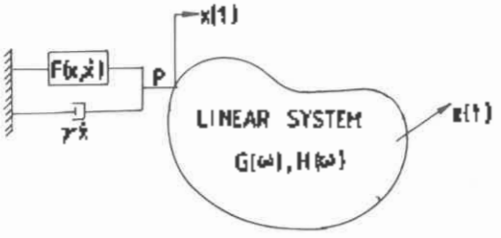

Figure 1. General linear system attached to a non-linear constraint

The constraint force is assumed to consist of separate contribution from a linear viscous element and a nonlinear elastic or hysteretic element modelling soil-structure interaction.The linear system is assumed to be undamped.The motion of point P,including the control input(earthquake action)and white noise disturbance is governed by the equation

$$(13) \qquad m\ddot{x} + F(x,\dot{x}) + \beta\dot{x} = u(x,t) + w(t), \quad x(0)=0, \dot{x}(0)=v_0$$

or equivalently

$$(14) \qquad \ddot{x} + f(x,\dot{x}) = u(x,t) + w(t)$$

The control u consists of a feedback and constitutes the basic active controller structure(Wolf,Madden 1981).

4 DIMINISHING OF THE SEISMIC RESPONSE OF NONLINEAR ISOLATION SYSTEM

A general performance index has the usual form:

$$(15) \qquad J = \int_0^T (a_1^2x^2 + a_2^2\dot{x}^2 + \rho u^2)\, dt$$

where ρ is a scalar weighting parameter.The performance index is an acceptable compromise between achieved system response and control energy expended.

The optimization problem (14) and (15) is equivalently with Mayer's problem

$$(16)\quad \dot{x}_o = a_1^2x_1^2 + a_2^2x_2^2 + \rho^2u^2\ ,\ \dot{x}_1 = x_2,$$
$$\dot{x}_2 = u(x,t) + w(t) - f(x_1,x_2),\ y(t) = x_o(t),$$
$$x_o(0) = 0,\ x_1(0) = x_o\ ,\ x_2(0) = v_o\ .$$

With notations

$$(17)\quad P^0 = a_1^2x_1^2 + a_2^2x_2^2 + \rho^2u^2,\ P^1 = x_2,$$
$$P^2 = u(x,t) + w(t) - f(x_1,x_2)\ .$$

The conditions (10) wrote for i=1,2 and ϑ=0,1,2 are

$$(18)\quad \sum_{k=0}^{2} p^k ad^{\vartheta} F_u^k = 0,\quad \vartheta=0,1,2$$

Eliminating the components of the adjoint vector p^k,k=0,2 between equations(18)we obtain the necessary optimum condition

$$(19)\quad \begin{vmatrix} ad^0F_u^0 & ad^0F_u^1 & ad^0F_u^2 \\ ad^1F_u^0 & ad^1F_u^1 & ad^1F_u^2 \\ ad^2F_u^0 & ad^2F_u^1 & ad^2F_u^2 \end{vmatrix} = 0$$

With (8),(9) and (17) from (19)we obtain the following partial differential equation of second order

$$(20)\quad a_{11}\frac{\partial^2 u}{\partial x_1^2} + 2a_{12}\frac{\partial^2 u}{\partial x_1 \partial t} + a_{22}\frac{\partial^2 u}{\partial t^2} + a_{10}\frac{\partial u}{\partial x_1} +$$
$$+ a_{10}\frac{\partial u}{\partial t} + a_{00} = 0$$

for the optimal control u.In (20)we have:

$$a_{11} = \rho^2x_2^2,\ a_{12} = \rho^2x_2^2,\ a_{22} = \rho^2\ ,\ a_{10} = \rho^2(u-w-f-x_2\frac{\partial f}{\partial x_2}),$$
$$a_{01} = -\rho^2\frac{\partial f}{\partial x_2}\ ,a_{00} = a_1^2x_1^2 - a_2^2(u+w-f) + \rho^2u\frac{\partial f}{\partial x_1} - \rho^2u(u+$$
$$+w-f)\frac{\partial^2 f}{\partial x_1^2} - \rho^2ux_2\frac{\partial^2 f}{\partial x_1 \partial x_2}$$

The initial conditions from differential equation (20) it results from u(T,x) calculated with p(T)=0.

If in the functional (15) ρ=0,(20) degenerates in the

following algebraic equation:

$$(21) \qquad u = \frac{a_1^2}{a_1^2} x_1^2 + f - w$$

For the linear system, a shear beam and for the non-linear soil-structure interaction, the function with a cubic elastic part

$$f(x,x) = kx_1(1+\varepsilon x_1^2) + \delta x_2$$

we obtain the differential equation, similarly with (20), for the optimal control of non-linear problem. The equation (20) can be solved numerically and the results for many practical situations will be prepared and published in the future.

5 CONCLUSIONS

In the paper is given a general method for to obtain the optimal control for the non-linear differential systems, particularly, for to determine the active optimal loop control for to reduce the seismic response of reactor component. In the example, the nonlinearity is confined to soil-structure interaction. The effectivity of the method proposed will be proof by numerical results.

REFERENCES

Wolf, J.P. 1981. An assessment of the application of active control to reduce the seismic response of nuclear power plants. Nuclear Eng. Design. 66:383-397.

Miller, R.K. 1978. The peak harmonic response of locally non linear systems. Earth. Eng. Struct. Dyn. 6:79-87.

Fliess, M. 1984. Lie brackets and optimal nonlinear feedback regulation. Proc. IX-th IFAC World Congress. Budapest.

Willemstein, A.P. 1977. Optimal regulation of nonlinear dynamical systems on a finite interval. SIAM J. Control Optimiz. 15:1050-1069.

Ozgoren, M.K. & R.W. Longman & C.A. Cooper 1975. Application of Lie transform based canonical perturbation methods to the optimal control of bilinear systems. Proc. AAS-AIAA Astrodynamics Specialist Conf. Nassau, Bahamas

Poterasu, V.F. 1985. Damping characteristic identification for a nonlinear seismic isolation system. Nuclear Eng. Design. 84:59-87.

Poterasu, V.F. 1985. Active protection of domains of coupled solid-fluid model by means of optimal control theory. Trans. 7-th SMiRT Bruxelles, Belgium, In Computer Methods for Structural Analysis. B2/11:93-98. North-Holland.

Poterasu, V.F. 1983. Active control for extinction in minimum time of fluid coupled coaxial cylinders vibrations. 6-th SMiRT Chicago. U.S.A. K(b):567-574. North-Holland.

Dynamic characteristics of base-isolated reactor building subjected to various types of travelling waves

I.Takahashi, Y.Koyanagi, N.Fukuwa & K.Yoshida
Ohsaki Research Institute, Shimizu Construction Co. Ltd, Tokyo, Japan

1 INTRODUCTION

Studies on the base isolation systems applied to nuclear reactor building have been reported recently (Kunar 1979). In the isolation systems, laminated elastomer bearing pads (LEBPs) are widely used to decrease the responses of structure by lengthening the natural period (Jolivet 1977). Therefore, the characteristics of input earthquake motions should be studied in the seismic design of isolated structures. Most of the devices having LEBPs are effectively operated only for the horizontal motion, but they are ineffective for the vertical or rocking motions. For the structure subjected to seismic waves with phase difference, such as obliquely incident waves or surface waves, the rocking and torsional movements of the structure are additionally produced. However, there have been few studies on the responses of the structure with the base isolation systems subjected to the motion with phase difference (Richili 1981, Wolf 1983).

This paper describes the earthquake response analysis of a typical BWR MARK-II type reactor building supported by the laminated elastomer pads, which is subjected to obliquely incident SH and SV waves. Dynamic characteristics of the base-isolated reactor building and base isolation device are investigated. In order to solve this problem, the frequency domain analyses are carried out for a linear system using the substructure technique where the soil system is analysed by boundary element method (Yoshida 1984) and the structure is modeled by a spring-mass system. Since the sliding characteristics are greatly influenced by variation of axial forces when the structure is subjected to SV wave, nonlinear analyses are further conducted for a reactor building supported by sliding laminated elastomer bearing pads (SLEBPs).

2 INVESTIGATION ON THE STRUCTURE SUPPORTED BY LAMINATED ELASTOMER BEARING PADS

2.1 Analytical model and conditions

A BWR MARK-II type reactor building on the half-space medium shown in Fig.1 is chosen as a typical model. This reactor building is assumed to have no eccentricity, and is supported by 1,600 LEBPs which are set up at equal distance between the two square bases. The isolation frequencies of LEBPs are assumed to be 1.0Hz and 0.5Hz for the horizontal motion, 20.0Hz for the vertical motion. The damping factors of both the reactor building and isolation device are 5%.

The input earthquake motion is generated artificially and its maximum acceleration amplitude is 286Gal. The incidence angles of SH and SV waves are selected as 0°,10°,20° and 30°. The analyses are carried out using the dynamic substructure technique in the frequency domain.

In Tables 1 and 2, the properties of soil and isolation devices are indicated. Figs.2 and 3 show the time history and response spectrum of the input earthquake motion, respectively.

2.2 Results of analysis

The foundation input motions are shown in Figs.4 and 5 in the form of transfer functions. They indicate that the torsional and rocking motion are excited by obliquely incident SH and SV waves, respectively.

The dynamic response of the reactor building subjected to SH and SV waves are shown in Figs.6 and 7, respectively. Those results are compared with those for a non-isolated reactor building. When the isolated structure is subjected to vertical incident SH or SV waves, the response curves have sharp peaks only at the isolation frequency, while the responses are suppressed in the other frequency range. However, when the isolated structure is subjected to obliquely incident SV waves, the response curves have second peaks caused by the rocking motion. As the incidence angle increases, the responses are getting large not only at the isolation frequency but also in the other frequency range.

Next the results of the earthquake response analyses are considered. The maximum response accelerations of the base-isolated and non-isolated reactor buildings subjected to SH waves are shown in Fig.8 in the case of f_H=1.0Hz. The isolated reactor building moves horizontally as like a rigid body, and the horizontal motion decrease considerably. LEBPs are also effective to decrease the torsional motion which contributes to the horizontal motion at most 10%. The maximum response to SV waves is shown in Fig.9. The horizontal responses at the top of the structure are increased and furthermore, the vertical motion of the structure is generated considerably by obliquely incident SV waves.

In Tables 3 and 4, the maximum values of the horizontal or vertical response accelerations at a height of 50.5m are indicated. The response caused by the horizontal, torsional and rocking motion of the base are also shown. When the base-isolated structure is subjected to obliquely incident SH waves, the responses are independent of the incidence angle. When subjected to SV waves, however, the responses are increased by the rocking motion as the incidence angle becomes large. Especially in the case of the incidence angle θ=30°, which is more than the critical angle (24°), the horizontal accelerations caused by the rocking motion are over 150 gal whether or not the isolation device is provided. It is indicated that this type of isolation system is not effective to reduce the rocking motion.

Figs.10 and 11 show the floor response spectra. While the responses of the structure subjected to SH waves vary little according to the incidence angle, those to SV waves with a fairly large incidence angle increase by the rocking motion in the high frequency range. These results coincide with the tendency of the transfer functions.

The responses of the isolation devices are discussed as follows. Tables 5 and 6 show the maximum values of the relative horizontal displacement, and the relative torsional angle between the upper and lower bases. Obliquely incident SH waves produce the relative torsional angle, consequently the horizontal displacement increases at the edge of the base. However, even when the structure is subjected to SH wave with the incidence angle of 30°, the relative horizontal displacement increases only about 5%. Thus, it is pointed out that the torsional motion produced by obliquely incident SH waves have little effect on the responses of the isolation devices.

In the case of SV waves, the rocking motion is produced. Therefore, the vertical motion are enlarged at the edge. When the structure is subjected to SV waves with the incidence angle of 30°, the maximum relative vertical displacement is about 0.03cm and then, the axial forces of the isolation devices amount to about 95ton at the edge of the base. From these results, it becomes clear that the axial forces of the isolation devices possibly vary from 0.5 to 1.5 times of those produced by the weight of the structure.

3 INVESTIGATION ON THE STRUCTURE SUPPORTED BY SLIDING LAMINATED ELESTOMER BEARING PADS

From the results mentioned above, the axial forces of LEBPs possibly vary with the position when subjected to obliquely incident SV waves. Therefore, if the isolation systems consist of LEBPs, the friction forces of the pads may be different each other. In this section non-linear characteristics of structural responses caused by the variation of axial forces are investigated. The analyses are carried out using the substructure technique in time domain under the same conditions as those for the previous study. In this study, the dynamic impedance functions are simplified to the additional mass, viscous damping coefficient and stiffness evaluated at the isolation frequency. The force-displacement relationship of the isolation devices is shown in Fig.12. The horizontal motion of the isolation device is coupled with the axial force, and the device slides horizontally when the horizontal strains reach to the friction forces. The friction coefficient of the isolation device is assumed to be 0.2.

Fig.13 and Table 7 show the maximum horizontal and vertical response accelerations of the structure. When the structure is subjected to SV wave with a small incidence angle, similar tendency of the dynamic characteristics is recognized whether or not the sliding plates exist. However, there is a little difference when the incident angle is large. The horizontal floor response spectra are shown in Fig.14. It is indicated that the peaks at f_H=1.0Hz are reduced considerably by sliding of the isolation devices. Table 8 shows the maximum relative displacement between the upper and lower bases. The relative vertical displacement shows a tendency to increase. On the contrary, the relative rocking angle tends to decrease in comparison with the results of the structure supported by LEBPs. However, as the incidence angle increases, the both relative horizontal displacement and rocking angle becomes large. Figs.15 and 16 show the maximum axial force distribution of the isolation devices. The axial force distribution depends largely on the position within the base.

4 CONCLUSIONS

The dynamic characteristics of the base-isolated reactor building is studied. The results of this study is summerized as follows,

(1) The isolation devices supported by laminated elastomer pads are effective for decreasing the horizontal and torsional motions. However, they are ineffective for the vertical or rocking motions,

(2) The vertical axial force of the isolation devices possibly vary from 0.5 to 1.5 times of the axial force produced by weight of the structure,

(3) The characteristics of the structure supported by sliding laminated elastomer bearing pads are similar to those of the laminated elastomer bearing pads.

REFERENCES

Jolivet, F. et al., 1977, "Aseismic Foundation System for Nuclear Power Stations," Proc. of the 4th SMiRT, K9/2, San Francisco, USA

Kumar, R.,R, et al., 1979, "A Review of Seismic Isolation for Nuclear Structures" Special Report of Elastic Power Research Institute

Yoshida, K., et al., 1984, "Dynamic Response of Rigid Foundations Subjected to Various Types of Seismic Wave" Proc. of the 8th WCEE, Vol.III, pp.745-752, San Francisco, USA

Richili, M., et al., 1981, "Effect of Travelling Waves on a Shock Isolated Nuclear Power Plant Put on Rock Foundation," Proc. of the 6th SMiRT, K12/7, Paris, France

Wolf, J., P, et al., 1983, "Response of a Nuclear Power Plant on Aseismic Bearing from Horizontally Propagating Waves" Proc. of the 7th SMiRT, K16/1, Chicago, USA

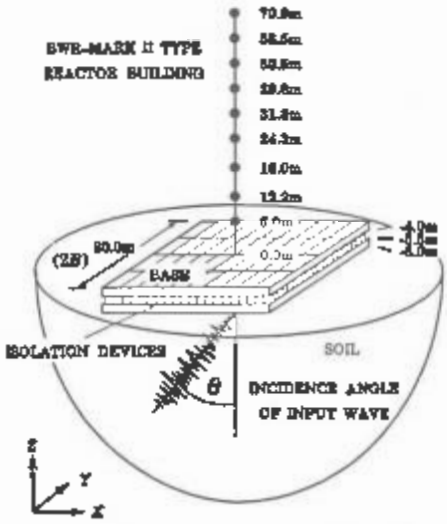

Figure 1. Description of model

Table 2. Properties of isolation devices

	Case-I	Case-II
Isolation Frequency for Horizontal Motion f_H=1/T_H	1.0	0.5
Isolation Frequency for Vertical Motion f_V=1/T_V	20.0	20.0
Total Horizontal Spring Constant K_H (t/m)	1.11×10^5	2.22×10^4
Total Vertical Spring Constant K_V (t/m)	4.52×10^6	4.52×10^6
Total Rocking Spring Constant $K_{R\theta-m}$	2.41×10^{11}	2.43×10^{10}
Total Torsional Spring Constant $K_{R\theta-m}$	1.26×10^8	3.01×10^7

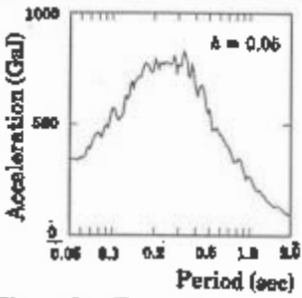

Figure 3. Response spectrum of input wave

Table 1. Properties of soil

	Constant
Shear Wave Velocity	1,000 m/sec
Poisson's Ratio	0.4
Damping Factor	0.02
Weight per Volume	2.0t/m³

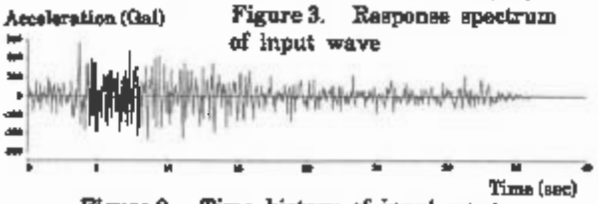

Figure 2. Time history of input wave

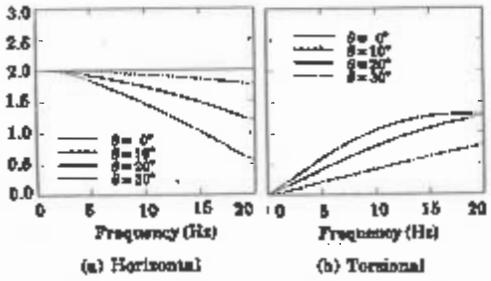

Figure 4. Foundation input motions due to SH waves

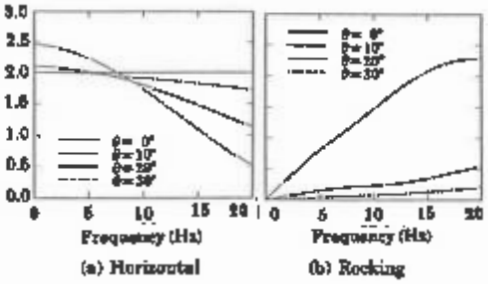

Figure 5. Foundation input motions due to SV waves

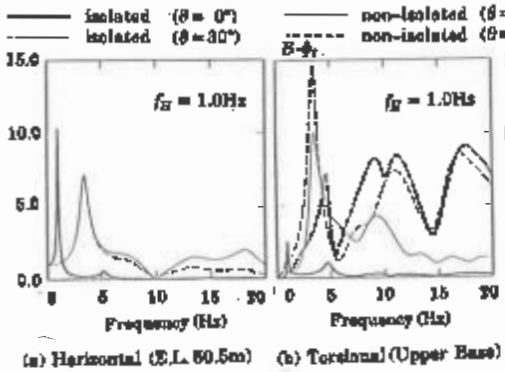

Figure 6. Transfer functions due to SH waves

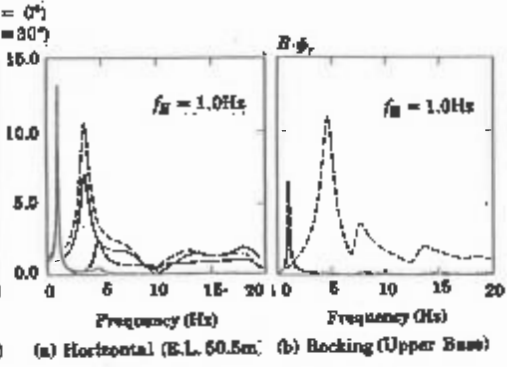

Figure 7. Transfer functions due to SV waves

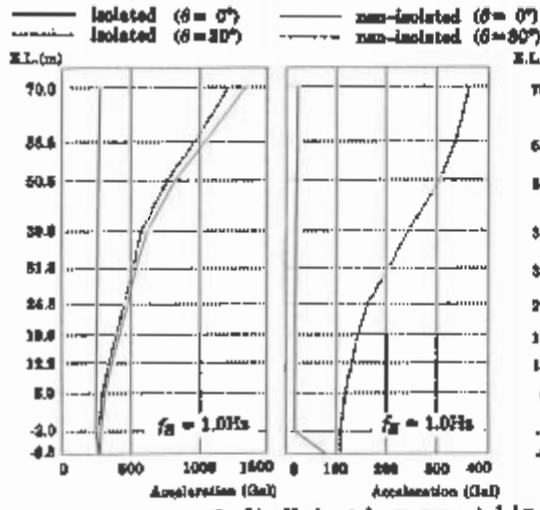

(a) Horizontal (b) Horizontal resp. generated by torsion(at the edge of the base)

Figure 8. Maximum response accelerations due to SH waves

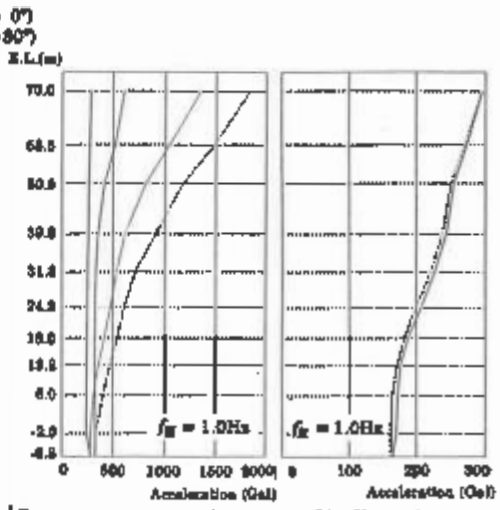

(a) Horizontal (b) Vertical

Figure 9. Maximum response accelerations due to SV waves

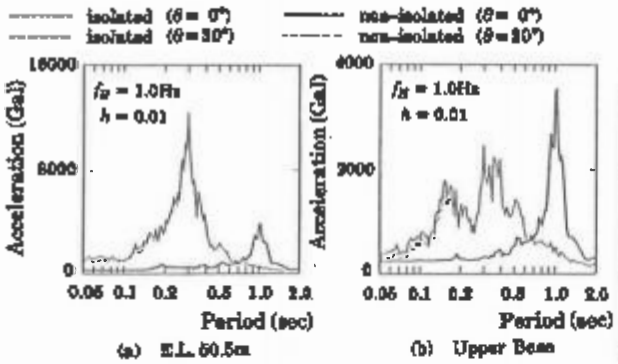

(a) E.L. 60.5m (b) Upper Base

Figure 10. Horizontal floor response spectra due to SH waves

Table 3. Maximum horizontal response due to SH waves

Case	Incident Angle (°)	Maximum Horizontal Response (gal) at the Center of Structure	by Horizontal Motion of Upper Base	by Torsional Motion of Upper Base
Isolated (f_H = 1.0Hz)	0	260.9	260.3	3.3
	15	250.7	249.5	5.8
	25	240.4	239.0	8.2
	30	236.0	233.4	8.0
Isolated (f_H = 0.5Hz)	0	89.5	86.9	6.8
	15	89.5	86.9	6.8
	25	89.3	86.8	6.8
	30	89.1	86.7	6.7
Non-Isolated	0	518.8	861.9	265.9
	30	758.5	861.7	146.7

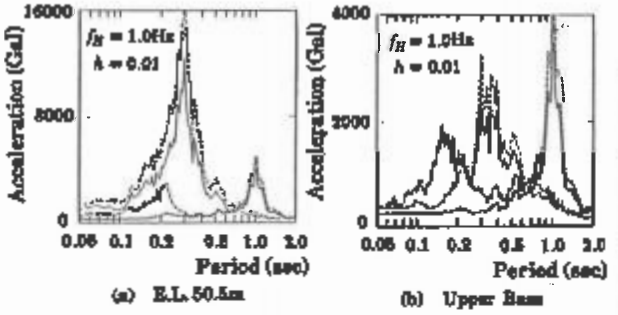

(a) E.L. 60.5m (b) Upper Base

Figure 11. Horizontal floor response spectra due to SV waves

Table 4. Maximum horizontal response due to SV waves

Case	Incident Angle (°)	Maximum Horizontal Response (gal) at the Center of Structure	by Horizontal Motion of Upper Base	by Rocking Motion of Upper Base
Isolated (f_H = 1.0Hz)	0	361.0	297.7	3.5
	15	345.0	296.7	22.0
	30	326.6	246.9	46.5
	35	411.0	251.0	160.5
Isolated (f_H = 0.5Hz)	0	88.0	86.9	0.4
	15	94.7	91.7	14.2
	30	115.0	96.2	37.5
	35	294.5	140.3	188.4
Non-Isolated	0	518.6	861.8	13.3
	30	1173.5	894.2	578.1

Table 5. Maximum Relative displacement of isolation devices due to SH waves

Isolation Frequency f_H (Hz)	Incident Angle θ(°)	Maximum Relative Displacement: Horizontal Displacement at the Center (cm)	Torsional Angle ($\times 10^{-4}$rad)	Horizontal Displacement at the Edge (cm)
1.0	0	6.27	0.0	6.27
	10	6.27	3.60	6.38
	20	6.26	7.09	6.44
	30	6.25	10.53	6.51
0.5	0	8.78	0.0	8.78
	10	8.78	3.25	8.82
	20	8.78	6.38	8.85
	30	8.77	9.31	8.88

Table 6. Relative displacement of isolation devices due to SV waves

Isolation Frequency f_V (Hz)	Incident Angle θ(°)	Maximum Relative Displacement: Vertical Displacement at the Center ($\times 10^{-2}$cm)	Rocking Angle ($\times 10^{-6}$rad)	Vertical Displacement at the Edge ($\times 10^{-2}$cm)
1.0	0	0.0	6.21	2.48
	10	0.26	6.23	2.52
	20	0.98	5.66	2.75
	30	1.22	8.45	4.01
0.5	0	0.0	2.13	0.85
	10	0.26	2.19	0.93
	20	0.38	2.44	1.09
	30	1.20	4.85	2.49

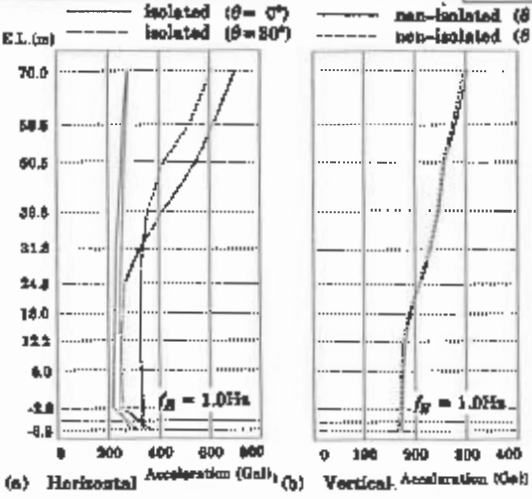

Figure 13. Maximum response accelerations

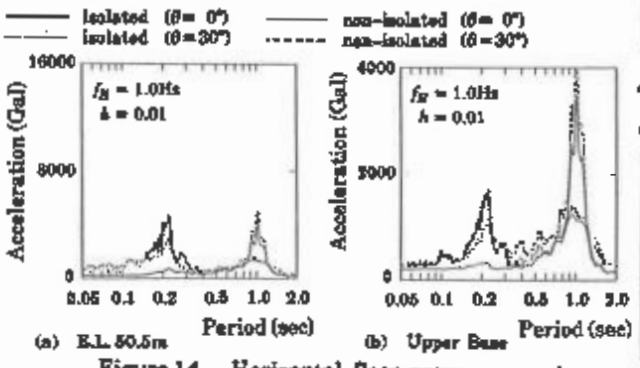

Figure 14. Horizontal floor response spectra

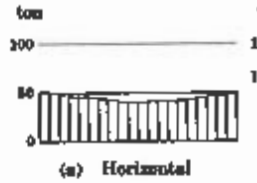

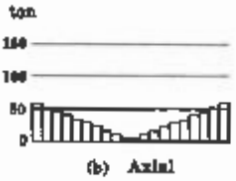

Figure 15. Forces of isolation devices (θ=0°)

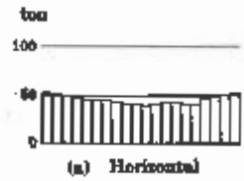

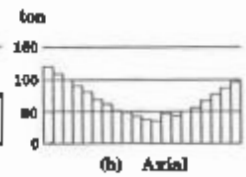

Figure 16. Forces of isolation devices (θ=30°)

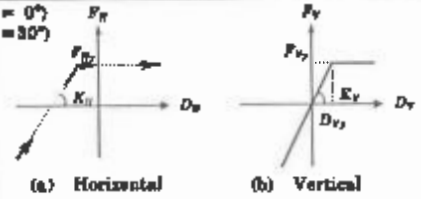

Figure 12. Force-displacement relationships of isolation devices

Table 7 Maximum horizontal accelerations (E.L. 50.5m)

Incident Angle θ(°)	Maximum Horizontal Response(gal): at the Center of Structure	by Horizontal Motion of Upper Base	by Rocking Motion of Upper Base
0	252.1	235.5	16.0
10	249.4	234.8	24.0
20	257.5	228.4	41.6
30	544.2	253.7	230.8

Table 8 Maximum Relative displacement of isolation devices

Incident Angle θ(°)	Maximum Relative Displacement: Vertical Disp. at the Center ($\times 10^{-2}$cm)	Rocking Angle ($\times 10^{-6}$rad)	Vertical Disp. at the Edge ($\times 10^{-2}$cm)
0	0.11	5.70	2.17
10	0.34	5.70	2.24
20	0.49	5.87	2.33
30	1.56	9.33	4.29

Conceptual design of seismic isolation for the PRISM liquid metal reactor

F.F.Tajirian
Bechtel National, Incorporated, San Francisco, Calif., USA
M.R.Schrag
General Electric Company, Sunnyvale, Calif., USA

1 INTRODUCTION

This paper reviews the seismic design considerations for the PRISM (Power Reactor Inherently Safe Module) pool-type liquid metal reactor (LMR). PRISM is a compact modular reactor of a size corresponding to about 135 MWe. It can be installed in standardized multiple blocks to provide a range of power plant sizes Tippets et al. (1986).

Each reactor building consists of an underground reactor silo embedded to a depth of 23.5m below grade. Figure 1 shows a section through one silo. The reactor module, passive auxiliary cooling systems, air flow passages, the reactor head access, and supporting structure are housed in the silo. The reactor vessel consists of a relatively long slender stainless steel vessel which is supported near the top of the operating floor. In general, LMR components are relatively thin walled because of near atmospheric pressure operation and to accommodate large thermal transients. While such components have desirable thermal features, they usually result in large seismic amplifications. To enhance seismic safety, it is desirable to minimize seismic input to the reactor and to reduce amplifications caused by the flexibility of the reactor components. Two options were considered: taking full credit for embedment in reducing seismic input, and seismically isolating the reactor. The analysis results, the design of the seismic isolators, and the advantages of the selected isolation scheme are discussed in this paper.

2 SEISMIC RESPONSE OF NON-ISOLATED REACTOR MODULE

Three-dimensional soil-structure interaction analyses were performed using the computer program SASSI (Lysmer et al. 1981) to compute the response of the non-isolated PRISM reactor system. The program is a general-purpose finite element program which uses the flexible volume substructuring approach (Tajirian 1981 and Tabatabaie 1982). It was selected to take full advantage of embedment in reducing response. In a previous study by Tajirian et al. (1984), the capabilities of the program in predicting the response of deeply embedded structures was demonstrated by computing the response of the Humboldt Bay Nuclear Power Plant during the Ferndale earthquake of June 7, 1976. The computed motions were shown to be in good agreement with those recorded inside the plant during the earthquake.

The reactor was housed in a concrete caisson embedded to a depth of 27m, somewhat similar to the PRISM silo.

The model used for the PRISM analysis consisted of 114 nodal points. The silo structure was modelled with 52 solid elements and the reactor with 20 beam elements and 13 lumped masses. Due to symmetry conditions, only one-fourth of the system was modelled.

A synthetic design earthquake time history scaled to a maximum acceleration of 0.3g was specified at grade. The response spectrum of this record envelopes the NRC Regulatory Guide 1.60 design spectra. The site was modelled as a damped uniform elastic halfspace with a shear wave velocity of 625 m/s.

Horizontal accelerations and response spectra at the reactor vessel (RV) support and at the core support plate were computed. The accelerations were 0.30g and 1.25g respectively. Although the maximum acceleration at the RV support was close to the input, there was a 4.2 times increase in acceleration at the core support plate due to vessel flexibility. The acceleration response spectra for 2% damping at the same points are shown in Figure 2 (no isolation). Near 5 Hz the spectral peak at the core support is 16.8 g, 12 times higher than the support acceleration.

Designing the PRISM reactor internals to accommodate these levels of acceleration, though feasible, would be a complex effort. A means of reducing the seismic response was sought. One option considered a series of seismic keys to reduce the response. Such an approach was not selected because it would complicate the design. The other option considered was to seismically isolate the reactor assembly from horizontal motions.

3 SEISMIC ISOLATION OF PRISM

3.1 Background

Many forms of seismic isolation have been proposed. Kelly (1986) gives a general review of applied methods and a comprehensive bibliography. The most promising system for nuclear applications and the one selected for PRISM is steel-laminated natural rubber bearings. This type of isolation has been used in the only seismically isolated building in the US, the Foothills Communities Law and Justice Center in Southern California Tarics et al. (1986). Substantial data exists on the behavior of these bearings. In addition, the bearings are simpler to design and do not rely on additional components to perform satisfactorily.

The rubber compounds used in these bearings have sufficient damping to assure a controlled response without the need for external damping devices which may cause high frequency amplifications in equipment response Tajirian et al. (1987). A minimum damping of 10% can be achieved for all applicable strains. Additionally, these rubber compounds have other beneficial properties: at low strains they have a high shear modulus, as high as 3.45 MPa, and at higher strains, the modulus drops to 1.45 MPa and remains fairly constant. The high rubber stiffness at low strains means that wind loads and small earthquakes can be resisted without appreciable movements, eliminating the need for mechanical fuses. The proposed bearings are self-centering, and tests have shown that the rubber properties do not change appreciably due to

cycling. Thus, they would be effective in the main shock and aftershocks, and there should be no need for replacing them after an earthquake.

The long experience with similar bearings in Europe, where they have been used to isolate buildings from ambient ground vibrations, indicates that no appreciable changes in the rubber properties are to be expected during the operating life of the plant. Such isolators would require minimum inspection and maintenance, and replacement during the life of the building is not foreseen, even though provisions are made for such replacement.

3.2 Design of PRISM seismic isolators

A 3-D schematic of the seismic isolation scheme is shown in Figure 3. The operating floor which supports the reactor module is supported on 20 isolators. The total weight isolated is 4450 tons. Details of a typical bearing can be seen in Figure 4. It consists of alternating layers of rubber and steel. The rubber is vulcanized to the steel plates. The bearing size and rubber compound were selected to give a horizontal isolation frequency of 0.75 Hz. Horizontal flexibility is controlled by varying the rubber properties, the total thickness of the rubber, and the diameter of the bearing.

In general, the total thickness of the rubber in the bearing depends on the maximum horizontal displacement expected to occur. For nuclear applications which require a high safety margin, the thickness can be selected such that the shear strain, which is the maximum horizontal displacement divided by the total thickness of rubber, is in the range of 50 to 60% when applying the maximum SSE displacement. Using this criteria the bearing shown in Figure 4 is designed to accommodate a maximum design horizontal displacement of 20 cm. It should be noted that tests on similar full scale bearings have shown that the bearings are able to accommodate shear strains in excess of 150% at full design load. Thus, even when the bearing is sheared to its design limit the available margin before failure is more than a factor of three. To minimize amplifications in vertical response, the bearing dimensions are selected to yield a high vertical to horizontal stiffness ratio in excess of 1000.

3.3 Results of seismic analysis

The dynamic response of the seismically isolated reactor module was computed. The same input motion and site properties described in Section 2 were used. In this analysis, embedment effects were neglected since the reductions in acceleration due to embedment would not affect the response of the isolated system.

Maximum accelerations and response spectra at the basemat (input to the isolators) and at the core support plate were computed. The horizontal accelerations were 0.31g and 0.25g respectively, a reduction of 1.24 times. A comparison of these response spectra is shown in Figure 2 (with isolation). The results show an even more dramatic decrease in accelerations. Spectral accelerations for frequencies above 1.2 Hz were substantially reduced. The maximum relative displacement between the isolated reactor module and the non-isolated silo was computed to be 11.5 cm.

A comparison of spectra at the core support plate for the isolated and the non-isolated plant shows that the peak spectral acceleration near 5 Hz was reduced from 16.5g to 0.25g. This is beneficial to all components with natural frequencies greater than 1.2 Hz.

Seismic analysis in the vertical direction has shown that vertical seismic response, without vertical seismic isolation is acceptable.

4 SUMMARY AND CONCLUSIONS

Seismic isolation results in substantial reductions in horizontal accelerations for all of the different reactor components. Incorporation of seismic isolation into the PRISM design results in reactor design simplification, reactor system safety and reliability improvements, and reactor design and licensing risk reduction.

Seismic isolation facilitates the standardization of the NSSS design, permitting a broad geographic deployment. Components developed for regions of low seismicity may be used in areas of high seismicity if the components are isolated. Furthermore isolation offers greater financial protection from the need to redesign the PRISM reactor due to the discovery of unexpected geological conditions or possible future upward revisions in design regulations.

REFERENCES

Kelly,J. M. 1986. Aseismic base isolation, review and bibliography. Soil Dynamics and Earthquake Engineering Vol. 5. No. 3.

Lysmer,J., M.Tabatabaie, F.F.Tajirian, S.Vahdani & F.Ostadan 1981. SASSI - A system for analysis of soil-structure interaction. Report No. UCB/GT/81-02. University of California, Berkeley.

Tabatabaie,M. 1982. The flexible volume method for dynamic soil-structure interaction analysis. PhD dissertation, University of California, Berkeley.

Tajirian,F.F. 1981. Impedance matrices and interpolation techniques for 3-D interaction analysis by the flexible volume method. PhD dissertation, University of California, Berkeley.

Tajirian,F.F.,M.Tabatabaie & J.Lysmer. 1984. Truly three-dimensional soil-structure interaction analysis of the Humboldt Bay power plant. Dynamic soil structure interaction, University of Minnesota.

Tajirian,F.F. & J.M.Kelly 1987. Seismic and shock isolation system for modular power plants. Submitted to ASME symposium on seismic shock, and vibration isolation. San Diego.

Tarics,A.G., et al. 1986. Quality assurance and control of fabrication for a high-damping-rubber base isolation system. ATC-17 Seminar on base isolation and passive energy dissipation, California.

Tippets,F.E., S.M.Davies, L.M.Salerno, & C.R.Snyder 1986. PRISM: a passively safe, economic and testable advanced power reactor. Proceedings of the American power conference. Chicago, Illinois.

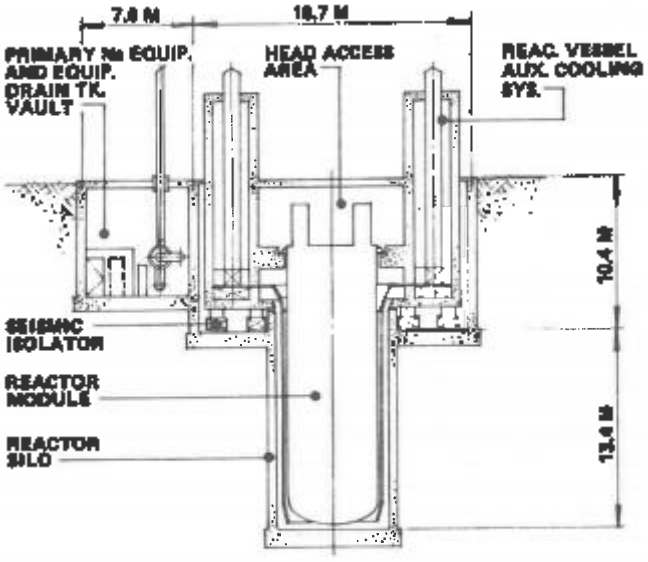

Figure 1. Section through PRISM silo

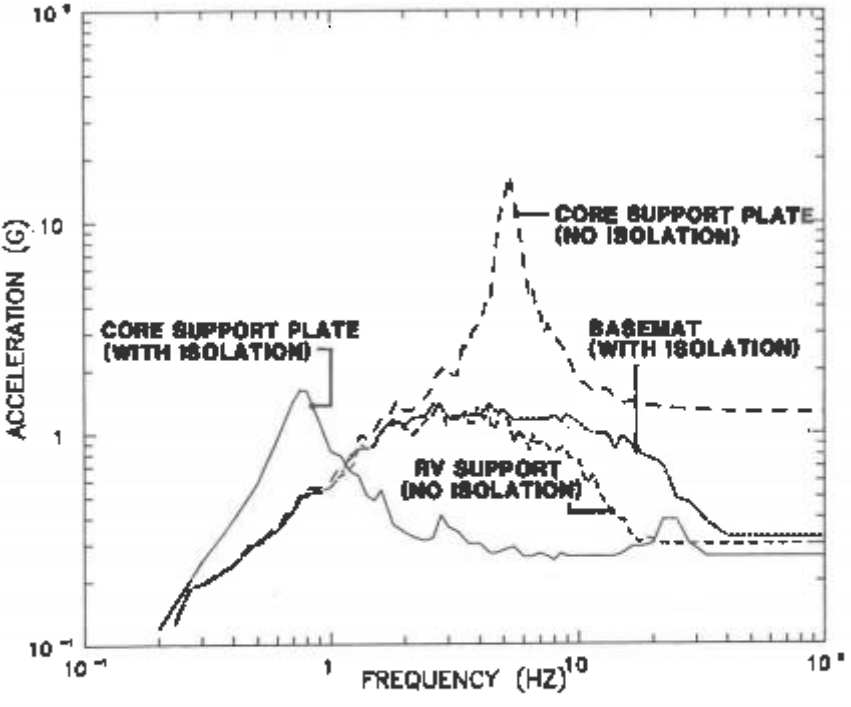

Figure 2. Comparison of response spectra damping = 2%

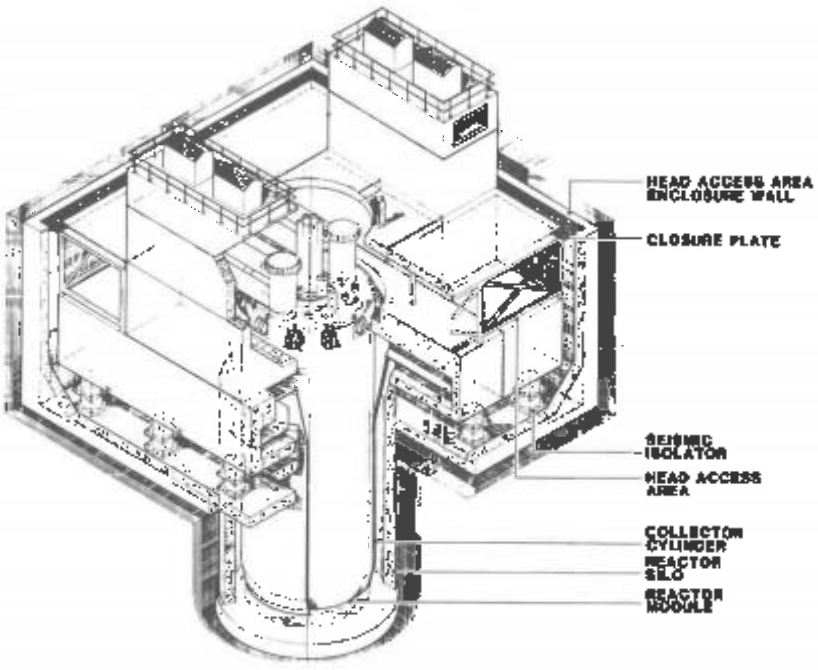

Figure 3. 3-D schematic of PRISM reactor module

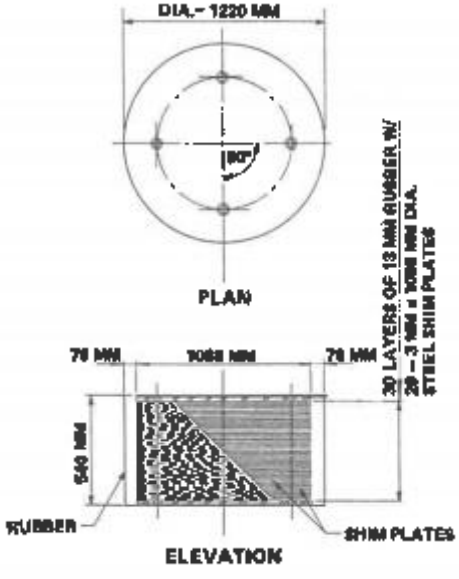

Figure 4. Typical seismic isolator

Qualification of seismic isolation for the PRISM liquid metal reactor

M.R.Schrag & J.N.Fox
General Electric Company, Sunnyvale, Calif., USA
F.F.Tajirian
Bechtel National, Incorporated, San Francisco, Calif., USA

ABSTRACT

Lateral seismic isolation has been included in the PRISM liquid metal reactor design in order to minimize seismic influence on the reactor design and to provide a design independant of site selection. The slender vertical orientation of the reactor provides high strength vertically while the lateral seismic isolation provides low response laterally. The seismic response analysis is presented for the isolated reactor concept. Additionally, testing is discussed for the isolators and isolation system.

1 BACKGROUND

The application of lateral seismic isolation to the PRISM liquid metal reactor (Berglund 1986, Tippets 1986) has been made in order to minimize seismic influence on the reactor design and to provide a design independant of site selection. The entire isolated PRISM nuclear structure weighs only 40 MN with an isolated basemat approximately 18 meters square (Figure 1).

Several isolation concepts were considered for use in this application. Concepts with a substantial base of technology, testing and application were given preference to facilitate acceptance by regulatory agencies.

The parameters considered in the design selection were simplicity, sufficient damping, self centering capability, and resistance to environmental factors and degradation.

The concept selected for this application is a layered natural rubber and steel bearing as developed by the Malaysian Rubber Producers' Research Association in England and the University of California at Berkeley. The design uses a special high damping rubber compound with damping capability in excess of ten percent of critical. This bearing is of the type used in the first base isolated building in the United States; the Foothill Communities Law and Justice Center, County of San Bernardino, California (Derham 1985, Tarics 1984).

A design that achieves a low lateral isolation frequency without unduly sacrificing vertical support stiffness (Figure 2) was developed. The lateral isolation frequency is 0.75 Hertz. To minimize vertical amplifications in response the vertical stiffness of the bearings is selected to be at least one thousand times stiffer than the lateral stiffness, and will be specifically determined by test. Details of the bearing design are discussed in Tajirian (1987).

2 SEISMIC RESPONSE ANALYSIS

A soil-structure interaction analysis was performed and documented in Tajirian (1987). In that analysis, the reactor is modeled in sufficient detail to evaluate levels of seismic response at component supports. Different damping values are included for the soil, seismic isolators and reactor structure. A synthetic time history is input, for which the response spectrum envelopes the NRC Regulatory Guide 1.60 spectrum, with a 0.3g zero period acceleration.

A response spectrum analysis is also performed, using the same structural model without including the soil. The isolators are included in the model. A single damping value of 3% is used. The analysis is intended to identify frequencies of vibration and mode shapes, as well as seismic response.

Fifty-seven degrees of freedom are modeled to evaluate any potential amplification through the isolated structure (Figure 3). The model is two dimensional and is used in both the horizontal and vertical analyses. The small size of the structure, and its direct support to ground through the isolators require that a coupled model be used in which all the major components are modeled. The input spectrum is obtained from the soil-structure interaction analysis at the foundation (Figure 4).

Results of the horizontal spectrum analysis (Table 1) show the structure to respond in a single significant mode of vibration at 0.75 Hertz. All modes of vibration couple with the dominant isolation frequency and all the secondary frequencies are insignificant. All motion is in phase. Acceleration response throughout the structure is nearly uniform. This behavior will allow the component seismic responses to be evaluated using simplified static analysis.

The displacement and acceleration response of the response spectrum analysis are excessively conservative. A response spectrum corresponding to 3% damping is used, while the isolators exhibit damping in excess of 10% of critical. The amount of conservatism is demonstrated in Table 1 where results from the soil-structure interaction analysis (Tajirian 1987) are also presented. These results show the response spectrum analysis results to be 2/3 greater. This is consistent with NRC Regulatory Guide 1.60 spectra, where at 0.75 Hertz the acceleration is also 2/3 greater for 3% versus 10% damping.

The vertical response of the system exhibits several significant modes of vibration between 14 and 32 Hertz. Individual modal responses are combined to derive the total response (Table 2). Amplifications in vertical response are small by comparison, which is why vertical seismic isolation is not included in this design.

3 VALIDATION TESTING

A series of static and dynamic tests are planned to confirm the material properties of the rubber compounds, design characteristics of the bearings, cyclic stability (degradation), and the safety margin of the bearings.

The test plan includes the following:

1. Material tests on the rubber compound to confirm properties such as damping, dynamic shear stiffness, and tensile strength.
2. Dynamic tests of the bearings under a combined static vertical load and a cyclical horizontal load to verify bearing stability under conditions far beyond the design basis SSE.
3. Vertical and horizontal stiffness tests of the bearings for various

strain levels.

4. Hysteric behavior determination of the bearings.
5. Fragility testing under vertical dead load.
6. Sustained compression set testing.
7. Property evaluation before and after cycling.

Full scale qualification using a prototype structure is being evaluated. Snap back tests conducted to verify response characteristics such as frequency and damping are under consideration(Popov 1986, Hunter 1986). The snap back test would be performed by applying a lateral force to the isolated basemat sufficient to induce a static deflection of several inches. The restraint is then released and the structure is allowed to respond. The resultant damped free vibration response is monitored; from which the dynamic stiffness and damping of the isolators, as well as the fundamental frequency of vibration is determined.

4 ACCEPTANCE TESTING

The physical properties (shear modulus and damping) of each batch of rubber used in manufacturing the bearings will have to be verified by testing. Each individual bearing must undergo acceptance testing prior to installation. Bearings shall be tested under the combined effects of vertical and horizontal design loads.

Prior to shipment, each bearing will be cycled through ten complete cycles at the maximum design displacement, currently 11.5 cm. Stiffness and hysteric properties will be measured to assure stiffness and damping properties are within design tolerance levels.

5 PERFORMANCE ASSURANCE/INSERVICE INSPECTION

The seismic isolation support system functions as vertical supports for the silo and reactor module at all times, but only in the case of a large seismic event is the seismic isolation function required. The seismic support system is classified as a nuclear safety class system for the PRISM design. It is essential to plant safety to insure that the system will function in the event of a large seismic event.

The seismic isolators are fabricated from layers of steel and rubber. Experience has shown this type of bearing and this type of natural rubber to be extremely age resistant. Additionally, a three inch protective rubber layer around the circumference is included in the design. This provides fire proofing for the bearing as well as protecting the steel plates from rusting.

The most appropriate inservice inspection (ISI) for this system is visual inspection. Sample rubber coupons and bearings will be located adjacent to the isolators and will be removed for functional testing and detailed examination if the visual examination indicates damage to the seismic supports. However, the seismic isolators are designed and expected to last the entire plant life without degradation or replacement. All bearings are replaceable on an individual basis.

REFERENCES

Berglund, R.C., et al. 1986. The PRISM reactor concept. Presented at ENC '86 Conf., Geneva, Switzerland.

Derham, C.J., J.M. Kelly and A.G. Thomas 1985. Nonlinear natural rubber bearings for seismic isolation. J. Nuclear Engineering and Design 84:417-428.
Hunter, K.W. and P.A. March 1986. Snapback excitation of structures using multiple force inputs. J. Sound and Vibration. Nov.:16-20.
Popov, E.P. 1986. Experiment as an aid to structural seismic design. J. Experimental Mechanics. June:194-208.
Tajirian, F.F. and M.R. Schrag 1987. Conceptual design of seismic isolation for the PRISM liquid metal reactor. Trans. 9th SMiRT Conf., Laussanne, Switzerland. K 12/10.
Tarics, A.G., D. Way and J.M. Kelly 1984. The implementation of base isolation for the Foothill Communities Law and Justice Center, county of San Bernardino, California. Reid and Tarics Associates, 20 Jones Street, San Francisco, California.
Tippets, F.E., et al. 1986. PRISM: a passively safe, economic and testable advanced power reactor. Proceedings of American Power Conf., Chicago, Illinois.

Table 1. Horizontal SSE seismic response.

Component	Response spectrum analysis Displacement* (cm)	Response spectrum analysis Acceleration (g's)	SSI analysis Acceleration (g's)
Isolated Basemat	**	0.44	0.25
Reactor Vessel	0.76	0.46	0.26
IHX	1.24	0.47	0.26
Sodium Pump	1.04	0.47	0.26
UIS	2.13	0.49	0.31
Core Support	0.80	0.47	0.26

* Relative to the isolated basemat (see Figure 2). All displacements in phase.
** Maximum isolator differential displacement = 11.5 cm (SSI analysis).

Table 2. Vertical SSE seismic response.

Component	Response spectrum analysis Displacement (cm)	Response spectrum analysis Acceleration (g's)
Isolated Basemat	small	0.19
Reactor Vessel	small	0.82
IHX	small	1.28
Sodium Pump	small	0.75
UIS	0.064	0.68
Core Support	0.112	0.90

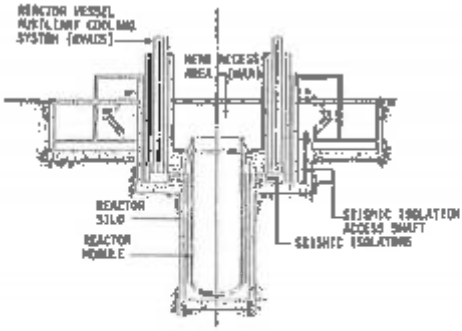

FIGURE 1 ISOLATED PRISM REACTOR MODULE

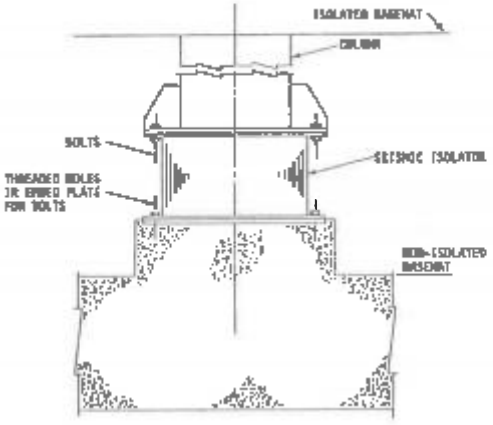

FIGURE 2 TYPICAL SEISMIC ISOLATOR MOUNTING

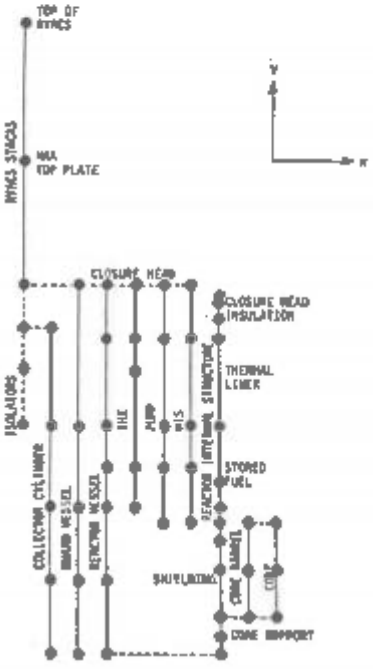

FIGURE 3 PRISM SEISMIC MODEL

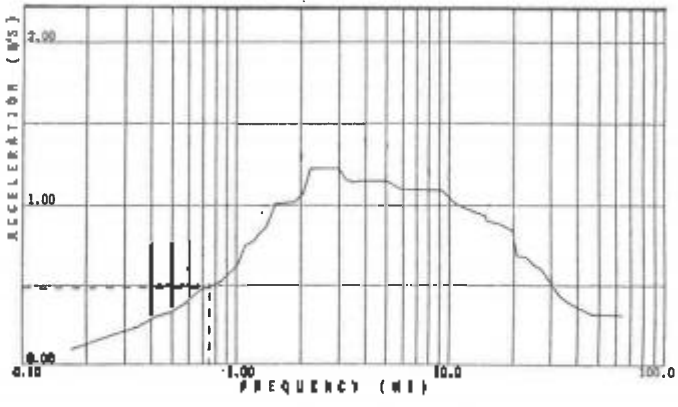

FIGURE 4 HORIZONTAL SPECTRUM, DAMP = 5%

Feasibility study on the seismic isolation of pool-type LMFBR 3. Experiments of lead and elastomeric bearings

A.Yasaka, M.Iizuka, Y.Fukushima & Y.Hirao
Kajima Corporation, Tokyo, Japan
Y.Sonoda & M.Kurihara
Hitachi Ltd, Tokyo, Japan

1. INTRODUCTION

The seismic base isolation systems are very efficient in protecting important internal equipments as well as buildings from earthquake vibration. Many advantages can be anticipated when this system is applied to the most important (in seismic rating) structures such as the FBR plant. The base isolation system composed of laminated rubber bearings and a certain kind of energy dissipators are considered to be the most practical at present. The lead and elastomeric bearing, which has been developed in New Zealand, is a laminated rubber bearing with a lead plug down its center. It provides the combined features of horizontal flexibility and energy absorption capability in a single unit. In order to investigate the feasibility of adopting the lead and elastomeric bearings to the seismic isolation systems of the pool type LMFBR plants, loading tests and shaking table tests were conducted. This paper describes the experimental results of the mechanical behavior and vibration characteristics.

2. LOADING TESTS

2.1 Specimens and testing apparatus

The test specimens are shown in Figure 1a. The specimens were designed to support the dead weight, W of 100tf and to have bilinear hysteretic loop parameters of elastic stiffness K1 = 0.1W/cm = 10tf/cm (f1 = 1.6 Hz), post-yield stiffness K2 = 0.01W/cm = 1tf/cm (f2 = 0.5 Hz) and yield force F = 0.05W = 5tf. These values were determined from the results of the earthquake and wind response analyses. Two methods of mounting details were adopted. One was the mounting by dowels, and the other by bolts. In the dowel type, 4 dowels on the flange plate were tailed in mortises of the bearing. In the bolt type, the flange plates were fixed to the bearing by bolts. The other details were the same with each other. The material used in the specimens were natural rubber (durometer hardness : 57, shear modulus : 8.1 Kgf/cm2) and lead of high purity.

Testing apparatus is shown in Figure 1b. Both shear force and axial force were provided by the actuators. A special link apparatus was used to constrain the specimens to deform in pure shear.

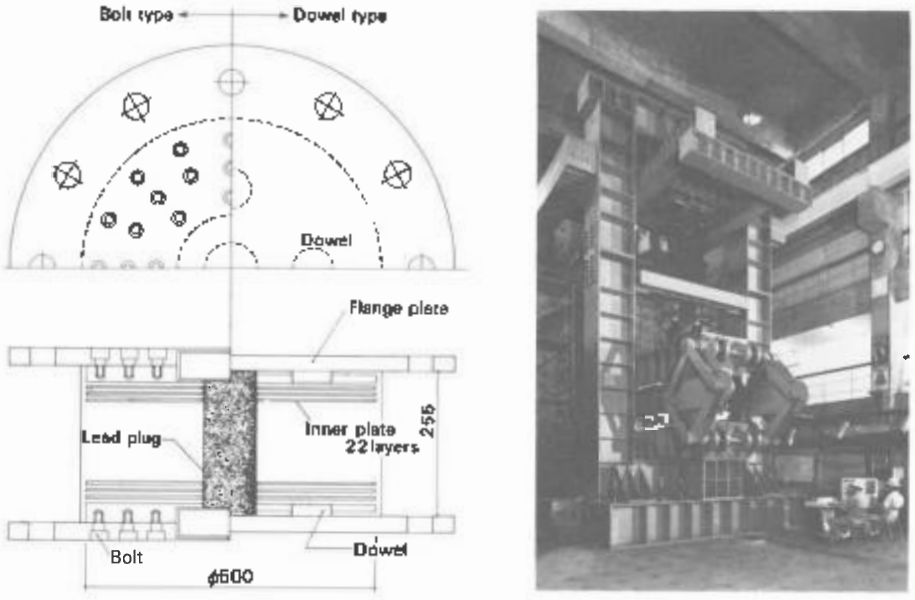

Figure 1. Specimen (right side: dowel type, left side: bolt type) (a); testing apparatus (b)

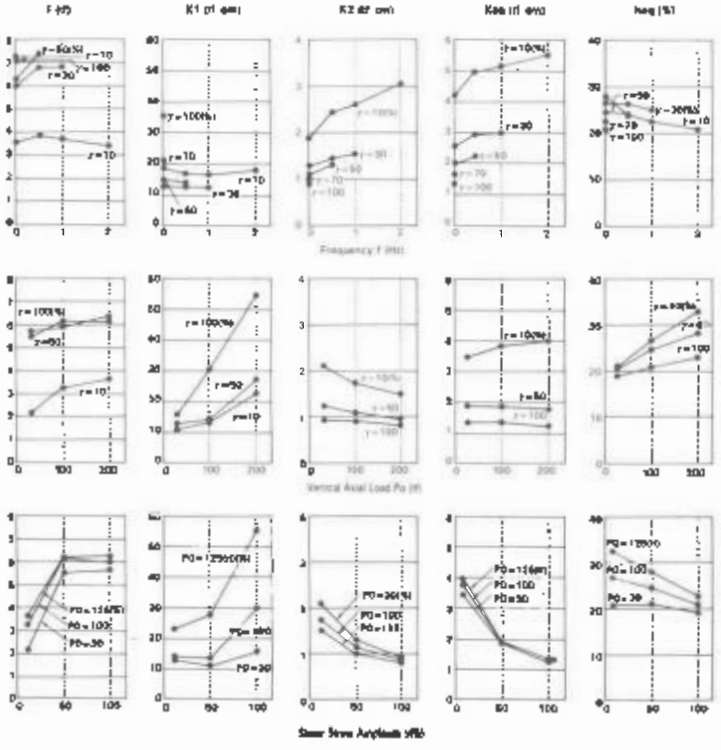

Figure 2. Effect of frequency f, vertical axial load Po and shear strain amplitude γ on hysteretic loop parameters.

2.2 Test results

In order to investigate the shear hysteretic characteristics, the specimens were dynamically loaded under constant axial load Po, shear strain amplitude $\pm\gamma$ ($\gamma = \delta H/h$; δH: horizontal displacement, h : effective elastomer height) and frequency f. Five hysteretic loop parameters of K1 (elastic stiffness), K2 (post-yield stiffness), F (yield force), Keq (equivalent stiffness) and heq (equivalent viscous damping factor) were determined from the load-deflection curves obtained by the tests. The relationships between these hysteretic loop parameters and loading conditions are shown in Figure 2. All of the hysteretic loop parameters were influenced by the shear strain amplitudes, and K1 and heq by axial loads. K2, Keq and heq in the small deformation range were affected by frequencies.

Shear fatigue tests were conducted. Cyclic shear loadings were applied to the specimens under Po = 100tf, γ = 50%, and f = 0.5 Hz. Loadings were repeated 8 times at intervals of 30 minutes. One set of loading was composed of ten cycles. The results of the 1st loading and the 8th loading are shown in Figure 3. In a set of serial cyclic loadings, restoring force gradually decreased, but with a time interval of 30 minutes, the properties recovered to the initial state.

Static shear tests for large deformation were carried out. Both types of the specimens could deform more than 200% shear strain bearing the axial load of 100tf without any damages. Test results are shown in Figure 4a. In the large deformation range, the restoring force characteristics were greatly affected by the mounting details.

Static pure tension test was conducted. Test results are shown in Figure 4b. The specimen failed at the rubber layer, when elongation ε($\varepsilon = \delta v/h$; δv:tensile displacement, h : effective elastomer height) reached 165%.

3. SHAKING TABLE TESTS

3.1 Specimen and earthquake input

A specimen used in the shaking table tests is shown in Figure 5a. The specimen is a scale model of a trial design model of a LMFBR plant. The specimen was designed to have the dynamic properties which were simulated to those possessed by a full scale model, on the basis of the similarity method. The specimen is a steel frame model with four-story and one-bay, which was mounted on four sets of 4tf bearings. The 4tf bearing is a scale model of a 500tf bearing which is applied in the trial design model. Therefore, the time scale factor is approximately $\sqrt{11}$. Two kinds of properties for the 500tf bearing were taken into account. They were different in the yield level α only, as follows.

1) Elastic stiffness : K1 = 0.04W/cm = 20tf/cm (f1 = 1.0Hz)
   Post-yield stiffness : K2 = 0.01W/cm = 5tf/cm (f2 = 0.5Hz)
   Yield force : F = 0.05W = 25tf (α = F/W = 0.05)
2) K1 and K2 are the same as above, F = 0.025W = 12.5tf (α = 0.025)

where W is supporting load of 500tf. These values were determined in consideration to the floor response spectrum. These properties were scaled down to those of 4tf bearing using the similarity method.

Two input earthquake motions were the El Centro 1940 NS component and an artificial earthquake motion. In generating the artificial earthquake motion, its frequency properties were determined in consideration to the fundamental natural frequency of the base isolation system.

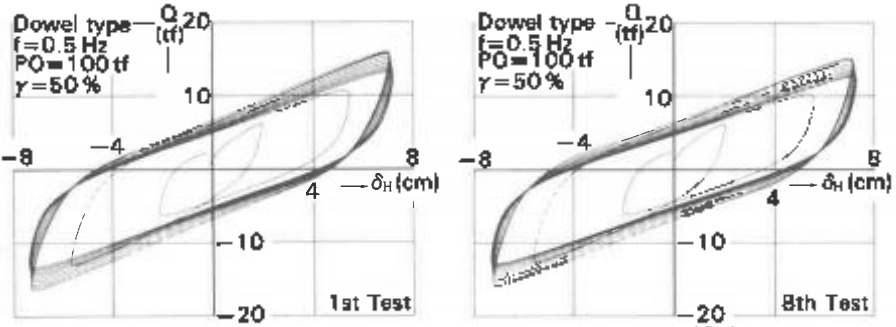

Figure 3. Shear force (Q) - horizontal displacement (δH) curves obtained by shear fatigue tests.

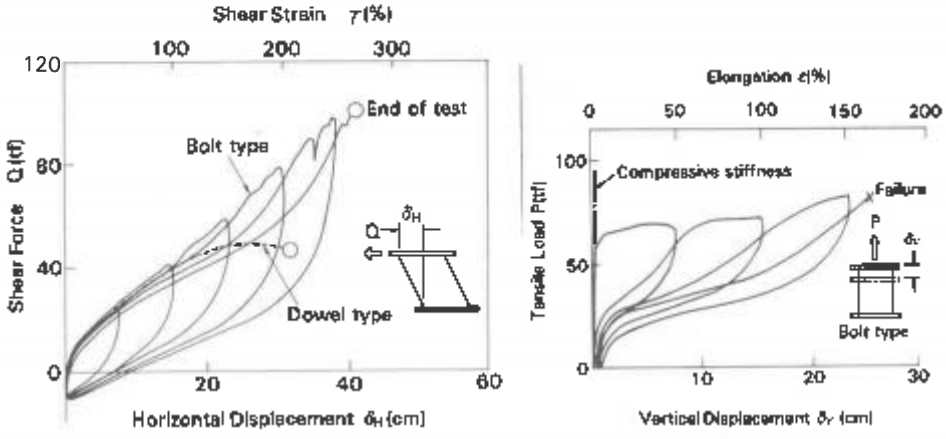

Figure 4. Restoring force characteristics in shear (a) and in pure tension (b).

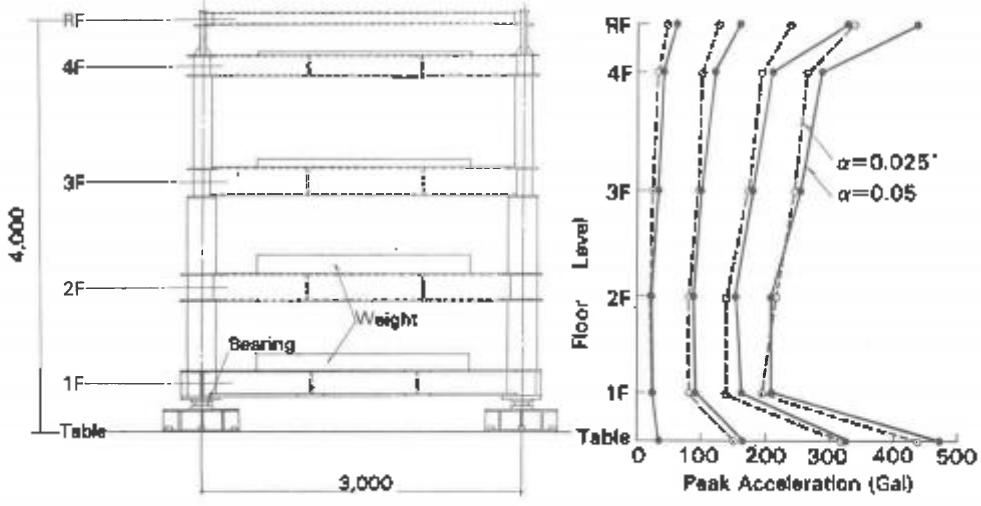

Figure 5. Specimen used in shaking table tests (a) ; peak response acceleration (b).

3.2 Test results

The test results for the artificial earthquake input are described hereunder. The results of the El Centro input were similar.

The peak response accelerations are shown in Figure 5b. The relationship between the relative displacement in the isolation story and the peak table acceleration is shown in Figure 6a, and the floor response spectra in Figure 6b. As shown in Figure 5b, the peak response accelerations were roughly constant with height and less than the peak table accelerations. And the lower yield level (smaller α) showed slightly lower acceleration responses. But, as shown in Figure 6a, the lower yield level showed slightly larger displacement responses. The floor response spectrum at the 2nd floor, where the reactor vessel is supported, was not influenced much by the yield level. But, as shown in the spectrum at the 4th floor, the lower yield level reduced the floor response spectrum in the short-period range.

3.3 Simulation analysis

Simulation analyses were performed to confirm that the analytical method was appropriate. The steel frame was represented by 5 lumped masses, and the isolation story was modeled as rocking and swaying springs. The swaying spring was assumed as the bilinear hysteretic spring which simulated the load - deflection curves of the isolation story obtained by the static loading tests.

Examples of the analytical results are shown in Figure 7. It can be seen that both calculated acceleration time history and calculated floor response spectrum agree well with the observed results.

4. CONCLUSION

The effectiveness of the lead and elastomeric bearings has been demonstrated by the tests. In the loading tests, the effect of the shear displacement amplitude, the axial load and the frequency on the shear hysteretic characteristics were quantified. And it was confirmed that the mounting details remarkably influenced the restoring force characteristics in the large deformation range. Furthermore, it was demonstrated that lead and elastomeric bearings had good fatigue properties, and they had sufficient ductilities in both shear and tension. From the shaking table tests, it was demonstrated that the peak response accelerations were greatly reduced. The effect of the yield level of the bearing on the responses was examined. And from the simulation analyses, it was recognized that the analytical method was reasonable.

It can be concluded that the lead and elastomeric bearings are very feasible devices to apply to the seismic base isolation systems of LMFBR plants, in view of both the mechanical performance and the vibration behavior.

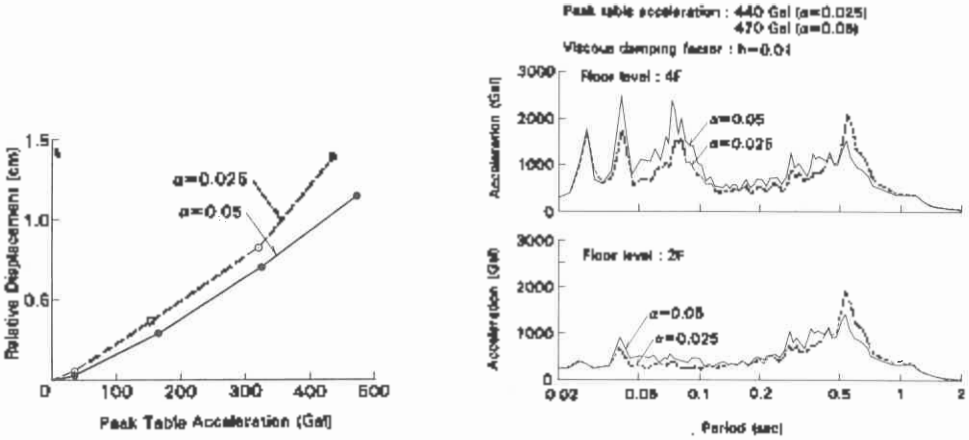

Figure 6. Relationship between relative displacement and peak table acceleration (a) ; effect of yield level on floor response spectrum (b).

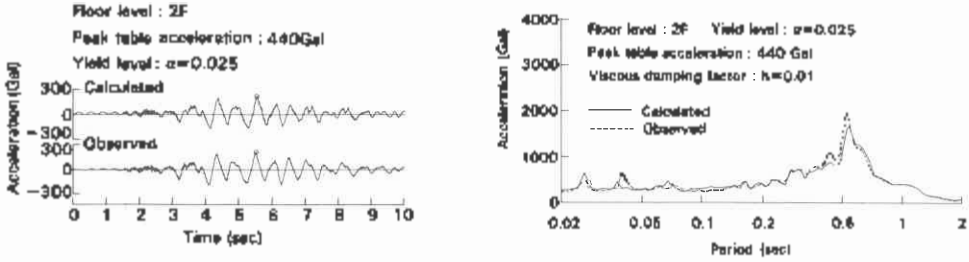

Figure 7. Comparison of calculated results and observed results in acceleration time history (a) and in floor response spectrum (b).

REFERENCES

Iizuka, M., Takabayashi, K., Yasaka, A., & Kurihara, M. 1986. Feasibility study of a seismic isolation system for fast breeder reactor plants. Proc. of the 7th Japan earthquake engineering symposium:1663-1668.

Robinson, W.H. 1982. Lead-rubber hysteretic bearings suitable for protecting structures during earthquakes. Earthquake Engineering and Structural Dynamics. 10:593-604.

Tyler, R.G. & Robinson, W.H. 1984. High-strain tests on lead-rubber bearings for earthquake loadings. Bulletin of the New Zealand National Society for Earthquake Engineering. 17.2:90-105.

Kelly, J.M. & Hodder, S.B. 1982. Experimental study of lead and elastomeric dampers for base isolation systems in laminated neoprene bearings. Bulletine of the New Zealand National Society for Earthquake Engineering. 15.2:53-67.

Feasibility study on the seismic isolation of pool-type LMFBR
2. Development of a rubber bearing and a friction damper

M.Kurihara & H.Kasai
Mechanical Engineering Research Laboratory, Hitachi Ltd, Tsuchiura, Japan
M.Madokoro & T.Yashiro
Hitachi Works, Hitachi Ltd, Japan
A.Yasaka & K.Odaka
Kajima Corporation, Tokyo, Japan

1. INTRODUCTION

Development of seismic isolation devices is a most important factor for the realization of a seismic isolation system in FBR plants. In this study, the seismic isolation system is composed of laminated rubber bearings and energy absorbers. A friction damper is adopted as an energy absorber. The friction damper is able to be designed to provide large energy absorption capability. However, the radical change in friction force excites the high frequency vibration modes of the building (Kurihara 1986). A modified friction damper with an initial soft stiffness to reduce the radical change in the damping force has thus been designed. To investigate the feasibility of applying rubber bearings and modified friction dampers to a seismic isolation system in FBR plants, loading and shaking table tests were performed using scale models. This paper describes: 1) the fracture characteristics of rubber bearings after aging tests and fatigue tests; 2) the dynamic characteristics and durability of the modified friction damper; and 3) the vibration characteristics of the seismic isolation system.

2. LOADING TESTS OF THE RUBBER BEARING

2.1 Scale model and experimental method

Specifications of the laminated rubber bearing for an actual plant are shown in Table 1. To estimate its fracture characteristics, aging and fatigue tests, and fracture loading tests were carried out using 1/11 scale models. These scale models are shown in Fig. 1 and the testing apparatus is shown in Fig. 2. The rubber bearings were put in a room with a constant temperature of 90°C under the static compression load of 4.1 ft to simulate the plant lifetime.

2.2 Test results

The restoring force characteristics of the rubber bearing, to the allowable displacement, is shown in Fig. 3. The observed result is somewhat small in comparison to the designed value. For example, at the rated displacement of 10 mm, which corresponds to the maximum response displacement arising from an artificial earthquake motion (Sonoda 1986), the spring constant of the rubber bearing is smaller by 14%. However, the difference is negligible in a practical application. Load displacement characteristics for each experimental condi-

tion during the fracture are shown in Fig. 4. The spring constants of the rubber bearings in the allowable displacement after aging tests rise slightly, compared with that for rubber bearings experiencing no aging. The fracture displacement of a rubber bearing after aging tests comparable to 60 years plant life is smaller by 30% than that with no aging. However, this value is greater than the allowable displacement by 30%. Therefore, it is found that the increase in spring constant and the decrease in fracture displacement of the rubber bearing over a plant's lifetime does not appear to be serious in a practical application.

Table 1 Design specificatoins for a rubber bearing

Loading Weight W (tf)		500
Natural Freq. (Hz)	Horizontal f_2	0.6
	Vertical fv	20
Spring Const. (tf/cm)	Horizontal K_2	4.85
	Vertical Kv	8160
Allowed Value of Horizontal Deformation Δa (cm)		50

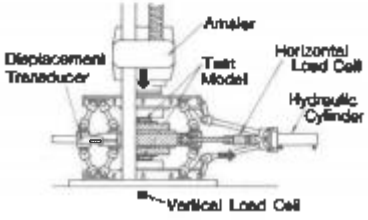

Fig. 2 Testing apparatus for rubber bearings

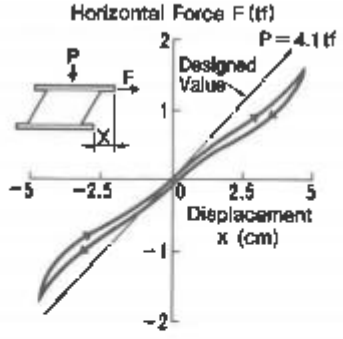

Fig. 3 Force-displacement relation of a rubber bearing

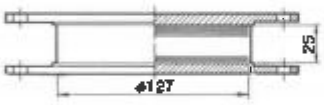

Horizontal Spring Const : K_2= 439 kgf/cm
Vertical Spring Const. : Kv = 7.39×10⁵kgf/cm
Allowed Value of Horizontal Displacement : Δa = 4.6 cm
Rubber:1mm×17, Steel :0.5mm×16

Fig. 1 Scale model of a rubber bearing

	Aging Condition of Model	Fatigue test Condition Amplitude (mm)	Frequency (Hz)	Cycle
Ⓐ	No-Aging	10	0.5	10^3
Ⓑ	No-Aging	1	5	10^5
Ⓒ	40 Years Aging	1	5	10^5
Ⓓ	60 Years Aging	1	5	10^5
※	No-Aging	No-Fatigue		

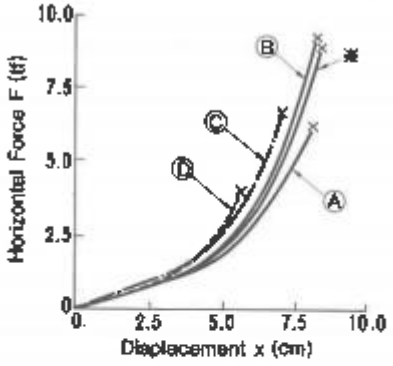

Fig. 4 Fracture characteristics of rubber bearings

3. LOADING TESTS OF THE MODIFIED FRICTION DAMPER

3.1 Scale model and experimental method

A diagram of the modified friction damper is shown in Fig. 5. This damper, which has elasto-plastic hysteresis characteristics, is characterized by the thin rubber layer called a pot bearing in series with friction plates. The plates

composed of a stainless steel plate and a brake pad are given a constant compressive load by the coned disc springs.

Loading tests for the damper were carried out with the testing apparatus shown in Fig. 6. The load-displacement characteristics and durability of the damper were investigated. In addition, conditions employed in the tests were a frequency of 0.5 Hz and a surface pressure of 100 kgf/cm^2.

3.2 Experimental results

The displacement effect on the spring constant of the pot bearing is shown in Fig. 7. The restoring force characteristics of the pot bearing at frequency 0.5 Hz are also given. The difference between the designed spring constant and the experimental result at a rated displacement of 0.91 mm is 10% at most. Therefore, the experimental result is considered to agree well with the designed value. The hysteresis loop of the damper at frequency 0.5 Hz is shown in Fig. 8. The displacement effect on the damping characteristics is shown in Fig. 9. From this figure, it can be seen that the friction force is almost constant, and that the loss energy increases in proportion to displacement. Therefore, it is found that the damper has stable damping characteristics at least to the same degree as the allowable displacement for the rubber bearing. The damper's durability for cyclic loading is shown in Fig. 10. The friction force increases slowly as the number of cycles increases, which means that the loss energy tends to increase as well. However, since the friction force increases by about 10% of the initial value at around one hundredth cycle, it is found that the damper is very durable as regards cyclic loading.

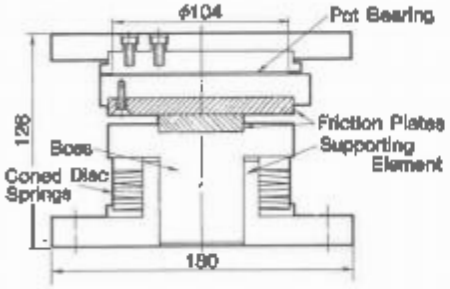

Fig. 5 Structure of the modified friction damper

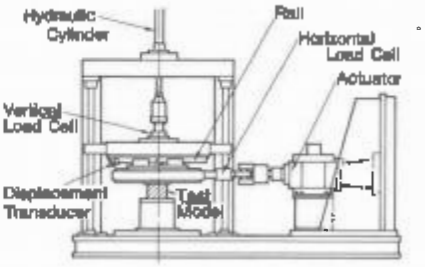

Fig. 6 Testing apparatus for dampers

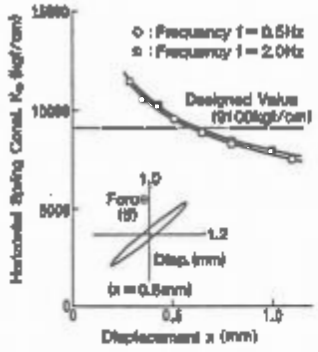

Fig. 7 Displacement characteristics of a pot bearing

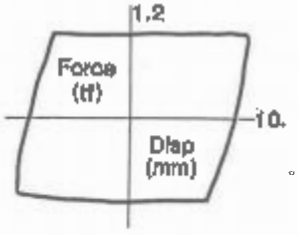

Fig. 8 Hysteresis loop of the modified friction damper

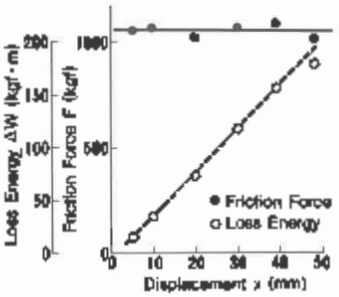

Fig. 9 Displacement characteristics of the modified friction damper

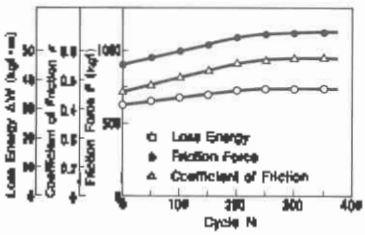

Fig. 10 Durability of the modified friction damper for cyclic loading

4. SHAKING TABLE TESTS

4.1 Isolated building model and experimental method

As shown in Fig. 11, the building model is a four-story, one-bay, steel-frame structure used to simulate vibration properties in the design model of a FBR building. The model is 18000 kgf in weight. The natural frequencies of the first and second modes of the model under a fixed base condition are 9.8Hz and 22.9Hz, respectively. The damping ratio of each mode is about 0.005. The model was mounted on four rubber bearings which had the same design specifications as those used in the loading tests. The first stiffness K_1, the second stiffness K_2 and the apparent yield force Q of the combined isolation device composed of four rubber bearings and two modified friction dampers were designed as shown in Table 2.

In order to obtain hysteresis characteristics of the combined isolation device, loading tests were performed using the hydraulic cylinder as shown in Fig. 11. Next, shaking table tests were carried out using the artificial earthquake motion that was reduced in time by $1/\sqrt{11}$ according to the similarity law.

4.2 Test results

The hysteresis loop of the combined isolation device is shown in Fig. 12. The isolation device operated as expected. Time histories of earthquake response accelerations on roof floor level and the relative displacement in the isolation story are shown in Fig. 13. Maximum response accelerations on each floor level are shown in Fig. 14. Also the results for an isolated building model with modified friction dampers is compared with those for one with ordinary friction dampers and a non-isolated building model. From Fig. 14, it can be seen that seismic isolation systems drastically reduce response accelerations when compared to a non-isolated type. However, the effectiveness in reducing response accelerations depends on the type of damper employed. In Fig. 14, one can see that the modified friction damper reduces response accelerations on each floor level by 1/2, compared with the ordinary friction damper. The relationship between the response acceleration on the second floor, the installation level of the reactor, and maximum input acceleration level is shown in Fig. 15. Floor response spectra on the second floor are shown in Fig. 16. The relationship between the floor response spectra on the second floor above the 5 Hz frequency and maixmum input acceleration level is shown in Fig. 17. From Fig. 16 and 17, it can be seen that the floor response spectra for the modified friction damper are less than 1/2 of those for the ordinary

friction damper, except in the neighborhood of the first mode. Therefore, supplying suitable elasto-plastic hysteresis characteristics to an ordinary friction damper is effective in reducing floor response spectra.

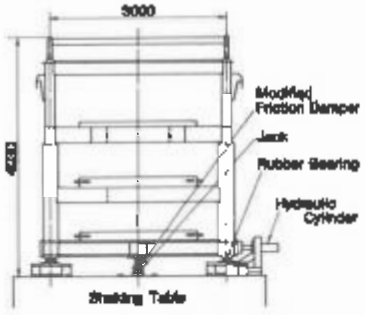

Fig. 11 Isolated building model

Table 2 Design specifications for the isolation device

	Designed Specification	
	Scale Model	Actual Model
K_1 (kgf/cm)	7,280	728,000
$\omega_1=\sqrt{K_1 g/w}$	3.9	1.0
K_2 (kgf/cm)	1,730	18,400
$\omega_2=\sqrt{K_2 g/w}$	1.8	0.8
Q (kgf)	925	100,000
$\beta=Q/w$	0.06	0.06

K_1: First Stiffness Q: Apparent Yield Force
K_2: Second Stiffness w: Weight of Building Model

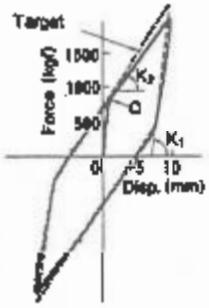

Fig. 12 Hysteresis loop of the isolation device

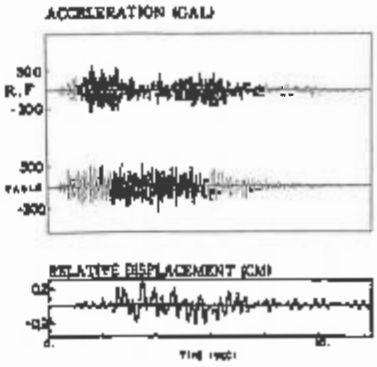

Fig. 13 Response waves of the isolated model with the modified friction damper

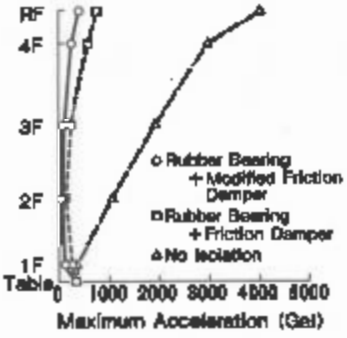

Fig. 14 Maximum response acceleration distribution

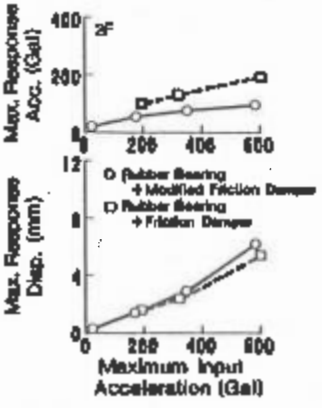

Fig. 15 Relationship between maximum response and maximum input acceleration

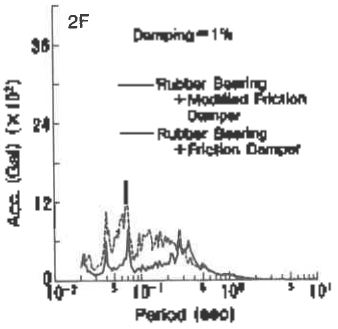

Fig. 16 Response spectra on 2nd floor (maximum input acc.=351 Gal)

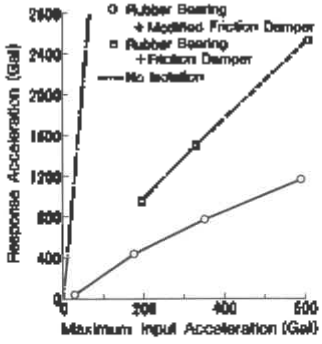

Fig. 17 Relationship between maximum response spectra on 2nd floor above 5Hz and maximum input acceleration

In this paper, simulation analysis results are abbreviated, but they agree approximately well with test results.

5. CONCLUSIONS

This paper presents a study on the feasibility of a seismic isolation system composed of rubber bearings and modified friction dampers for FBR buildings. The following conclusions are reached on the basis of loading and shaking table tests of the isolation device.

1. The increase in spring constant and the decrease in fracture displacement of a rubber bearing aged 60 years does not appear to be serious in a practical application.

2. The modified friction damper has almost ideal elasto-plastic hysteresis characteristics in a large displacement range and shows good durability for cyclic loading.

3. It is recognized that the modified friction damper greatly controls the excitation of high frequency vibration modes in isolated buildings.

4. The bilinear hysteretic parameters of the isolation device can be designed independently and accurately. Consequently, it is expected that a seismic isolation system which has the adequate hysteresis characteristics can applied to FBR buildings.

REFERENCES

Kurihara, M., et al., 1986. Feasibility study of a seismic isolation system for fast breeder reactor plants 2. Proc. of the 7th Japan earthquake engineering symposium: 1657 - 1662.

Sonoda, Y., et al., 1986. Feasibility study of a seismic isolation system for fast breeder reactor plants 1. Proc. of the 7th Japan earthquake engineering symposium : 1651 - 1656

Seismic isolation design analysis on pool-type LMFBR

A.Sakurai, S.Shiomi, S.Aoyagi & T.Matsuda
Central Research Institute of Electric Power Industry, Chiba, Japan
N.Tanaka & H.Isogai
Mitsubishi Atomic Power Industries, Inc., Tokyo, Japan
K.Fujita
Mitsubishi Heavy Industries Ltd, Takasago, Japan
T.Shimomura
Mitsubishi Heavy Industries Ltd, Kobe, Japan

1 Introduction

A pool-type LMFBR is studied in Japan as one of the candidates of the future LMFBR, which has a large diameter main vessel (M/V). But in our country we have so severe regulations, that it is difficult to design a M/V without any seismic supports. So we have studied a seismic isolation design in which a M/V is supported by an isolation system in expectation that the seismic response acceleration of a M/V would become lower and that the seismic loads would be reduced. In this study a M/V and a building are modeled to beam elements with lumped masses respectively and connected by a non-linear spring which represents the isolation system. Then we have carried out the seismic response analysis and have investigated the feasibility of the isolation.

2 Model and case of analysis

We performed two kinds of analyses, one of which was to investigate the influence of an isolated M/V to the response of a building using a coupled model of the M/V and the building, the other was to survey the appropriate parameters of the isolation systems using a single model of the M/V.

2.1 Model of analysis

The building in a conceptual design was supposed to be approx. 90m in width, 70m in length and 88m in height and approx. ¢14,000 ton in weight including components and a base mat. And the M/V was supposed to be approx. 18m in dia. and 15m in height and approx. 10,330 ton in weight including core internals, sodium and so on.

In the analysis of the coupled model, the M/V and the building were modeled to lumped masses and beams, and the isolation systems were modeled to a non-linear spring (Fig. 1).

In the analysis of the single model, only the M/V was modeled (Fig. 2). Equations of motion are as follows,

$$\left.\begin{aligned} &[M]\{\ddot{X}\} + [C]\{\dot{X}\} + [K]\{X\} = -[M]\{1\}\ddot{Z} + \{Y\} \\ &\{Y\} = [\,-F\ 0\ldots0\,]^T, \end{aligned}\right\} \quad \ldots (1)$$

Where F is the imposed force on the supported point of the M/V from the isolation system, which depends on its properties, and $\ddot{Z}$ is the acceleration of the M/V's floor. Solving the equations (1), we got seismic responses.

The data of the models are shown in Tables 1 and 2.

2.2 Input of seismic wave

The input of a seismic wave in the analysis was determined as follows. At first, we selected a seismic wave having strong component at relatively low

frequency regions out of the ones recorded recently in Japan. The wave was enlarged so that the peak acceleration of the wave was equaled to 300 Gal. Then we applied the acceleration time-history of the wave to the mass of a rock in Fig. 1.

2.3 Case of analysis

For the coupled model, we chose two values i.e. 0.5 H_Z and 1.0 H_Z as a frequency of the isolation system, and selected two kinds of yielding loads of the isolation system. And also we calculated seismic responses according to the model without isolation systems for comparison.

In the analysis of the single model, we selected several parameters for searching the most appropriate parameters of the isolation systems. We considered three kinds of the systems ; a hysterisis damper model, a series model of a friction damper and a spring, and a parallel model of a friction damper and a spring. In the analysis of the single model, we applied the response accelerations at the M/V floor obtained from a seismic response analysis of the building.

3 Results

3.1 Analysis of the coupled model

Natural frequencies and mode shapes of the coupled model are shown in Fig. 3.

Peak seismic response accelerations of the building and the M/V are shown in Fig. 4. Floor response spectra of the M/V floor are shown in Fig. 5 for the two cases of yielding acceleration under the condition that the isolation frequency was 1 H_Z. The following observations were obtained through the results.

(i) The peak acceleration at the M/V floor was increased up to 450 ~ 600 Gal while the input to the rock was 300 Gal. And the peak value was similar with or without isolation systems. And also it was not so affected by the isolation frequency, and by the yielding acceleration.

(ii) The spectrum was not so affected by the yielding acceleration.

3.2 Analysis of the single model

Results of analyses of the single model are shown in Table 3 and Figs. 6 ~ 9.

(1) Hysterisis damper. We could control the both responses of the acceleration and the displacement of the M/V at low value using an appropriate isolation condition. The peak acceleration was 300 ~ 600 Gal and the maximum relative displacement was about 35mm when the ratio of initial stiffness to yielded stiffness was 6 ~ 8 in the case of this study (Fig. 6).

The examples of response acceleration time history are shown in Fig. 7 for the input of sine wave. It is observed that the M/V responded having components of high frequency and having inversed phases at the upper part and at the bottom.

(2) A parallel model of a friction damper and a spring. We could control the both responses of the acceleration and the displacement of the M/V at low value using an appropriate isolation condition. The peak acceleration was 500 ~ 750 Gal and the maximum relative displacement was about 25mm when the isolation frequency was near 1 H_Z in the case of this study (Fig. 8).

The example of the relation between the peak accelerations and the coefficients of friction are shown in Fig. 9 for each level. When a coefficient of friction is zero, the M/V responses uniformly at each level, but when the coefficient is increased, the M/V responses intensely at the top and at the bottom.

Table 3 shows suitable parameter combinations of the isolation systems which could control both seismic responses of the acceleration and the displacement of the M/V at low value.

4 Discussions

(1) The M/V supported by the isolation systems did not have influence on

seismic responses of the building, and the analysis using a single model was adequate for searching appropriate parameters of the isolation systems.

[2] The fundamental frequency became low when the M/V was supported by the isolation system, but the response wave of the M/V's acceleration had high frequency components. The cause of this phenomenon was estimated to be that the isolation system had a discontinuous stiffness at the yielding points then the M/V suffered the impact when the isolation system yielded.

[3] The both responses of acceleration and displacement of the isolated M/V could be controlled at low value when the parameters of the isolation system were appropriately chosen.

[4] The isolated M/V should be modeled in a multi mass model when the seismic responses of the M/V was calculated, judging from the fact in Fig. 9.

5 Conclusions

From the results of analysis, we estimated that selecting suitable parameters of the isolation system, we could reduce the peak response acceleration of the M/V from about 2500 Gal to 1000 Gal for the strong seismic motion in Japan, and then the maximum relative displacement became about 50mm between the M/V and the floor. Each model of the systems would become effective on controlling the M/V's both responses of acceleration and displacement at low value if parameters were appropriately chosen. But even if the M/V was isolated, the M/V might respond having vibration components of higher frequency. So the designer should pay attention to such facts in designing the seismic components on the isolated M/V.

For one example we designed a conceptual isolation system which supports a M/V using coil springs and friction dampers in parallel (Fig. 10). In future we have to solve the following problems. The first is whether we could design and fabricate such isolation systems that have constant and reliable properties of an isolation. The second is whether we could have piping systems connected to the M/V which tolerate displacement of about 50mm. After successful solution of such problems we could have a M/V of a large pool-type LMFBR without seismic supports which coud keep the integrity against strong seismic motions.

Table 1 Data of analysis for a coupled model (see Fig.1)

Structure	No. of mass	Level of mass (El. m)	Weight (ton)	No. of element	Area of shear (m^2)	Second moment of area (m^4)
Reactor building	R308	32.5	10,000	6	160	252,870
	R307	19.0	19,570			
	R306	14.0	45,700	7	216	373,514
	R305	10.0	43,250	8	481	630,200
	R304	7.5	45,110	9	817	694,879
	R303	0.6	47,350	4	868	794,829
	R302	-- 6.6	38,982	3	1013	913,038
	R301	-13.0	46,400	2	1013	913,038
	R317	-15.5	--	1	1044	913,238
	R316	-22.5	12,520	0	Isolation systems	
	R315	-25.5	--			
Reactor main vessel (M/V)	R311	9.9	4,560	11	1,495	112.9
	R312	-- 8.7	1,840	12	1,495	112.8
	R308	-- 7.5	2,260	13	1,496	112.9
	R314	-10.0	630	14	1,288	91.3
	R315	-12.7	1,860			
Total weight of structures (with components)			418,930 ton	Moment of inertia		$I_{XX}=7.48\times10^7$, $I_{YY}=6.21\times10^4$ ($ton\cdot m^2$)

Table 2 Data of analysis for a single model (see Fig.2)

Part	Mass ($kg\cdot s^2/mm$)		Spring stiffness (kg/mm)		Coefficient of viscosity ($kg\cdot s/mm$)
Load pad	M_1	488.5	K_1	41,860	C_1	87.07
M/V upper	M_2	66.8	K_2	2,680,000	C_2	283.07
M/V middle	M_3	289.6	K_3	2,680,000	C_3	628.96
M/V bottom	M_4	74.4	K_4	1,440,000	C_4	287.80
Sodium	M_5	82.3	K_5	116	C_5	1.30
RIS	M_6	31.7	K_6	70,500	C_6	15.00
Core tolerant	M_7	748.3	K_7	2,000,000	C_7	547.01

Table 3 Optimum parameters of the isolation system and maximum responses for a single model

Shape	Trapezoids	Friction in series	Friction in parallel	Rigid support
Parameters	spring coefficient 3.0×10^5 kg/mm	frequency 2Hz	frequency 1Hz	frequency 100Hz
Results of response	y_0/y_p 0.6	mm 0.38	mm 0.1	--
	yield load 1.0×10^6 kg	--	--	--
Max. of $\ddot{x}_1$(Gal)	490	670	3000	9000
Max. of $\ddot{x}_2$(Gal)	473	585	732	2600
Max. of x_1 (mm)	31	50	21	4
Rel. disp. of x_2-x_1(mm)	5	10	4	18
Residual disp. (mm)	0	0	0	0

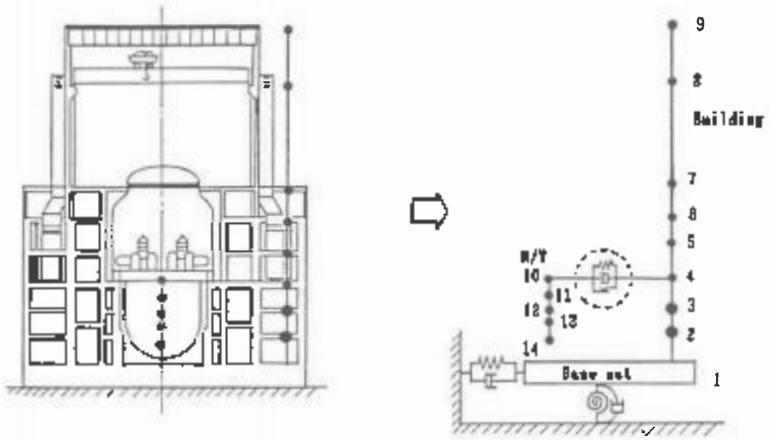

Fig.1 A Coupled model of a building and a M/V

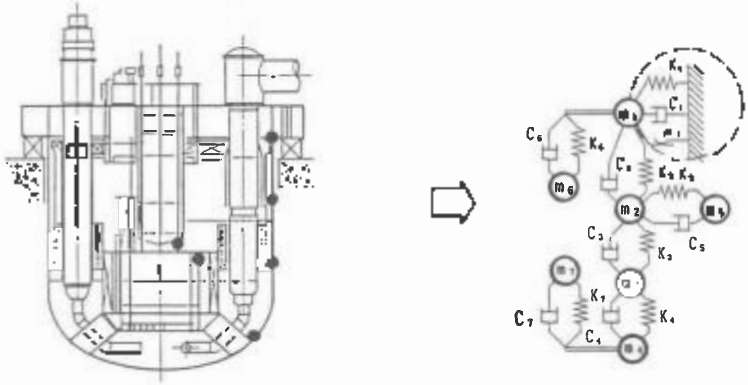

Fig.2 A Single model of a M/V

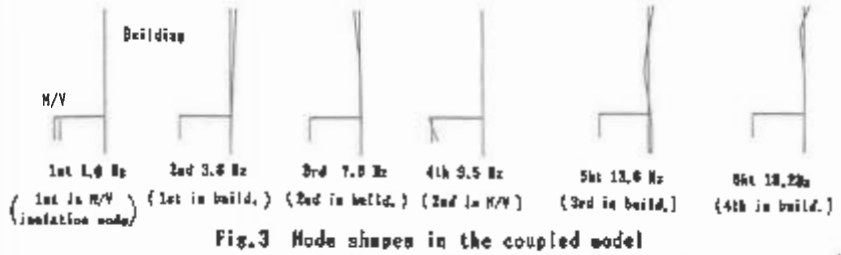

Fig.3 Mode shapes in the coupled model

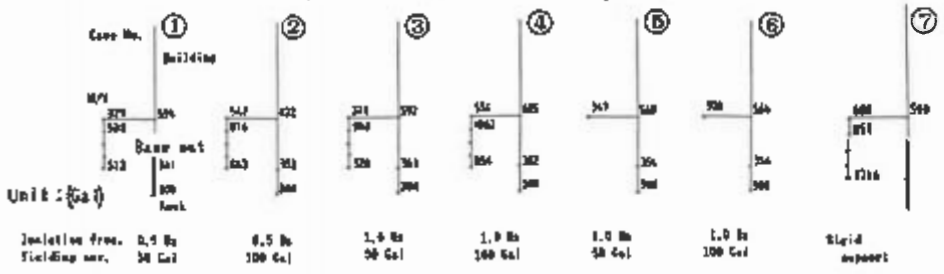

Fig.4 Peak acceleration responses in each case for the coupled model

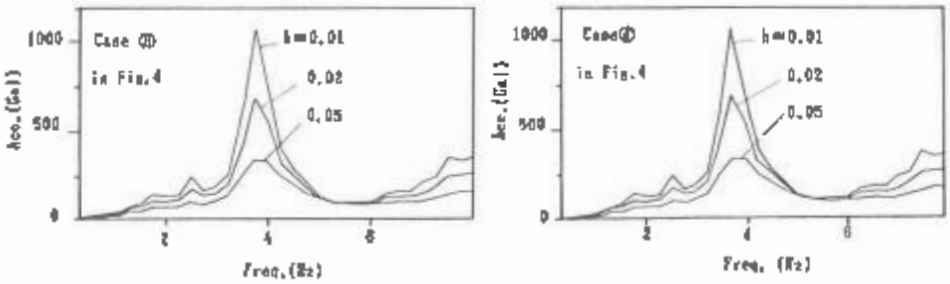

Fig.5 Comparison of floor response spectra of the building

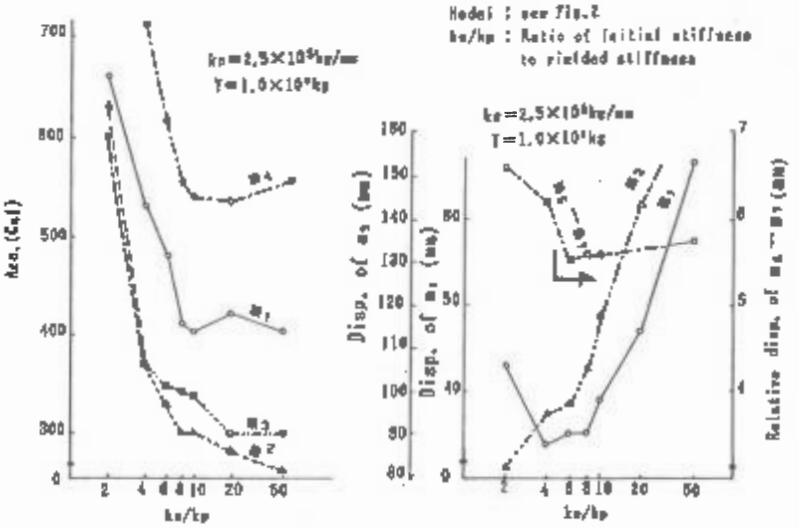

Fig.6 Responses for the models with hysteresis damper

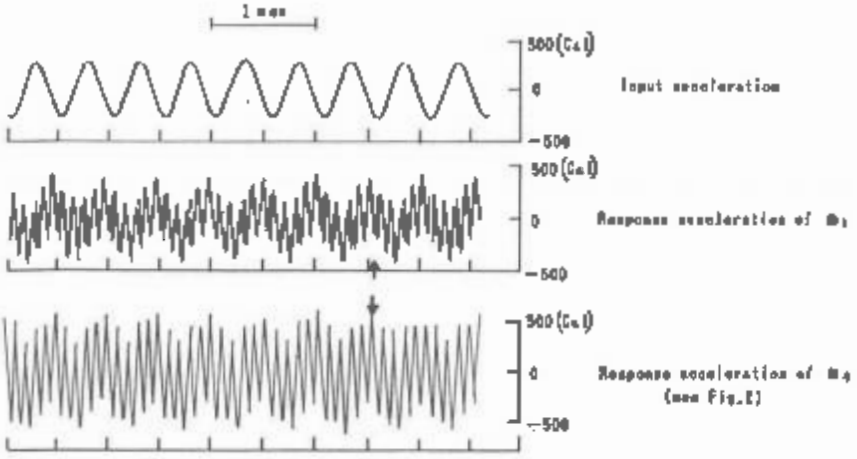

Fig.7 Time history sample of response acceleration of the H/V for the single model isolated

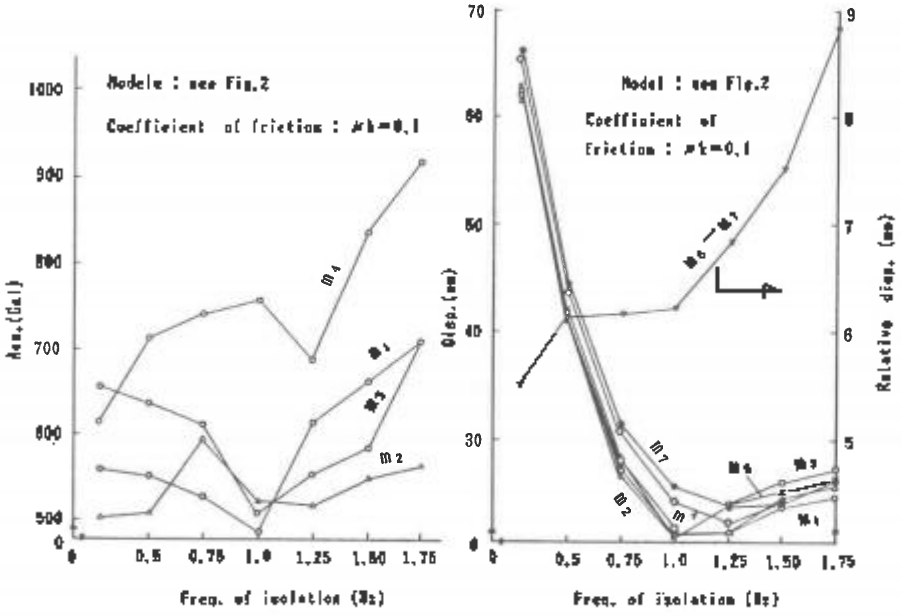

Fig.8 Responses for the parallel models of a friction damper and a spring

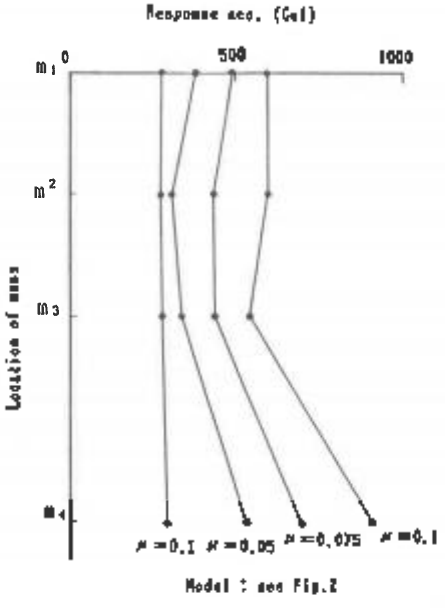

Fig.9 Peak response acceleration distribution in the H/V isolated

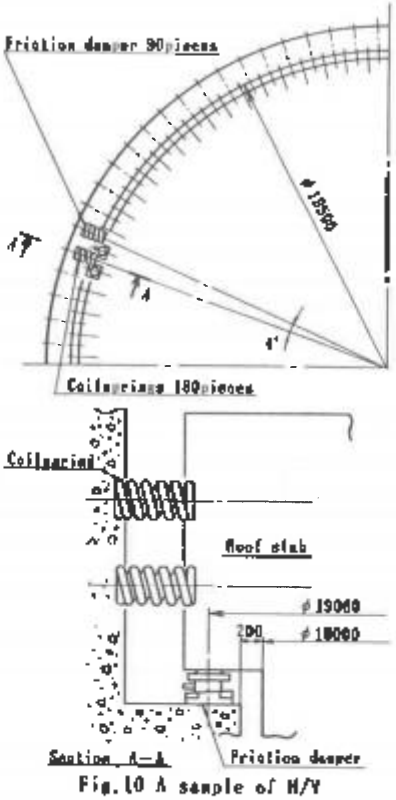

Fig.10 A sample of H/V isolation supporting system

Comparative studies of isolation systems applied to a compact LMR reactor module*

T.-S.Wu, B.J.Hsieh & R.W.Seidensticker
Argonne National Laboratory, Ill., USA

ABSTRACT

We investigated the responses to horizontal input ground motions of a compact LMR reactor module incorporated with three different isolation systems: a steel plate reinforced elastomer pad design without friction plates (called the linear system); the same pad with friction plates (called the bilinear system); and the Alexisismon design which uses rubber springs and teflon pot bearings to carry horizontal and vertical loads, respectively. Essential parameters characterizing the isolation systems, such as isolation frequency, are chosen consistent with those available in the open literature for these systems.

All three isolation systems significantly reduce the horizontal shear force transmitted to the reactor system. The bilinear system, due to the friction plates, limits the maximum shear force transmitted to a preset value. The Alexisismon design, which may use a very soft spring and, therefore, exhibits a much lower isolation frequency than the other two designs, gives the most reduction in shear force.

Among these three isolation systems, the linear system yields the smallest maximum acceleration for the isolated reactor. The Alexisismon design not only produced the highest maximum acceleration, but also showed amplification in acceleration. Acceleration amplification is also observed in the bilinear system for some of the ground motions considered. It appears at this time that this acceleration amplification is caused by the nonlinearity of the isolation systems. Further study is definitely warranted.

1 INTRODUCTION

Because of current requirements on safety and reliability, nuclear power plants are to be designed against seismic events even for the areas once thought seismically inactive. The conventional approach to a seismic design is to provide sufficient strength and ductility in the structures and components to resist the earthquake forces. This may result in heavy-walled vessels, pipings, and structural components.

*Work performed under the auspices of the U.S. Department of Energy.

An alternate approach is to use a seismic isolation scheme which reduces the seismic forces transmitted to the isolated structure by shifting the important natural frequencies of the structure away from the more damaging frequency range of the strong motion of earthquakes. The shifting of structural frequencies is usually accomplished by incorporating a flexible support to the structure, such that the isolated structure has lower natural frequencies and thus avoids the damaging high-frequency power range of earthquakes.

For reactors designed for low pressure but severe thermal transients, thin-walled components are generally preferred. It is, therefore, not an easy task to design them against strong earthquakes and severe thermal loadings simultaneously. Seismic isolation, therefore, becomes especially attractive in these reactors.

With seismic isolation, the seismic loading transmitted to the structure is reduced. Reliability and design margins of the structure in resisting earthquake loads are also increased. These, in turn, reduce the sensitivity of the plant's response to local soil environment; therefore, the effects of uncertainty involving soil properties are much reduced.

2 DESCRIPTION AND MODELING OF THE REACTOR

The reactor module of a compact liquid metal reactor (LMR), shown in Fig. 1, has a diameter and height of approximately 6m (20 ft) and 18 m (60 ft), respectively. Not included in this figure are the reactor vessel auxiliary cooling system (RVACS) and the head access area (HAA). Note that the bulk of the mass of the reactor module is concentrated at discrete locations such as the reactor closure or deck, and the core and shielding, a spring-mass system is considered adequate for the present investigation. Figure 2 is the analysis model which is intentionally made simple in order to efficiently evaluate linear and nonlinear systems under various seismic loadings as well as different soil conditions.

Before this simple spring-mass model (Fig. 2) was chosen as the basic model in this study, other spring-mass models were also examined. It is observed that these models yield almost the same results. Furthermore, it has been pointed out in [1] that there is little difference between the results from a simple model and from a more detailed model for a reactor with seismic isolation. The model of Fig. 2 is thus used in most of the seismic isolation studies for the reactor module under horizontal seismic loadings.

In the analysis, the reactor module is attached either to the ground when there is no isolation, or to one of the isolation systems described in Section 3 when there is isolation. In the unisolated case, the structure is assumed built upon either soft soil with a shear velocity of 600 m/s (2,000 f/s), or upon hard soil with a shear velocity of 1800 m/s (6,000 f/s).

Springs and dampers have been used to simulate different isolation systems. In these simulations, the springs can be linear or bilinear. The bilinear spring considered here behaves linearly until a maximum spring force has been reached. After that, the spring force remains constant during loading but behaves linearly during unloading. The dampers are either of linear viscous or of Coulomb friction type. Other than that inherent in the material of the isolation system, no additional damping has been included in the modeling. Free surface sloshing of the reactor coolant is not examined in this investigation.

3 ISOLATION SYSTEMS AND TIME HISTORIES

Three isolation designs have been studied: They are: (1) reinforced elastomer design without friction plates [1], or linear system, (2) reinforced elastomer design with friction plates [1], or bilinear system, and (3) Alexisismon design [2], which uses rubber springs and pot bearings to carry horizontal and vertical loads, respectively.

In the linear system, isolation is provided by the reinforced elastomer, i.e., elastomer embedded in steel plates. During an earthquake, the elastomer, or seismic isolator, acts as a soft horizontal spring and responds linearly. The isolated structure will vibrate and return to its initial position after the earthquake. There will be no permanent displacement as long as strains remain in the elastic range.

In addition to the reinforced elastomer, as in the linear system, the bilinear system uses friction plates to limit the maximum horizontal force transmitted to the structure. During earthquakes, the elastomer deforms linearly with force, as in the linear system. When the earthquake becomes stronger and the force of the elastomer reaches or exceeds the limiting or maximum force, slipping between the plates occurs. As a result of this slipping, horizontal displacement of the elastomer is limited, thus avoiding the potential buckling of the elastomer or seismic isolator. Note there is no limitation on the horizontal displacement of the structure except it design performance limit. For low-intensity earthquakes, this design behaves just as the linear system. For earthquakes of higher intensity, relative displacement (slipping) between the friction plates occurs. The structure could exhibit some permanent displacement after an earthquake (usually just a few inches).

In the Alexisismon design, horizontal isolation is mainly provided by the rubber spring or bearing which does not support any vertical load. Vertical load is supported entirely by the pot bearing. There will be some horizontal friction force when the pot bearing has sliding motion. Because of this friction, the isolated structure may exhibit some small amount of permanent displacement after an earthquake.

In the limiting case when the friction force is zero, the Alexisismon design reduces to the linear system. However, in the Alexisismon system, the isolation frequency (i.e., the lowest natural frequency of the isolated structural system) can be very low compared with other designs. This is because the rubber bearing which provides the horizontal stiffness of the isolation system does not carry any vertical load, thus eliminating the concerns for buckling of the rubber bearing from large relative horizontal displacement. This is not true for the linear system, where the vertical weight of the structure is carried by the elastomer, which may buckle when the relative horizontal displacement becomes excessive. Thus, the attainable isolation frequencies for the linear system may be different from those of the Alexisismon designs. Hence, different isolation frequencies are used in analyzing the reactor module with the different isolation systems.

Isolation frequency, which relates the total mass of the system being isolated and the stiffness of the isolator, is generally very low to be away from the damaging frequency range of strong earthquake motions. The isolation frequencies used in this analysis are 0.5, 0.67, and 0.17 Hz, respectively, for the linear system, the bilinear system, and the Alexisismon design. The maximum frictional force between the friction plates for the bilinear system is 20% of the

total weight of the structure and 5% for the pot bearing in the Alexisismon design. These parameters are consistent with those used elsewhere.

To obtain some measure of the effectiveness of the isolation systems, responses of unisolated systems under the same earthquake loadings are also obtained. The unisolated systems are modeled by assuming that the structure is built upon a soft soil site (with soil shear velocity of 600 m/s) or a hard soil site (with soil shear velocity of 1800 m/s), respectively. The necessary equivalent linear spring and damper corresponding to an infinite soil media are obtained from known relations [3].

A total of eight well characterized and representative acceleration time-histories have been used in this investigation. These include one synthetic time-history whose spectrum envelopes that suggested in USNRC Guide 1.60, the well known El Centro record, and the 1935 record at Helena, Montana which is close to a potential plant site. The other five time-histories based on their strong motion duration, local magnitude, and frequency content, have been included in a study on the engineering characterization of earthquakes ground motion for nuclear power plate design [4].

4 SUMMARY OF RESULTS

When an isolation system described previously is incorporated into the reactor module where the site soil shear velocity is either 600 m/s or 1800 m/s, results show an insignificant effect of the site soil property on the responses. Such results have also been observed in [1]. This is expected, since the stiffness of an isolation system with an isolation frequency of 0.67 Hz or less is much softer than the soil stiffness considered here. Accordingly, such low-frequency seismic isolator can be modeled as fixed at the bottom, or neglecting the soil stiffness when the soil shear velocity is equal to or higher than 600 m/s.

Table I presents the shear force transmitted to the reactor module for different isolated and unisolated environments. It is evident that when seismic isolators are present, there is a significant reduction in the shear force transmitted. The bilinear system, due to the use of friction plates, limits the maximum shear force transmitted to the preset value of 20% of the total weight of the system. The Alexisismon isolator, which has a much lower isolator frequency or very soft spring, shows little increase in the shear force transmitted even when the maximum ground acceleration is increased from 0.3 g to 1.2 g.

Table I also indicates that when the input maximum acceleration (or ZPA) is scaled to higher values, responses of the linear system will increase proportionally. The bilinear system, by its design, limits the force transmitted to a preset value (20% of the total system weight in this study) under any seismic input. The increment in force transmitted with respect to ZPA is smaller in the Alexisismon design than the other two designs. Maximum acceleration of the reactor system generally increases with the input ZPA except in the two instances marked in Table I, which could be the result of the nonlinearity of the isolation system.

In Table II, a summary of responses for the reactor module isolated with different isolation systems under different acceleration time-histories is presented. Results indicate that all three isolation

designs reduce the shear force transmitted. Among the three isolation designs, the Alexisismon design generally gives the most reduction in shear force. The bilinear system, with the coefficient of friction used in this study, limits such shear force to 20% of the reactor system's total weight.

The maximum acceleration of the entire reactor system given in Table II occurs mostly at the core location. Of the three isolation designs investigated, the linear system yields the smallest maximum acceleration. The Alexisfsmon design not only produced the highest maximum acceleration, but also has the maximum acceleration of the entire system higher than the maximum input acceleration of 0.3 g, i.e., there appears to be acceleration amplification. Such amplification could be the result of the nonlinearity introduced by the Coulomb friction force of the system. When the Coulomb friction force is kept unchanged while the maximum input acceleration is scaled to higher values, such amplification is reduced or there is no amplification (Table I). Alternatively, amplification can be reduced or elfminated by reducing the Coulomnb friction force (or friction coefficient) when there is no change in the input acceleration. Acceleration amplification is also observed when the bilinear system is subjected to the time-histories obtained from the synthetic time-history and that recorded at Hollywood Storage P. E. lot.

Table II also summarizes the peak relative displacement for each of the three isolation designs. It is of interest to note that the bilinear system, which has the highest isolation frequency in this study, does not always yield the smallest relative displacement among these three isolation designs.

REFERENCES

Plfcon C., R. Gueraud, M. H. Richlf, & J. F. Casagrande 1980. Protection of Nuclear Power Plants Against Setsm," Nuclear Technology, Vol. 49, pp. 295-306.

Ikonomou, A. S. 1985. Alexisismon Isolation Engineering for Nuclear Power Plants," Nuclear Engineering and Design, Vol. 85, pp. 201-206.

Richart, F. E., Jr., J. R. Hall, Jr., & R. D. Woods 1970. Vibrations of Soils and Foundations," Prentice Hall, Inc., NJ.

Engineering Characterization of Ground Motion, Task I: Effects of Characteristics of Free-Field Motion on Structural Response. NUREG/CR-3805, May 1984.

Table 1. Variations of Responses with ZPA of an Isolated Reactor Module

Time Histories	ZPA (g)	Maximum Shear Transmitted (% total wt) With Isolation Linear (.5 Hz)	Bilin. (.67, Hz)	Alexis. (.17 Hz)	Without Isolation site shear vel (m/s) 600	1800	Peak Acceleration (g) Linear (.5 Hz)	Bilin. (.67 Hz)	Alexis (.17 Hz)
Synthetic	0.3	22.6	20	7.4	63	112	.26	.32	.36
	0.6	45.2	20	9.7	—	—	.51	.32*	.46
	1.2	90.4	20	11.0	--	—	1.02	.62	.57
El Centro	0.3	13.2	20	5.8	66	76	.15	.25	.41
	0.6	26.4	20	7.4	--	--	.30	.35	.60
	1.2	52.8	20	12	--	—	.60	.50	.76
Helena Montana	0.3	3.4	6.0	5.3	84	92	.06	.10	.61
	0.6	6.8	14.0	5.4	--	--	.11	.20	.62
	1.2	13.6	20	6.8	--	—	.22	.34	.46*

*Peak acceleration did not increase with input ZPA

Table 2. Peak Acceleration and Relative Displacement of an Isolated Reactor Module Under Different Time-Histories

Time Histories*	Peak Acceleration (g)			Peak Rel. Displ. (cm)		
	Linear (.5 Hz)	Bilin. (.67 Hz)	Alexis. (.17 Hz)	Linear (.5 Hz)	Bilin. (.67 Hz)	Alexis. (.17 Hz)
Synthetic	.26	.32	.36	19.2	22.3	21.3
El Centro	.15	.25	.41	6.4	13.1	13.1
Helena, Montana	.05	.10	.51	1.5	3.7	4.0
Taft, California	.15	.26	.30	5.5	14.0	15.5
Olympia, Washington	.12	.21	.35	7.0	10.7	10.4
Cholame, California	.25	.28	.36	17.1	22.9	22.3
Pacoima Dam	.13	.28	.44	3.1	12.3	13.4
Hollywood	.16	.32	.37	6.2	11.3	18.0

*Maximum acceleration was scaled to 0.3 g

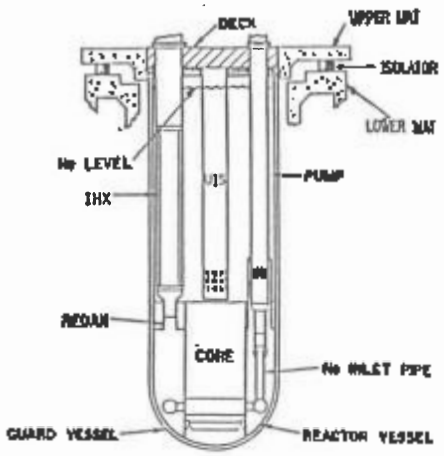

Fig. 1. Schematic of a Reactor Module with Seismic Isolation

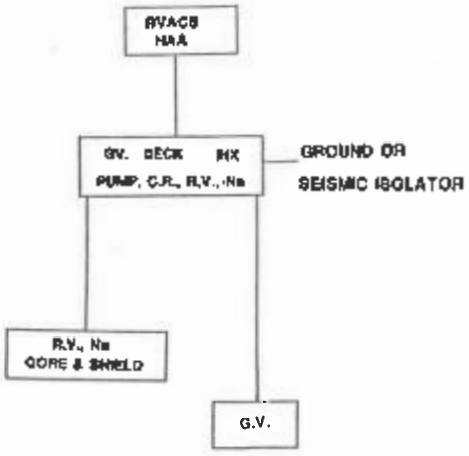

Fig. 2. Analysis Model for an Isolated Reactor Module

Optimization of mechanical properties of structures from the point of aseismic design

N.Model
Central Institute of Cybernetics and Informations Processes, Berlin, GDR
P.Dineva & L.Hadjikov
Institute of Mechanics and Biomechanics, Sofia, Bulgaria

I. INTRODUCTION

The vibroinsulation problem is solved by passive and acti ve dynamic systems control methods.The attacking of the problem by design of vibroisolators that passively extinguish the harmful vibration has begun historically earlier (Piculev I975,Petersen I979).Quite in the latest years some attention has been drawn on the possibility about dynamical system's active control.But the question about the technical realization at the optimal and the modal regulators making the behaviour safe during earthquake remains open until now.

The optimal control theory application to the aims of the dynamical systems stability motion (systems being described as rigid,nondeformable solids)by a passive vibroinsulation is done (Model I979).Thus the optimal dynamic system properties are identified without one having to solve the problem about a technical realization of active control equipments.

An aim of this paper is an application of an optimal control theory to obtaining optimal elastic and dissipati ve characteristics of the buildings at their aseismic de sign.

2. MECHANO-MATHEMATICAL DESCRIPTION OF THE STRUCTURE MOTION UNDER SEISMIC LOAD

The motion equations of a structure under seismic load have the form:

$$(I) \quad M\ddot{X} + C\dot{X} + KX = -Mb\ddot{x}_0$$
$$X(0)=\dot{X}(0)=0$$

where:M,C,K is the mass,damping and stiffness matrix,$X,\dot{X},\ddot{X}$ are vectors of displacement,velocity and acceleration, b is a cosine-director's vector of external action,$\ddot{x}_0$ is the external seismic action's acceleration,n is the number of equations as well as the number of the system's degrees of freedom.

3. THEORY OF OPTIMAL CONTROL APPLICATION TO OPTIMIZATION OF THE MECHANICAL PROPERTIES OF BUILDING STRUCTURES AT THEIR ASEISMIC DESIGN

3.I Formulation of the active control problem

The structure dynamics description in the case of a free motion and controlling active forces present in the state space has the form:

(2) $\dot{y}(t)=Ay(t)+Bu(t)$

there:

$y(t)=\begin{Bmatrix} X \\ \dot{X} \end{Bmatrix}$ is a state vector with a dimension 2n

$A=\begin{bmatrix} [0] & [I] \\ -M^{-I}.K & -M^{-I}.C \end{bmatrix}$ is a matrix of mechanical properties with a dimension 2nx2n,[0] and [I] are a zero and a unit matrix correspondingly with a dimension nxn,B is a vector showing the places of action of the controlling forces,u(t) is a vector of control having a dimension m, where m is the number of control inputs.All components of the X vector are assumed directly measurable.

The task for solving is set to find such a control u(t) for the system(2) that the quadratic functional of quality:

(3) $J(u)=\frac{1}{2}\int_0^{\infty}((y(t)-w(t))^T.Q.(y(t)-w(t))+u^T.R.u)dt$

to be minimized with respect to all smooth and continous u(t).There R is a positively defined weight matrix with a dimension mxm,Q is a nonnegative weght matrix with a dimension 2nx2n,w(t)is a function of assign.

The problem of vibroisolation(active and passive) coincides with the problem about synthesis of an optimal regulator u(t) with w(t)=0.

The optimal control has the form:

(4) $u(t)=-R^{-I}.B^T.P.y(t)$

where P is determined by the matrix algebraic equation of Riccati:

(5) $A^T.P+P.A-P.B.R^{-I}.B^T.P+Q=0$

Following this formulation the authors (Hadjikov,Dineva, Ivanova 1986)obtain numerical results for examples of real buildings showing effective decreasing of the dangerous peaks in their seismic motion.As we have already mentioned in part I.,the difficulty of the active control problem consists in its technical realization.

3.2 Optimization of the mechanical properties of structures from the point of view of aseismic design

We are going to consider the control forces from (4) u(t) as hypothetic control forces whose reoresentation in the form of a feed-back leads us to the task about an identification of the dynamic optimal system.After replacing(4) in (2) we obtain a motion equation for the system have already been optimized:

$$(6)\quad \dot{y}(t)=(A-BR^{-1}.B^{T}.P)y(t)=\tilde{A}opt.y(t)=\begin{bmatrix} [0] & [I] \\ -M^{-1}.\tilde{K}opt. & -M^{-1}.\tilde{C}opt. \end{bmatrix} y(t)$$

Eq.(6) gives us the new elastic properties $\tilde{K}opt.$ and the new dissipative $\tilde{C}opt.$ at the dynamic system having already been optimized.With the obtained $\tilde{K}opt.$ and $\tilde{C}opt.$we can predict how a given structure must change it's elastic and dissipative characteristics in order to have a more stable behaviour during an earthquake.For the purpose it is necessary the reverse task to be solved,namely,out of the new optimal matrices of stiffness and damping the new optimal mechanical characteristics of the system to be obtained.Using the complex eigenvaluefrequencesω_i^* and modes of the optimized system(6),following Sotirov,Dineva, Hadjikov(1984)we can obtain an optimal complex stiffness matrix $\tilde{K}opt.$ by the formula:

$$(7)\quad \tilde{K}^{M}_{opt.}=Diag(\ \omega_i^{*2}\ ).M$$

Out of $\tilde{K}opt.$ it is easy to find the optimal complex stiffnesses of the separate finite elements having the form:

(8) $k_e^{*}=k_e+i\alpha_e.k_e$, k_e-real stiffness of the "e" finite element, α_e is the damping coefficient of the same element.

From (7) and (8) the optimal elastic modulusses of the structure material as well as the optimal damping coefficient for the separate element are to be simultaneously determined.

Some interest offer the case when in the building's motion under a seismic action, the soil mechanic properties influence is being into account.Then in the matrices K and C from eq.(I) the elastic and damping soil characteristics will participate.After implementing the presented methods of optimization we are going to obtain the optimal complex stiffnesses of the soil.

A numerical example has been solved about a mechanical parameter optimization of the soil-structure system for an illustrative nuclear power plant shown on Fig.I.It is shown on Fig.2 the displacement of mass N7 from the dynamic scheme before and after optimization of the system. In table I the mechanical parameters of the soil under the structure are shown before and after the optimal vibroprotection.

3.3 Theory of modal control application to mechanical characteristic optimization of structures

This part deals with the modal control theory for obtaining of the new mechanical parameters of a dynamic system having a new,beforehand assigned eigenvaluespectrum.This is especially important to avoid the dangerous resonance cases.

If the system $\dot{X}(t)=AX(t)+Bu(t)$ is controllable and $\varphi(\lambda)=\lambda^{n}+f_{1}\lambda^{n-1}+\ldots+f_{N}$ is a given arbitrary polynome of order N and with real coefficients,then there exists a feedback vector $u(t)=-KX(t)$ such,that $\varphi(\lambda)$ stands for a characteristic polynome of the closed system $\dot{y}(t)=(A-BK)y(t)$. The control vector u(t) can change both a part of the eigen oscillation and the whole eigen spectrum of the dynamic system.The system obtained has a new optimal matrix $\tilde{A}opt$ and new elastic $\tilde{K}opt$.and damping $\tilde{C}opt$. properties,as well as a new eigenvaluespectrum identical to the one beforehand given.

4. CONCLUSION

A new way is to apply the active optimal and modal control theory to optimization of the elastic and dissipative characteristics of structures at their aseismic design.For this purpose is created a fortran code that allows computing the optimal parameter of arbitrary building or defining the optimal vibroinsolation characteristics of additional devices.The code can be employed also for identifying the optimal complex stiffnesses of the soil in the case of soil-structure interaction problem.

The task has been solved in the case of a free motion at the building.A future work is going to be dedicated to a passive control of a building subjected to a dynamic stohastic action where in the structure's optimized mechanical properties,the stohastic model parameters of the concrete geological column will participate too.

REFERENCES

Piculev,N.A.1975.K voprosu proectirovania gruppi vibrogasitelei s utchetom rasstroec.J.Stroitelna mechanika i raschet soorujenii.N5 /in Russian/

Petersen,N.R.1979.Designe of Large-Scale Tuned Mass Dampers ASCP,I

Mogel,N.1979.Untersuchungen zur optimalen steuerung stochastisch gestorter dynamischer systeme.Diss.Technische Hochschule Leuna-Merseburg

Hadjikov,L.,Dineva,P.,Ivanova,J.,Patarinski,S.1986.Control of Earthquake Exited Structures.ICCM86-Tokyo, Japan

Sotirov,P.,Dineva,P.,Hadjikov,L.1984.Varhu sastavane na matricata na satihvane pri reschavane na dinamitchni sadachi.J.Theoretical and Applied MechanicsN4 /in Bulgarian/

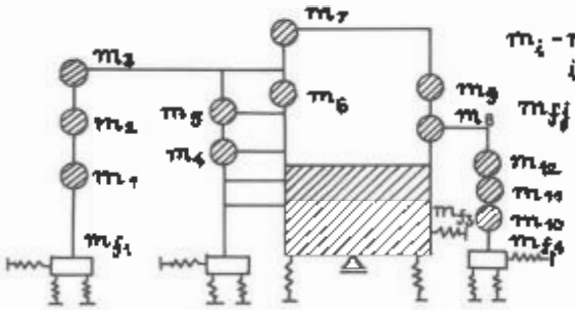
m_7
m_3
m_2
m_1
m_5
m_6
m_4
m_9
m_8
m_{12}
m_{11}
m_{10}
m_{13}
m_{f1}
m_{f4}
m_i - mass concentration in the i knot
m_{fj} - mass of the j-foundation

Fig. 1

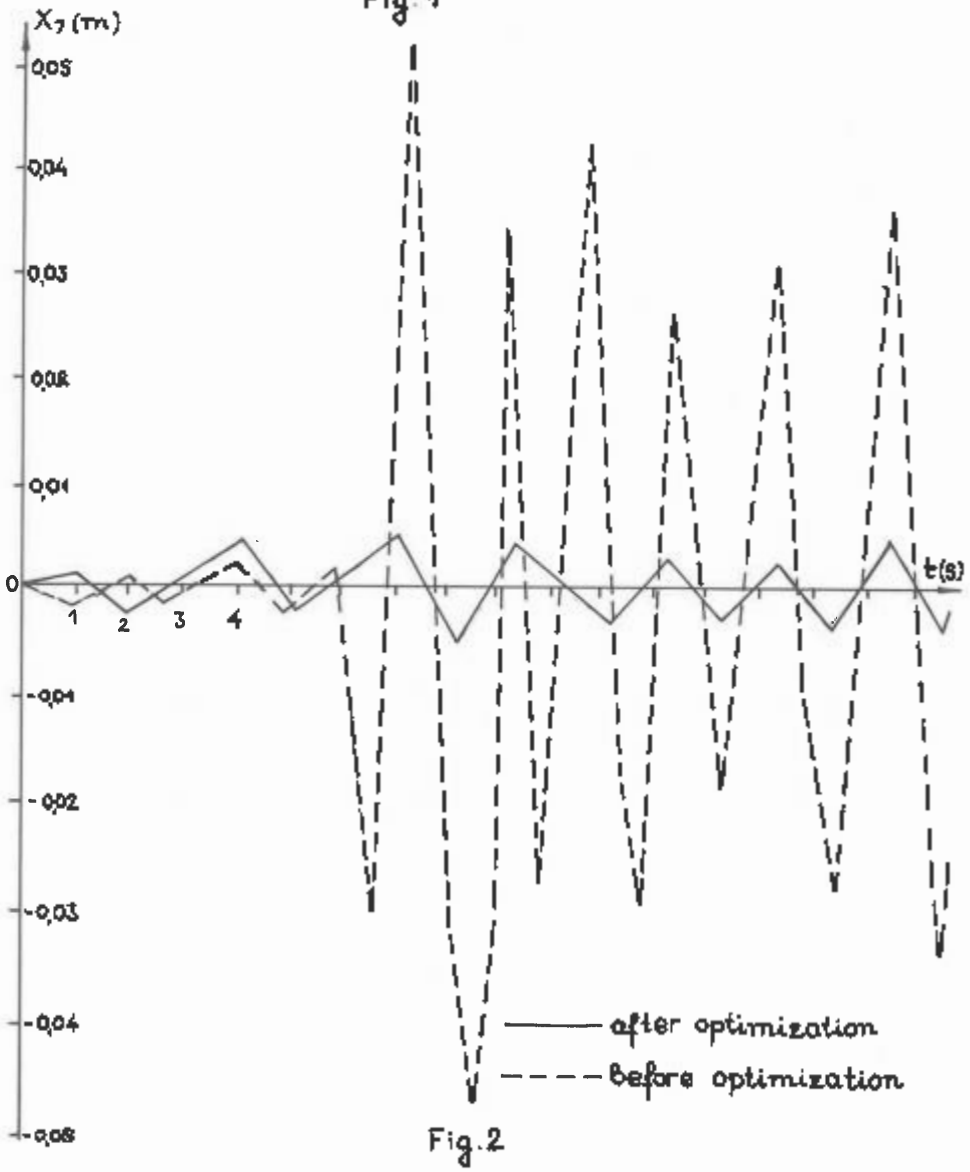
X_7 (m)
0,05
0,04
0,03
0,02
0,01
0
-0,01
-0,02
-0,03
-0,04
-0,05
1
2
3
4
t(s)
after optimization
before optimization

Fig. 2

Table I. The mechanical properties of soil before and after optimization

Soil properties	$C_{f_1}=C_{f_2}=C_{f_3}=C_{f_4}$ [t/m³] 1t = 10³kgf	$C_{\varphi_1}=C_{\varphi_2}=C_{\varphi_3}=C_{\varphi_4}$ [t/m]	$\alpha_{f_1}=\alpha_{f_2}=\alpha_{f_3}=\alpha_{f_4}$	$\alpha_{\varphi_1}=\alpha_{\varphi_2}=\alpha_{\varphi_3}=\alpha_{\varphi_4}$	C_f^3 [t/m³]	C_φ^3 [t/m³]
Before optimization	572	1195	0,3	0,2	777	1204
After optimization	5726	12325	0,3	0,2	8123	12039

here: $k^*_{fj}=k_{fj}+\alpha_{fj}k_{fj}$; $k^*_{\varphi j}=k_{\varphi j}+\alpha_{\varphi j}k_{\varphi j}$;

$k_{fj}=C_f.F_j$ $\quad$ $k_{\varphi j}=C_\varphi.J_{\varphi j}$

j - number of foundation

$j=1,2,3,4$ (see fig.1)

k_{fj} - stiffness for horizontal displacement of the j foundation with cross section F_j

$k_{\varphi j}$ - stiffness for the rotation of the j foundation with geometric inertial moment J_j

C_f, C_φ - soil characteristics of an ideal elastic foundation that undergoes displacement and rotation respectively

$\alpha_{fj}, \alpha_{\varphi j}$ - damping hysteresis coefficients

Seismic response analysis of nuclear power plant founded on sliding elastomer bearing pads

K.Uchida, K.Emori, K.Mizukoshi & Y.Takenaka
Kajima Corporation, Tokyo, Japan
J.Betbeder-Matibet
Electricité de France, Paris
J.-P.Noël-Leroux & P.Ulrich
Spie Batignolles, Vélizy-Villacoublay, France

1 INTRODUCTION

Introduction of base isolation concept to the seismic design of nuclear power plant (NPP) has recently been expected in Japan as an effective measure to reduce drastically the seismic force for both buildings and equipament and piping. An analytical study on earthquake response of a French type base isolation system for NPP is carried out as a joint study between Kajima Corporation of Japan and Électricité de France (EDF) and Spie Batignolles (SB) of France. The purpose of this study is to grasp the seismic behavior of a base-isolated NPP using the sliding elastomer bearing pads (hereafter referred to as "aseismic bearings") which were developed and actually applied to Koeberg NPP in South Africa by EDF and SB (Jolivet & Richli 1977, et al.), and to evaluate the feasibility of application of the base isloation system in Japan.

In this base isolation system, a pair of friction plates of each aseismic bearing can slip relative to each other when the horizontal shear force reaches a level of friction force. And it is anticipated that, during earthquake, the friction force level may fluctuate every moment and every location with the fluctuation of contact force applied to the friction plates. In this study, the base-isolated structure is modeled as a two dimensional multi-stick lumped-mass model in which the flexibility of the upper and lower rafts is taken into account and the aseismic bearings are modeled as fourteen nonlinear elements being capable of expressing above-mentioned complex sliding phenomenon of friction plates caused by fluctuating contact force. Using this model, a series of nonlinear earthquake response analyses are perfomed by applying horizontal and vertical earthquake ground motions simultaneously. And then, the dynamic behavior of the base-isolated reactor buildings and aseismic bearings are clarified , and the effectiveness of the system is discussed in comparison with the response of a non-isolated buildings.

2 OUTLINE OF BASE ISOLATION SYSTEM

The base-isolated NPP treated in this paper is a standard twin units French PWR 900MW, CP1 type, which consists of two reactor buildings, two fuel storage buildings, two connecting buildings, one electrical building, and one nuclear auxiliary building which are constructed on

a common upper raft (149 m x 86 m) to form a "nuclear island" weighing about 390,000 tons. The nuclear island is supported by a lower raft founded on the bedrock through about 2000 aseismic bearings.

The basic concept of the base isolation system is shown in Fig.1. Low intensity earthquakes only cause linear distortion of the laminated elastomer pads, and high intensity earthquakes cause both distortion of the laminated elastomer pad and slippage between the friction plates. The system thus works as a filter which transmits no shear force larger than the friction force to the upper buildings. The detail of the laminated elastomer is shown in Fig.2.

3 ANALYTICAL MODEL

The NPP is assumed in this study to be built on a hard rock site (shear velocity Vs = 1,500 m/s) without embedment.

As shown in Fig.3, the buildings and upper and lower rafts are modeled as a two dimensional multi-stick lumped-mass model representing the nuclear island in the longitudinal direction in which each mass point has three degrees of freedom, namely vertical, horizontal and rotational directions. For the building structures, the Rayleigh type damping with 5% of critical damping at both 0.9Hz and 10Hz is assumed.

The upper and lower rafts are connected with each other using fourteen non-linear elements (refer to Fig.4) representing in the plane a half of the aseismic bearing rows. Assumed for these non-linear elements is the internal viscous type damping with 5% at 0.9Hz for the horizontal deformation and 7% at 12Hz for the vertical deformation. As for the Coulomb friction elements representing the friction plates, the two states depending on the occurrence of the slippage are considered as follows;

$$\text{Non-slip state:}\quad Fs = Ks\,(\Delta s - \Delta r) + Cs\,\dot{\Delta}s$$
$$Fv = Kv\,\Delta v + Cv\,\dot{\Delta}v$$
$$\text{Slipping state:}\quad Fs = \mu Fv\,\mathrm{sgn}(\dot{\Delta}s)$$
$$Fv = Kv\,\Delta v + Cv\,\dot{\Delta}v$$

where
- Fs, Fv; Shear (friction) force, contact force
- Ks, Kv; Horizontal and vertical stiffnesses
- Cs, Cv; Horizontal and vertical damping coefficients
- Δs, Δv; Horizontal and vertical deformations
- Δr; Accumulated slip amount
- μ; Coulomb friction coefficient (= 0.2)

The condition for the change from non-slip state to slipping state is expressed as "$|Fs| \geq \mu Fv$"

Each mass point of the lower raft is supported by vertical and horizontal Winkler-type soil springs representing elastic deformation of the ground. The soil spring is estimated from static stiffness of semi-infinite elastic soil medium assuming that the vertical or horizontal reaction force to the soil surface is uniform. The internal viscous type damping is assumed for the soil springs considering radiation effect, where the damping factors of 2.3% and 26% are given at the horizontal and vertical fundamental frequencies (0.9Hz and 8.7Hz), respectively.

4 EIGENVALUE ANALYSIS

The natural frequencies and participation factors of the linear model for the isolated building, where the slippage of friction plates is restricted, are shown in Table 1, and Fig. 5 shows its typical mode shapes. For comparison, the natural frequencies of the non-isolated building are shown in Table 2.

As to horizontal input, only the mode at 0.89Hz in which the overall nuclear island moves horizontally as a rigid body predominates for the isolated building, in contrast with the non-isolated building having the higher modes with relatively large participation factors. As to vertical input, several predominant modes accompanying with local deformations of the upper and lower rafts appear in the range of 8 to 10Hz.

5 EARTHQUAKE RESPONSE ANALYSIS

5.1 Input Earthquake Ground Motions

As shown in Table 3, the El Centro 1940 NS and UD waves and the synthesized waves for the far field S2 earthquake are used as the input ground motions for the response analysis. The response spectra of these ground motions are shown in Fig.6. The S2 earthquake is the wave proposed by the "Seismic Design Sub-committee of MITI on Improvement and Standardization of Light Water Reactor" of Japan.

The analytical cases presented herein are shown in Table 4.

5.2 Response of Buildings

The horizontal response acceleration time histories obtained from the analysis show that the response of the isolated building has a smaller quantity of high frequency component than that of the non-isolated building. The isolated buildings oscillate mainly at the fundamental frequency of 0.89Hz, and the acceleration amplification in the direction of height is small.

The maximum responses of the reactor building (R/B) are shown in Fig.7. As was expected, the isolated buildings have much smaller horizontal acceleration and shear force, but conversely larger horizontal displacement, than the non-isolated buildings. The responses in the vertical direction against the same wave are almost the same for isolated and non-isolated buildings (Cases 1 and 3).

Fig.9 shows the horizontal acceleration floor response spectra for the damping factor of 1% at the points A and B shown in Fig.8. The spectral values are markedly reduced by introducing the base isolation in the frequency range higher than 2Hz, which may result in a great advantage for the aseismic design of equipment and piping.

5.3 Response Behavior of Aseismic Bearings

The horizontal shear force vs. displacement hysteresis loops of the aseismic bearings at the typical locations are shown in Fig.10. It is found that the hysteresis loop pattern differs depending on its location, which results in making the maximum and residual slippage of friction plates as well as residual shear deformation of elastomer after earthquake be uneven depending on its location.

Fig.11 shows the distribution of the maximum response values of the

fourteen aseismic bearing elements in the model. The variation of contact force which is shown as shaded region in Fig.11(a) is not uniform but not large enough to cause uplift. Fig.11(b) indicates that the horizontal relative displacement between the upper and lower rafts is a litte less than 10 cm and is uniformly distributed due to the large in-plane stiffness of the upper raft, but, the maximum and residual slippage between friction plates is not uniform because of the uneven variation in contact force as shown above. Fig.11(c) shows the residual horizontal deformation of elastomers after earthquake which variate within 2cm depending on the location.

6 CONCLUDING REMARKS

As the results of the analyses, the dynamic response behavior of the base isolated buildings and aseismic bearings during earthquakes are clarified. Especially, it is suggested that all aseismic bearings throughout the foundation do not necessarily behave uniformly because of the uneven fluctuation of the contact force applied to the friction plates during earthquakes.

In spite of such local complex behavior of each aseismic bearing, it is also shown from analytical results that the response acceleration, shear forces and floor response spectra of the reactor building are markedly reduced in comparison with a non-isolated building. Furthermore, it is confirmed that no uplift nor excessive slippage between friction plates are caused even under S2 earthquake specified in Japan.

REFERENCES

Jolivet, F. and Richli, M. 1977. Aseismic foundation system for nuclear power stations. Proc. 4th SMiRT. K9/2

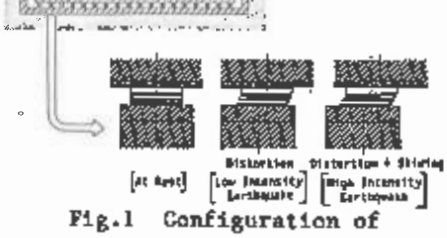

Fig.1 Configuration of Base-isolated N.P.P.

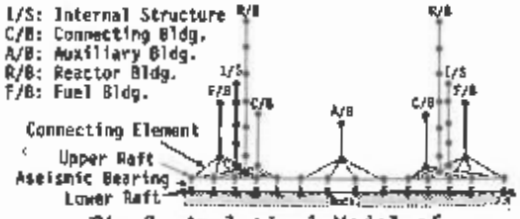

Fig.3 Analytical Model of Isolated Building

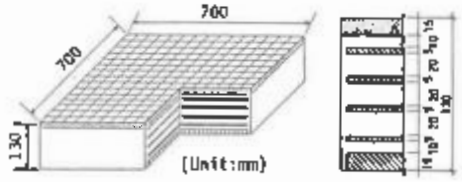

Fig.2 Detail of Aseismic Bearing

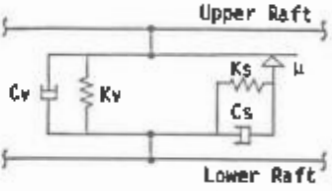

Cv: Vertical Damping Coef.
Kv: Vertical Stiffness
Cs: Horizontal Damping Coef.
Ks: Horizontal Stiffness
μ: Coef. of Friction

Fig.4 Non-linear Element for Aseismic Bearing

Table 1 Eigenvalues of Isolated Building

Mode	Freq. (Hz)	Participation Factor		Mode
1	0.891	1.0148	0.0003	Overall Horiz. Motion
2	3.65	0.0341	0.0368	R/B Horizontal Bnd
3	4.10	0.0063	0.0285	R/B Horizontal 2nd
4	5.02	0.0005	0.0003	
5	5.91	0.0169	0.0342	
6	6.36	0.0008	0.0231	
7	6.93	0.0085	0.0382	
8	7.05	0.0091	0.0256	
9	7.32	0.0012	0.0028	
10	8.03	0.0212	0.2462	
11	8.70	0.0035	1.2581	Overall Vert. Motion
12	9.05	0.0004	0.2140	
13	10.0	0.0001	0.2539	
14	10.3	0.0002	0.3012	

Table 2 Eigenvalues of Non-isolated Building

Mode	Freq. (Hz)	Participation Factor		Mode
1	3.74	2.1332	0.0217	R/B Horizontal 1st
2	5.86	1.7727	0.0001	R/B Horizontal 2nd
3	9.13	0.0050	0.0108	
20	9.33	0.2124	1.9115	Overall Vertical Motion

Table 3 Input Ground Motions

Name	Horizontal Max. Acc.	Vertical Max. Acc.	Duration
El Centro 1940	341.7Gal	206.3Gal	10.0sec
S_2 (M=8.1, Δ =40km)	467.3Gal	317.1Gal	40.0sec

Table 4 Analysis Cases

Case	Foundation	Input Ground Motion	Analysis
Case 1	Isolated	El Centro 1940	equi-linear
Case 2	Isolated	S_2 (M=8.1, Δ =40km)	non-linear
Case 3	Non-Isolated	El Centro 1940	linear

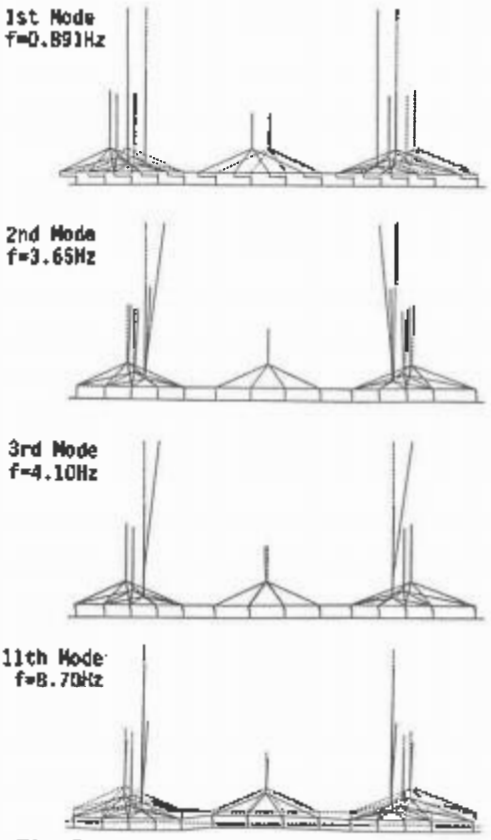

Fig.5 Typical Mode shapes of Isolated Building

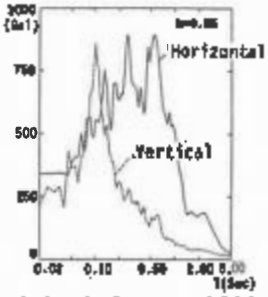

(a) El Centro 1940

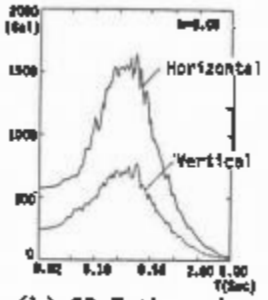

(b) S2 Earthquake

Fig.6 Response Spectra of Input Ground Motion

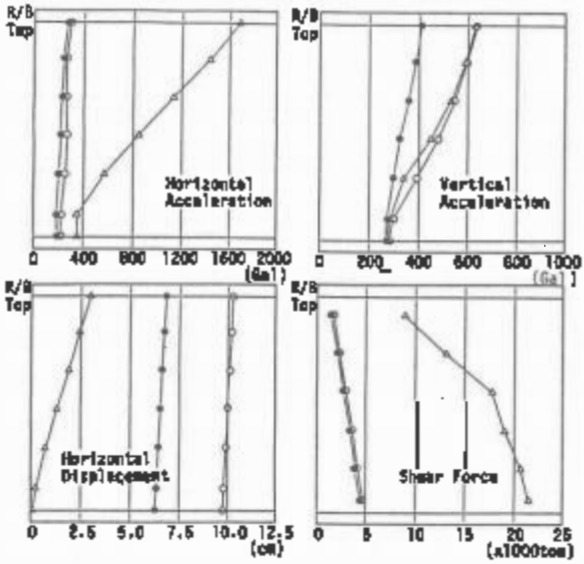

○ Case 1 (El Centro) ● Case 2 (S2) ▲ Case 3 (El Centro Non-Isolated)

Fig.7 Maximum Response of Unit 1 R/B

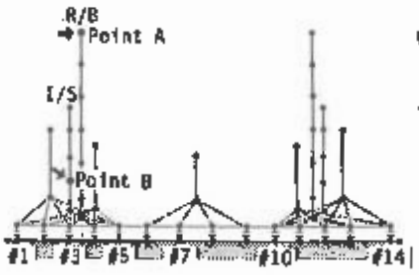

Fig.8 Location of Output

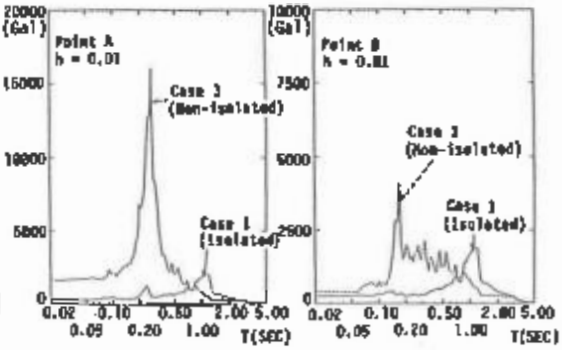

Fig.9 Horizontal Floor Response Spectra (Case 1, Case 3, El Centro)

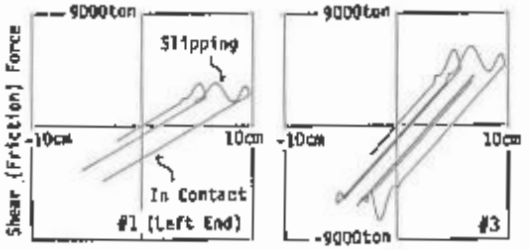

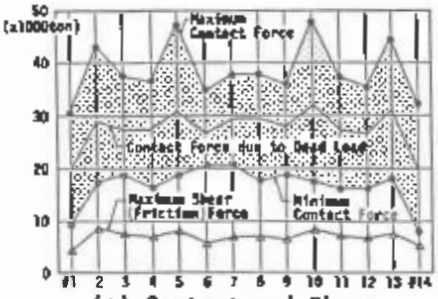

(a) Contact and Shear (Friction) Force

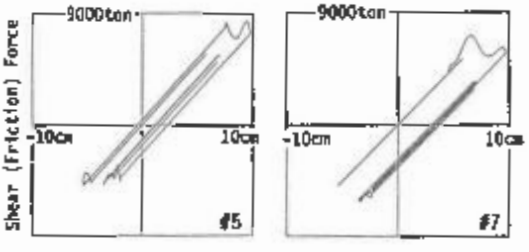

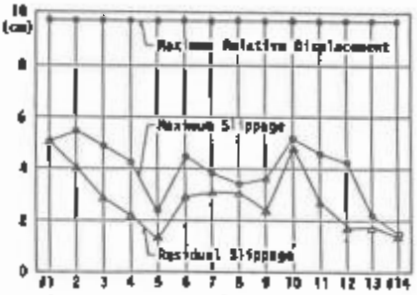

(b) Relative Displacement and Slippage

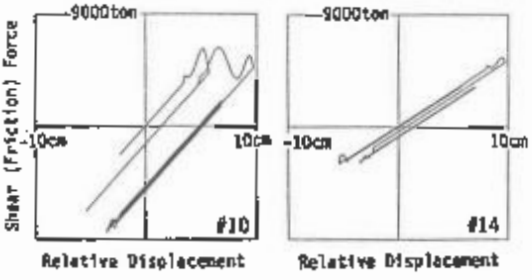

Fig.10 Histeresis Loop of Aseismic Bearings (Case 1, El Centro)

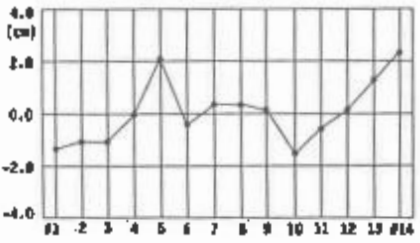

(c) Residual Deformation of Elastomer

Fig.11 Response of Aseismic Bearings (Case 1, El Centro)